PHOTOCATALYTIC AND PHOTOCHEMICAL DECOMPOSITION OF VARIOUS PER- AND POLYFLUOROALKYL SUBSTANCES (PFAS) IN WATER

by

NUSRAT JAHAN CHOWDHURY

Presented to the Faculty of the Graduate School of

The University of Texas at Arlington in

Partial Fulfillment of the Requirementsfor the Degree of

DOCTOR OF PHILOSOPHY

THE UNIVERSITY OF TEXAS AT ARLINGTON

August 2021

ACKNOWLEDGMENTS

Foremost, I would like to express my sincere gratitude to my adviser Dr. Hyeok Choi for his continuous support and guidance of my Ph.D. study and research. His patience, motivation, enthusiasm, valuable insights, and organized approach to challenges have enabled me to tackle many problems in an efficient and timely manner. Besides my advisor, I would also like to thank rest of my committee members Dr. Melanie Sattler, Dr. Srinivas Prabakar, and Dr. Junha Jeon for their encouragement, valuable comments, and constructive questions, I also express my appreciation to the staff and other faculty in the Department of Civil Engineering at The University of Texasat Arlington (UTA). Their assistance and dedication to their duties has allowed me, and so many other students, to successfully earn our degrees.

I would like to express my gratitude to all the colleagues I have had during this journey, most especially Akshay Parenky and Naomi Gevaerd de Souza (now doctors). Thank you all for their help and comradeship in the lab. This also includes all environmental engineering graduate students. I also want to thank my friend Shammi Rahman and Tamanna Rahman for being friend and supporting my decision. Specifical thanks go to my father and late mother not only for their unconditional love but also for guiding me to the person that I am at this moment. My brothers have been a source of inspiration, love, and support through this journey, and I will always be grateful to them.

Finally, I would like to thank my husband and children for giving me a wonderful home, and surroundings and for making the biggest sacrifice that has allowed me to take the time off to work on my Ph.D. I appreciate their love and sacrifices.

July 28, 2021

TABLE OF CONTENTS

LIST OF FIGURES

LIST OF TABLES

Problem Statement

Per- and polyfluoroalkyl substances (PFAS) comprised of a perfluoroalkyl backbone and a terminal functional group are a class of man-made chemical compounds known to be resistant to heat, water, and oils [Fujii et al., 2007]. The C-F chain of typical PFAS is hydrophobic while their functional groups such as sulfonic group and carboxylic group are hydrophilic. It gives these chemicals a unique property of repelling both water and oil (i.e., hydro- and oleophobic) [Zaggia et al., 2016]. Due to the low molecular polarity, strong C-F bond energy (536kJ/mol), strong biological resistance, and the amphiphilic nature, PFAS have been frequently incorporated into a variety of industrial and commercial products such as non-stick cookware, stain resistant clothing, food packaging, and firefighting foams [Rahman et al., 2014; Jian et al., 2018]. These chemicals are persistent and resist degradation in the environment. They also bioaccumulate, meaning their concentration increases over time in the blood and organs. Growing health data have indicated that exposure to PFAS can lead to various adverse health effects, such as low infant birth weight, thyroid hormone disruption, impairment on the immune system, and even cancers. According to US Environmental Protection Agency (EPA), certain PFAS have adverse health effects in laboratory animals due to exposure to these chemicals. PFAS have been frequently detected in the aquatic ecosystems, particularly near relevant industries or municipal facilities such as landfill, wastewater treatment plants and firefighter training sites [USEPA, 2017]. PFAS can be categorized into two groups, namely long-chain PFAS and short chain PFAS. USEPA has placed long chain PFAS on the contaminant candidate list 3, unregulated contaminant monitoring rule 3 [Post et al., 2012a], and established provisional health advisories for perfluorooctanesulfonic acid (PFOS) and perfluorooctanoic acid (PFOA) based on a risk assessment performed by the European Food Safety Authority [Clarke et al., 2010; Kwok et al., 2010; Zhang et al., 2011; Shaw et al., 2013].

Since year 2006, PFOA and PFOS have been voluntarily phased out by PFAS manufacturers and end-users and switched to short chain surrogate PFAS (not regulated yet), which has similar physical properties of long chain ones. While long-chain PFAS have been the center of active research in the past decades, industrial production, and applications of short chain PFAS continue to rise. Very few studies have focused on short chain PFAS remediation in the environment [Conder et al., 2008; Giesy et al., 2010; Houtz et al., 2013]. Short chain PFAS may pose soon another significant environmental problem, assuming their decomposition is independent of carbon chain length or functional group. It reveals an urgent need to compare reactivity of PFAS in water as a function of alkyl chain length and head group and advance our knowledge on the degradation mechanism. Previously, the efforts to develop effective treatment technologies have been given to long chain PFAS. While short chain PFAS are increasingly detected in the environment, there is a need to develop effective in-situ treatment technologies for remediation of PFAS contaminated groundwater.

Abstract

Nusrat Chowdhury (Liza)

The University of Texas at Arlington, 2021

Supervising Professor: Hyeok Choi

Per- and polyfluoroalkyl substances (PFAS) are anthropogenic compounds comprised of a perfluoroalkyl backbone and a terminal functional group. Their detrimental health effects of in humans, like other halogenated chemicals, have been well documented and thus the frequent occurrence of PFAS in the water environment is a recent global concern. After US Environmental Protection Agency (EPA) released a drinking water health advisory for the two most detected long chain PFAS (such as perfluorooctanoic acid (PFOA) and perfluorooctanesulfonic acid (PFOS)), industrial production and application of short chain PFAS continues to rise. Feasible and sensible treatment strategies are in dire need for environmental remediation and water treatment. No studies so far have demonstrated the reactivity of PFAS as a function of alkyl chain length and functional group in TiO_2 photocatalysis, which is considered as one of the promising advanced oxidation technologies (AOTs) and the most cost-efficient technologies for PFAS remediation. This research is presented in two subsections, where decomposition of selected PFAS was evaluated under various TiO_2 photocatalytic and photochemical conditions inducing AOTs.

In the first study, we carefully selected 9 PFAS based on chain lengths, functional groups, and structural properties, namely 4 perfluorocarboxylic acids (PFCAs) including PFOA, 3 perfluorosulfonic acids (PFSAs) including PFOS, hexafluoropropylene oxide dimer (GenX), and 6:2 fluorotelomer sulfonate (6:2 FTS) and investigated dependency of the photocatalytic decomposition of PFAS on their properties. In addition, various chemical oxidants and reductants

were introduced with titanium dioxide (TiO_2) photocatalysis and elucidate the decomposition mechanism of both carboxylic and sulfonic PFAS. Some notable findings include long chain PFCAs and 6:2 FTS were removed in the TiO_2/UVC system mostly via chemical decomposition while GenX, PFSAs, and short chain PFCAs were removed mostly via physical adsorption. Sulfate radicals (SRs, $SO_4^{\bullet-}$) generated with PS played an important role in decomposing both long and short chain PFCAs, while these radicals were ineffective to PFSAs. Hydrated electron produced from activation of sulfite by UVC defluorinated both PFCAs and PFSAs significantly. Overall susceptibility of PFAS to the chemical reactions was explained with their properties and the reactivity of reactive species produced in each system.

In the second study, lead-doped TiO_2 coated with reduced graphene oxide (TiO_2-Pb/rGO) was developed as a ternary photocatalyst to overcome the limitation of the poor reactivity of neat TiO_2 photocatalysts caused by quick electron-hole recombination. Degradation kinetics of PFOA using this catalyst was compared to that of bare TiO_2, TiO_2-Pb, TiO_2 /rGO, and TiO_2-Pb/rGO under UVC. High photocatalytic activity of TiO_2-Pb/rGO was observed, which is attributable to the effects of rGO and Pb addition on TiO_2 bandgap energy, surface interfacial charge transfer mechanisms and oxygen diffusivity. The role of Pb and rGO in TiO_2 was investigated, and the reactive species responsible for the reaction was identified. The radical quenching experiments implied the main roles of hole and oxygen on the highly efficient photodegradation of PFOA. Significant byproduct and fluoride release were observed upon decomposition of PFOA. This system showed great potential for in situ application of polyfluorinated compounds and long chain PFCAs remediation. The efficacy of these systems for a wider range of PFAS was evaluated. The reaction mechanism for the system was complex and future studies should identify an appropriate TiO_2-metal/rGO pair capable of decomposing sulfonic PFAS.

Here, first study compared photocatalytic a decomposition of 9 PFAS mainly PFCA and PFSA but future studies should explore other PFAS and compare reactivity to current study. In addition, it would be important to understand the effect of organic and inorganic contaminants present in water in photocatalytic and photochemical decomposition of PFAS. In second study, only long chain PFCA were successful degraded by TiO_2-Pb/rGO under UVC. Follow up studies investigating various TiO_2-Pb/rGO oxidant/reductant combinations could potentially decompose other PFAS groups.

CHAPTER 1

Introduction and Literature Review

1.1 Chemistry

Per- and polyfluoroalkyl substances (PFAS) are a group of organofluorine compounds that have alkyl chains but with the hydrogen atoms replaced by fluorine atoms [Rayne and Forest, 2009]. They are part of the larger group of fluorinated alkyl compounds, where at least one hydrogen has been substituted by a fluorine atom [Lange et al., 2006; Knepper et al., 2011]. The C-F bond is the strongest bond known in organic chemistry [O'Hagan, 2008] with bond strength of 530 kJ/mol, which attribute a specific property to these group, that they are chemically and thermally stable; and for this reason, they are commonly referred to as persistent organic pollutants (POPs) [Teng et al., 2009; Zhang et al., 2014; Bao et al., 2014; Arvaniti et al., 2015]. Typically, PFAS have the molecular formula $CF_3(CF_2)_nR$, where R could be any functional group such as hydroxyl, carboxylic or sulfonic acid among a few other possibilities [Rayne et al., 2009; Knepper et al., 2011].

PFAS is divided into polymeric and non-polymeric PFAS. Polymeric PFAS include three sub-groups: fluoropolymers, sidechain fluorinated polymers, and perfluoro polyether; whereas nonpolymeric PFAS include four sub-families: perfluoroalkyl acids (PFAAs), fluorotelomer (FT), per- and polyfluoroalkyl ethers (PFPE), and compounds derived from perfluoroalkane sulfonyl fluoride (PASF) [Buck et al., 2011].

1.1.1 PFAAs:

PFAAs are some of the most basic PFAS molecules. PFAAs are surfactants with unique physical-chemical properties such as an extraordinary high surface tension. They consist of a fully fluorinated carbon chain of typically three to fifteen. They are essentially non-degradable. The chemical structure of each PFAAs includes a hydrophobic alkyl tail in which all hydrogens are replaced by fluorine and a hydrophilic acid head group as shown in Figure 1.1.

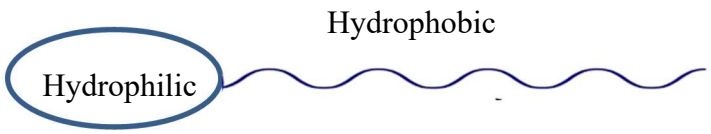

Figure 1.1. Schematic representation of fluorinated surfactants

The PFAAs class is divided into three major groups:

Perfluoroalkyl phosphonic acids (PFCAs): General chemical formula is $C_nF_{2n+1}COOH$, and it can be categorized into two groups; namely long chain (n >8) and short chain (n<6) PFCAs. The most frequently studied long chain PFCA is PFOA. The most important short chain PFCA is perfluoro butanoic acid (PFBA), which is an alternative of the most use surfactant PFOA.

Perfluoroalkyl sulfonic acids (PFSAs): General chemical formula of this group is $C_nF_{2n+1}SO_3H$; and typically, long chain PFSAs contain n ≥6 carbons. The most frequently studied PFSA is long chain PFOS. PFOS derivatives have been used as surfactants in oil well stimulation to recover oil trapped in small pores. PFOS has recently been classified as a persistent, bioaccumulative and toxic substance. The most important short chain PFSA is perfluoro butane sulfonic acid (PFBS), which is another alternative of the most use surfactant PFOA. Alternatives

fluoro surfactants of PFOS are short chain PFSAs such as PFBS (C4), perfluoro pentane sulfonic acid (, PFPeS, C5) and perfluoro hexane sulfonic acid (PFHxS, C6).

Among all PFAS compounds, PFOA and PFOS are the most prevalent and most studied of the PFAS [Wang et al., 2014]. Their properties are listed in the Table 1.1 below:

Table 1.1. Physical and chemical properties of PFOA and PFOS [Kucharzyk et al., 2017].

Property	PFOS (potassium salt)	PFOA (free acid)
Chemical Abstract Service (CAS) Number	2795-39-3	335-67-1
Physical description (atroom temperature and pressure)	White powder	White powder
Molecular weight (g/mol)	538	414
Water solubility at 25 °C (mg/L)	550 to 570 (purified) 370 (fresh water) 25 (filtered sea water)	9.5×10^{3} (purified)
Melting point (°C)	400	45 to 54
Boiling point (°C)	Not measurable	188 to 192
Vapor pressure at 20 °C (mm Hg)	2.48×10^{-6}	0.017
Octanol-water partition coefficient (log Kow)	Not measurable	Not measurable

Henry's constant (atm-m^3/mol)	3.05×10^{-6}	Not measurable
Half-life	Atmospheric: 114 days Water > 41 years (at 25 °C)	Atmospheric: 90 days Water> 92 years (at 25 °C)

Alternatives fluoro surfactants of PFOS are short chain PFSAs such as PFBS (C4), perfluoro pentane sulfonic acid (, PFPeS, C5) and perfluoro hexane sulfonic acid (PFHxS, C6).

Perfluoroalkyl phosphonic acids (PFPAs): PFPAs are another subgroup of PFAAs that recently gained scientific interest around the world. The chemical formula of PFPAs is $C_nF_{2n+1}PO_3H_2$. Perfluoro butane phosphonic acids (PFBPA), Perfluoro hexane phosphonic acids (PFHxPA) are mostly used Perfluoroalkyl phosphonic acids (PFPAs).

1.1.2 Precursor and raw materials:

6:2 FTS: The most common substitute for PFOS is typically used in hard metal plating. It is not fully fluorinated, but the C6 perfluorinated tail is persistent, and the chemical is a precursor of some PFCAs such as PFHxA.

Perfluoroalkane sulfonamides (FASAs): Typically, FASAs are used as raw material to make perfluoroalkyl sulfonamide substances that are used for surfactants and surface treatments. Examples include Perfluoro butane sulfonamide ($C_4F_9SO_2NH_2$), Perfluoro hexane sulfonamide ($C_6F_{13}SO_2NH_2$) are used as a raw material for surfactant. N-Methyl perfluoro butane sulfonamide (MeFBSA) and *N*-Ethyl perfluoro butane sulfonamide (EtFBSA) are intermediate environmental transformation product [Shahid Ullah, 2013]. Molecular structures of some PFAS (Figure 1.2) are shown below:

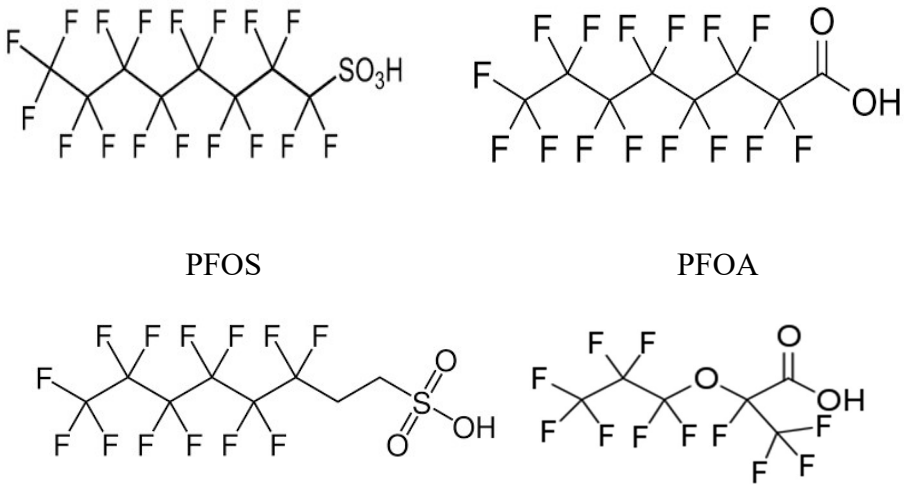

Figure 1.2. Molecular structures of some PFAS. PFOS represents PFSAs group such as PFBS and while PFOA represents PFCAs group such as PFBA. Chain lengths and functional groups vary in PFSAs and PFCAs. 6:2 FTS represents a polyfluoroalkyl substance with vulnerable 4 C-H bonds while GenX has a hetero-atom O in the middle of an alkyl chain.

PFAS classification chart (Figure 1.3) is shown below:

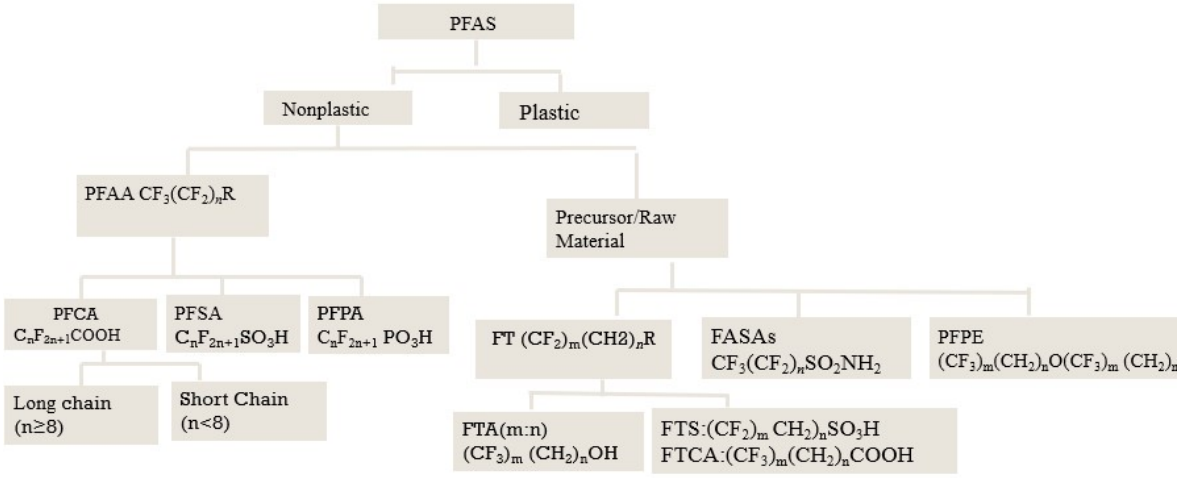

Figure 1.3. PFAS classification chart

1.2 Usage

PFAS are a class of man-made chemical compounds known to be resistant to heat, water, and oils. These compounds are frequently incorporated into a variety of industrial and commercial products such as non-stick cookware, stain resistant clothing, food packaging and firefighting foams. The most well-known compounds in this group are PFOA and PFOS. [Fujii et al., 2007] The sodium or potassium salt form of PFOA is used to produce useful fluoropolymers such as polytetrafluoroethylene (PTFE, more popularly known as Teflon). [Lindstrom, Strynar, and Libelo, 2011] PFOS, which is usually used as a potassium or sodium salt, is main ingredient in Scotchgarde and other similar stain repellents [Ochoa-Herrera et. al., 2008]. It is also used in hydraulic fluids in commercial airliners [Lau et al. 2007].

1.3 Occurrence

PFAS have been manufactured and used worldwide since 1940s, resulting in massive release to the environment upon industrial production and applications [Giesy et al., 2001]. PFOA and PFOS have been detected in every part of the world as well as in all manner of matrices- sediment, soil, seawater, groundwater and even drinking water [Skutlarek, Exner, and Farber, 2006; Benford et al., 2008; Vecitis et al., 2009]. This makes it unsurprising that it has been detected in the serum of many human subjects. In Australia, PFOS (16 ng/L) and PFOA (9.7 ng/L) as well as other shorter chain PFAS in surface waters are detected [Thompson et al., 2011]. During the period 1960s-1990s, internal studies at DuPont showed the presence of PFOA in the blood of some of its workers. This data was however not reported to the authorities, which eventually led the company to pay a settlement fee to the USEPA in 2005 [Hogue, 2005a].

Since year 2006, PFOA and PFOS have been voluntarily phased out by industry. Yet, they remain persistent in the environment [Wang et al., 2009]. From 2002, 3M company and many other major global producers of PFAS began to replace long chain PFAS with short chain PFAS [3M, 2000; Ritter et al., 2010]. Among the most common replacement short chain PFAS are hexafluoropropylene oxide (HFPO) dimer acid and its ammonium salt (referred to as GenX chemicals) and PFBS and its potassium salt (K+PFBS). The short chain PFCAs have more recently been detected in surface water and in precipitate, and their levels are higher than that of PFOA [Scott et al., 2006]. GenX chemicals have been detected in surface water, groundwater, finished drinking water, rainwater, and air. PFBS was selected as a replacement for PFOS. PFBS has been identified in the environment and consumer products including surface water, wastewater, drinking water, dust, carpeting and carpet cleaners, floor wax, and food packaging. PFBS and GenX chemicals are persistent in the environment, and mobile in groundwater and surface water [US EPA, 2018]. As the market demands, these short chain PFAS continue to grow, particularly in the developing countries. The environmental releases and impacts are expected to rise [Li et al., 2020].

With respect to chemicals, PFBA, PFBS, PFPeA, PFHxA, and PFHpA are the most widely detected short chain PFAS of which PFBA and PFBS account for >50% of the total concentration of short-chain PFAS. The concentration of PFBA in the aquatic systems varied widely from 5.26–144ng/g (dry weight) in sediment/solid waste; and the concentration of PFBS in aquatic systems ranged from 0.01 to 4520 ng/L (0–114ng/g dry weight) in soil/sediment. In contrast, the concentration of other short chain PFAS was up to one order of magnitude lower than those of PFBA and PFBS. Moreover, PFBA and PFBS were also the most frequently detected short chain PFAS in the atmosphere and ice/snow in the polar area, while PFHxA and PFHpA were least detected [Cai et al., 2012].

1.4 Health/Regulatory Aspects of PFASs

Once PFAS released, they are not (or rarely) decomposed in either natural environments or treatment facilities due to the chemical inertness of the extraordinarily strong, highly polarized C−F bonds. This significantly contaminate surface and ground waters that serve as sources of municipal drinking water, and thus threaten the public health. Mounting evidence have revealed that exposure to PFAS could cause serious health problems. Reduced birth weight and elevated infertility were observed due to exposure to PFAS [Fei et al. 2007, 2009]. According to a 2012 story in Chemical and Engineering News (C&EN), the C8 science panel (an independent research team) reports a connection between exposure to PFOA and high cholesterol [Benford et al., 2008]. In addition, exposure to PFOA was associated with thyroid diseases [Melzer et al., 2010]. In 2015, Chemours (a spin-off from Dupont) was ordered by a Federal U.S. jury to pay an Ohio woman $1.6 million after she claimed that the PFOA, which was used to make Teflon, was responsible for her kidney cancer [Reisch, 2015]. Others reported that exposure to long chain PFAS (e.g., PFOA, PFOS, and PFHxS) resulted in onset of early menopause in women and increased impulsivity and delayed puberty in children. [knox et al., 2011; Gump et al. 2011.] PFASs have also been linked to pre-eclampsia [Stein et al., 2009], attention deficit and hyperactivity disorder in children aged 12-14 [Hoffman et al., 2010].

Previously, toxicological studies have been focused on PFOA and PFOS. Little is known about the toxicity of short-chain PFAS such as PFBA, PFBS, and PFHxA, though it is often assumed that short chain PFAS can cause similar or lesser effects than PFOA and PFOS. In laboratory animal studies, it was reported that exposure to high levels of PFBA (up to 100mg/kg) induced increased thyroid and liver weight and cellular changes in both organs, changes in thyroid hormones, decreased cholesterol, and delayed development and decreased red blood cells and

hemoglobin [Chang et al., 2008]. However, another study performed a 90-day toxicological evaluation of PFHxA in gavage tests with rats, and observed some adverse effects, including hepatic peroxisomal beta-oxidation, and hepatic and thyroid changes [Kjølholt et al., 2015]. Based on a study of human autopsy tissues, PFHxA was prevalent in the liver and brain. Others reported that exposure to PFBS resulted in lower body weight, delayed development and adverse female reproductive effects on offspring of mothers as well as changes in thyroid hormone levels and cellular changes in kidneys [Health Risk Assessment Unit, 2017].

It was reported that perfluoroalkyl compounds with shorter carbon chains are less toxic than PFOA. In humans, the half-life is 3– 4 years for PFOA, 32 days for PFHxA and 3 days for PFBA [Cecon et al., 2011]. Another study revealed that C4–C6 PFAS were less hazardous to daphnia than C7–C8 perfluoroalkyl substances [Barmentlo et al., 2015]. Overall, toxicity data on these short chain PFAS are still incomplete and insufficient to assess environmental impact. For the possible toxicity of treated water, the detailed data is also known to be small. The deep analysis of mineralization mechanism would contribute to study concerning the toxicity of treated water.

In 2005, an advisory board listed PFOA as a “likely human carcinogen” and during the same year, a draft risk assessment was set for the entire group of these chemicals [Hogue, 2005b; Eilperin, 2005]. In 2006, EPA asked eight chemical companies to voluntarily eliminate the production of PFAS at their facilities although it was unclear at the time how many of those companies intended to heed such request [Hogue, 2006]. In November 2006, DuPont agreed to reduce the screening threshold near its West Virginia plant 300-fold, from 150,000 parts-per-trillion to 500 parts-per-trillion.

In May of 2016, USEPA released lifetime health advisories for PFOA and PFOS; recommending that drinking water containing PFOA or PFOS individually or in combination at concentrations greater than 0.070 µg/L should undergo further testing and efforts to limit exposure of public to PFAS.

1.5 Current Treatment Methods

The current treatment methods of PFAS could be grouped into two categories: physical adsorption and redox reaction. (Figure 1.4)

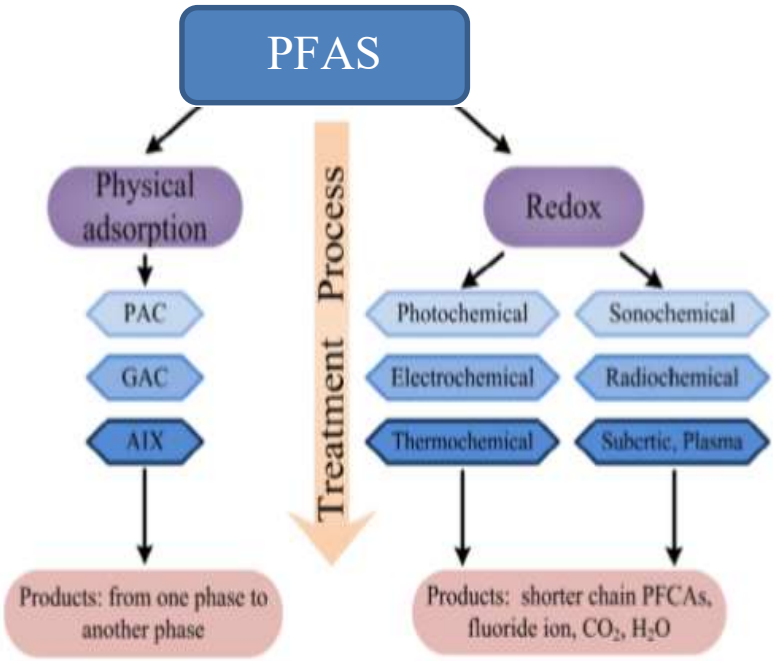

Figure 1.4. Summary of recent technologies for PFAS remediation

Over the course of the past decade, a lot of studies have been conducted and published on various techniques that have been developed for the treatment of PFAS in various matrices (Figure 1.5); however, many of such developed methods face varying degrees of challenges.

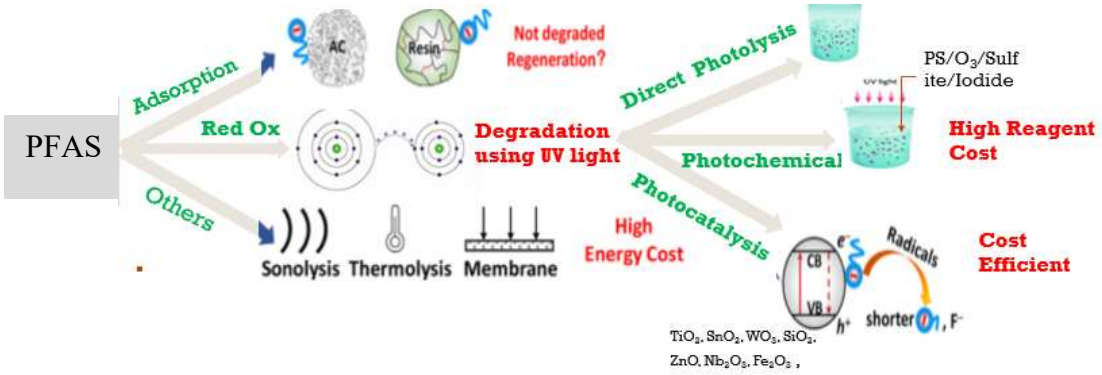

Figure 1.5. Schematic presentation of current treatment technologies

1.5.1 Physical Adsorption:

It involves the accumulation of a substance at the surface of another [Çeçen and Aktas, 2011]. In this case the target compound (adsorbate) adheres onto the surface of the adsorbent thus removing it from water. Physical adsorption on solid surfaces has been described in the hypotheses that: the adsorbate is not modified during adsorption. The adsorbate internal degrees of freedom are not excited during adsorption, and each adsorbed molecule fills one and only one adsorption site [Cerofolini et al., 1999].

Activated Carbon (AC), granular activated carbon (GAC) and powder activated carbon (PAC) have a long history in environmental applications because of their porous structure, large surface area, diverse surface chemistry [Rozwadowski et al., 1979; Qu et al., 2009]. Adsorption is an economical method to remove polar organic pollutants from water [Tzabar et al., 2012, Qin et al., 2014]. An investigation to remove PFOS and PFOA from water using PAC, GAC and anion-exchange resin (AIX400) showed that the GAC had the lowest sorption capacity for both PFOS and PFOA among the three adsorbents according to the Langmuir fitting. [Yu et al., 2009] Despite of high sorption capacity of AIX400, the high costs become the bottleneck in practical

applications. The presence of natural organic matter (NOM) affects the removal efficiency due to the competitive adsorption between NOM and PFAS. [Pramanik et al., 2015] Also, physical adsorption method merely transfers PFAS from water phase to another phase and cannot mineralize them. To avoid the secondary pollution, the subsequent destruction process such as incineration is necessary [Wang et al, 2017].

Another form of physical treatment for PFAS is membrane filtration. Two popular membrane filtration methods are nano-filtration (NF) with pore sizes of 0.00005-0.002 μm and reversed osmosis (RO) with pore sizes below 0.00005 μm [Knepper and Lange, 2011]. A study shows that RO is effective in removing PFOS from semiconductor wastewater [Tang et al., 2006] .The downside of the membrane filtration is that it cannot decompose PFAS. So, other steps such as incineration must be taken, which invariably leads to other concerns [Knepper et al. 2011].

1.5.2 Redox Technologies:

Redox technologies including photochemical, sonochemical, electrochemical, radiochemical, thermochemical, subcritical and plasma treatment processes are becoming promising methods for PFAS removal [Wang et al., 2015].

Sonochemical: Ultrasonic pressure wave force the quasi-adiabatic collapse of vapor bubbles formed from existing gas nuclei [Vecitis et al., 2008]. The transient collapse of aqueous cavitation bubbles raises average internal vapor temperature near 4000 K, whereas bubble-water interface temperature is in the range of 600 K to 1000 K. These transient high temperature lead to in situ pyrolytic reactions in the vapor and interfacial regions of each collapsing bubble, which breaks water producing hydroxyl radicals (HRs, $^{\bullet}OH$), oxygen atoms (O), and hydrogen atoms ($H^{\bullet}$). These transient radicals react readily with compounds at the bubble interface. Previous study

showed that acoustic cavitation driven by high-frequency ultrasound can significantly degrade aqueous solutions of PFOA and PFOS, and mineralize completely to CO, CO_2, F^-, and SO_4^{2-}. This occurs due to pyrolytic reactions at the surface of transiently collapsing bubbles. It was proposed that the degradation occurs at the bubble−water interface and involves the loss of the ionic functional group leading to the formation of the corresponding perfluoro olefin. The fluorochemical intermediates undergo a series of pyrolytic reactions in the bubble vapor leading to C1 fluoro-radicals. Secondary vapor-phase bimolecular reaction coupled with hydrolysis reaction and converts the C1 fluoro-radicals to carbon monoxide, carbon dioxide, and HF [Vecitis et al., 2008]. Although sonochemical technology is effective for PFAS remediation, applications are still limited largely due to high operating cost, the lack of understanding about their design, operational and performance characteristics. Uniform distribution of cavitational activity in reactor is another challenge in scale up design of sonochemical reactors [Seyedali et al., 2016].

Electrochemical process: Electrochemical oxidation is yet another method of destroying PFAS, which can either be destroyed by direct electron transfer from the anode (after being adsorbed) or in solution via strong oxidizing agents produced by electrolysis [Knepper and Lange, 2011; Merino et al., 2016]. The most used material here are boron doped diamond electrodes (BDDEs), and several researchers have successfully deployed them for the treatment of PFAS with varying degrees of success [Carter et al., 2008; Liao et al. 2009; Ochiet et al., 2011; Urtiaga et al. 2015].

Direct Photolysis: Direct Photolysis is the process of using light energy to break down molecules if the photon energy of the light source is greater than the bond energies present in the target compound [Merino et al., 2016]. Direct UV photolysis is another oxidation technique used for decomposing PFAS. However, the direct photolysis is ineffective for the degradation of PFAS

in aqueous solution, especially PFOS, under visible-light irradiation since PFAS does not absorb much light at wavelength >220nm [Hori et al., 2004; Taniyasu et al., 2012]. However, previous study showed that, PFOA can be broken down at short wavelengths (<200 nm) UV generated using a xenon mercury lamp. [Einaga et al., 2004]. Another study showed that defluorination profile of PFOA achieved with only 254 nm UV was very small compared to combined UV wavelengths of 254 nm and 185 nm [Giri et al., 2011]. Although the degradation efficiency of PFOA is improved with the irradiation of 185nm UV, the utilization of this is energy-intensive for wastewater treatment.

Photochemical process: These techniques can be classified into two main mechanisms, namely, photo-oxidation and photo-reduction degradation.

Photooxidation: The $^{\bullet}OH$ is the most used oxidant in water treatment industry. [Knepper et al., 2011] and this $^{\bullet}OH$ are often produced via advanced oxidation processes (AOPs). The most used AOP are the Fenton reaction, UV based processes, and ozone-hydrogen peroxide processes [Brillas et al., 1998; Rosenfeldt et al., 2004; Bautista et al., 2008; Knepper et al., 2011]. It was reported that PFOA was inert to $^{\bullet}OH$ (oxidantion potential 2.8 eV) since the energy of C-F bonds (530 kJ mol^{-1}) in PFOA was much higher than that of C-C bonds (410 kJ mol^{-1})[Pignatello et al., 2006; Vecitis et al., 2009].

Oxidative species e.g., carbonyl radicals ($CO_2^{\bullet-}$) [Thi et al., 2013], sulfate radicals (SRs, $SO_4^{\bullet-}$) [Chen et al., 2014],and Iodate radicals ($IO_3^{\bullet-}$) [Cao et al. 2010], or specific photocatalyst are effective in degrading PFAS. Sulfate radicals (SRs, $SO_4^{\bullet-}$) can be produced by UV irradiation/reduction mechanism or thermolysis (>40 ^{0}C) of persulfate anion (PS, $S_2O_8^{2-}$) or from the peroxymonosulfate ion (HSO_5^-) by transition metal [Vecitis et al., 2009; Knepper et al.; 2011].

PS photolysis is the most common photooxidative technologies used to remove PFAS in last 10-15 years [Hori et al., 2005; Liang et al., 2008; Vecitis et al., 2009; Lee et al., 2010; Nfodzo et al., 2011a; Nfodzo et al., 2011b]. Persulfate anion (PS, $S_2O_8^{2-}$) is an attractive candidate to photochemically decompose of PFCAs because photolysis of PS produces two SRs anions ($SO_4^{\bullet-}$) with quantum efficiency of unity, which can act as a strong oxidant in aqueous systems with oxidation potentials in the range of 2.5-3.1. SRs tend to react more selectively to transfer electron compared to HRs [Dogliotti et al., 1967, Bahnemann et al., 1994; Neta et. Al., 1988, Merino et al. 2016, Knepper et al., 2011]. SRs possesses stronger direct electron transfer ability than $^{\bullet}OH$. Relative high decomposition ratio of PFOA was achieved by SRs oxidation, and the decomposition rate would be higher when VUV irradiation replaced UVC irradiation in this process. Photolysis of PS (50 mM) produced highly oxidative SRs anions ($SO_4^{\bullet-}$), (Eq. 1.1), which efficiently decomposed PFOA and other PFAS bearing C4-C8 perfluoroalkyl groups (Eq 1.2). [Hori et al., 2005] Previous study reported that PFOS can also be decomposed significantly using PS activated by microwave heat and zerovalent iron particles [Lee et al., 2010]. Photoreduction and photooxidation study with six PFAS of various headgroup and perfluorocarbon tail length using KI and PS showed that PFAS kinetics is dependent on headgroup, chain length and initial PFAS concentration [Park et al., 2011].

$$S_2O_8^{2-} + h\nu\ (<270\ nm) \rightarrow 2SO_4^{\bullet-} \quad (1.1)$$

$$SO_4^{\bullet-} + PFOA \rightarrow SO_4^{2-} + C_7F_{15}COO^{\bullet} \quad (1.2)$$

$$PFOA + h\nu\ (<270\ nm) \rightarrow C_7F_{15}COO^{\bullet} \quad (1.3)$$

Previous study also proved photochemical decomposition of PFAS using sodium periodate ($NaIO_4$) [Cao et al., 2010]. It was showed that highly reactive species, such as iodate radicals

($IO_3^{\bullet}$), $^{\bullet}OH$, and $O^{\bullet-}$ generated by photolysis of IO_4^- [Wagner et al.,1982] have accelerated PFOA decomposition in UV/$NaIO_4$ system. $IO_3^{\bullet}$ radicals might directly abstract F^- from PFAS to form PFAS$^{\bullet}$ ($C_7F_{14}{}^{\bullet}COOH$), (Eq. 1.4) then reacted with $^{\bullet}OH$ to produce $C_6F_{13}COOH$ (Eq. 1.5), which underwent further photodecomposition and formed $C_5F_{11}COOH$. (Eq. 1.6)

$$C_7F_{15}COO^- + IO_3^{\bullet} \rightarrow PFOA^{\bullet+} + F^- \quad (1.4)$$

$$PFOA^{\bullet+} + {}^{\bullet}OH \rightarrow C_6F_{13}COOH \quad (1.5)$$

$$C_6F_{13}COOH \rightarrow C_6F_{13}COOH + F^- + H^+ \quad (1.6)$$

Carbonate radicals ($CO_3^{\bullet-}$) formed by reacting carbonate anions with $^{\bullet}OH$ under UV irradiation (Eq. 1.7)is effective in decomposing PFOA [Thi et al., 2013]. H_2O_2/$NaHCO_3$ solution can also produce $CO_3^{\bullet-}$ and directly oxidize the $C_7F_{15}COO^-$ to form $C_7F_{15}COO^{\bullet}$ radical as shown in Eq. 1.8 [Josh et al., 2006].

$$^{\bullet}OH + HCO_3^- \rightarrow H_2O + CO_3^{\bullet-} \quad (1.7)$$

$$CO_3^{\bullet-} + C_7F_{15}COO^- \rightarrow C_7F_{15}COO^{\bullet} + CO_3^{2-} \quad (1.8)$$

The common feature of PFAS photo-oxidative process is cleaving the C-C or C-S bonds between alkyl and functional groups in the beginning of the reaction [Yamase et al., 1983; Hori et al.; 2003, 2004]. Previous study proposed the common photo-oxidation pathways of PFOA as shown in Figure 1.6[Wang et al., 2017]. Possible pathway was concluded as follows: (i) an electron of the carboxylate terminal group was transferred to the oxidant, such as PS, phosphotungstic acid, Fe^{3+}/Fe^{2+}, forming perfluorinated alkyl radicals ($C_7F_{15}COO^{\bullet}$). (ii) Then the $C_7F_{15}COO^{\bullet}$ radical undergoes a Kolbe decarboxylation reaction that cleavage of C-C bonds between $C_7F_{15}{}^+$ and COO^- to produce the perfluoroalkyl radicals ($C_7F_{15}{}^{\bullet}$). (iii) The terminal carbon atom of $C_7F_{15}{}^{\bullet}$ radicals have higher electron density, and prone to react with H_2O molecule, $^{\bullet}OH$ and molecular oxygen,

yielding an unstable alcohol $C_7F_{15}OH$. (iv) The consequent $C_7F_{15}OH$ would eliminate HF to form $C_6F_{13}COF$. (v) The acid fluoride undergoes hydrolysis to generate PFHpA with one less CF_2 unit than the original PFOA. (vi)Then, step by step, PFHxA, PFPeA, PFBA, PFPrA, and TFA are produced.

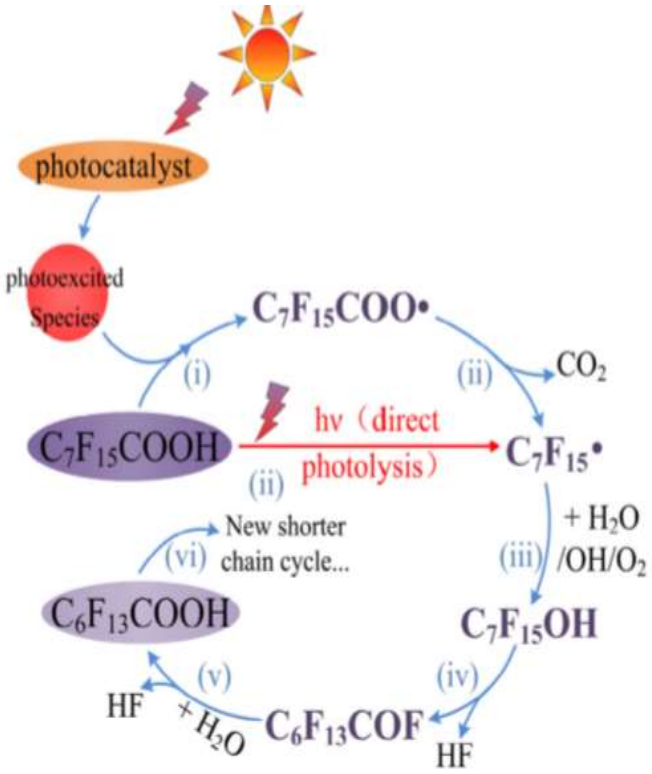

Figure 1.6. Common photo-oxidation pathways of PFOA

Two major oxidation reaction pathways of PFOS decomposition in water using alkaline 2-propanol was prosed previously [Yamamoto et al., 2007]. As shown in Figure 1.7, photo-oxidative process of degrading $C_8H_{17}SO_3^-$ by cleaving the C-S bonds and forming $C_8HF_{17}^{\bullet}$ radicals and $C_8F_{17}OH$, respectively, which resulted in shorter chain perfluoro compounds such as C_7HF_{15} and $C_7F_{15}OH$ by stepwise losing a CF_2 unit.

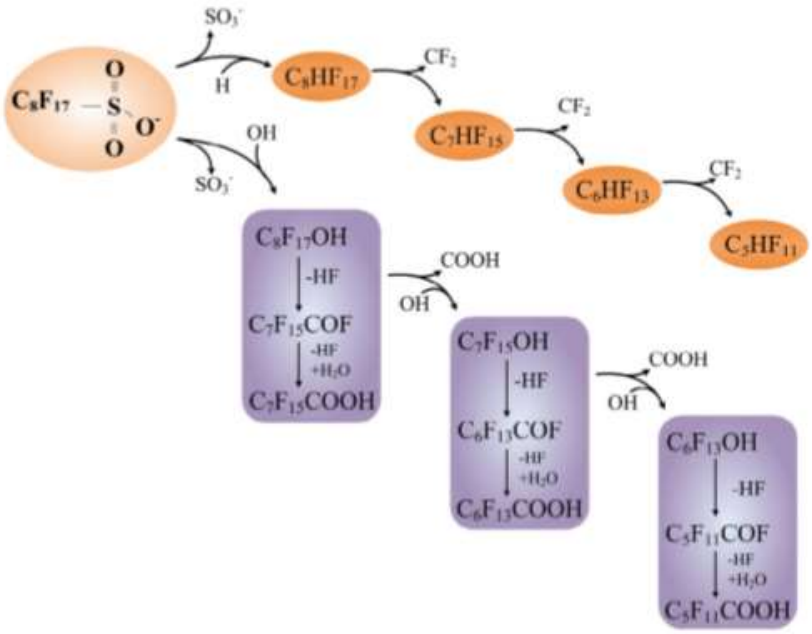

Figure 1.7. Photooxidation pathways of PFOS (Yamanto et al., 2007)

Photoreduction: Reductive dehalogenation is a method that has often been used to treat sites contaminated with halogenated pollutants [Knepper et al., 2011; Merino et al. 2016]. Such reductive transformations often occur via attack by highly reactive nucleophiles. Unlike photo-oxidation process, the C-F bonds are directly cleaved by hydrated electron (e_{aq}^-) as nucleophile in photo-reductive process. The e_{aq}^- is the key photo-generated reductive species responsible for PFAS photodegradation. These e_{aq}^- could be produced from the photolysis of KI solutions via charge-transfer-to-solvent (CTTS) states as shown in Eq. 1.9 [Park et al., 2009].

$$I^{\bullet-} + h\nu \rightarrow I^-_{CTTS} \rightarrow I^{\bullet} + e_{aq}^- \qquad (1.9)$$

Figure 1.8 depicts the possible photoreductive defluorination Pathways of PFOA. The fluorine atom is the reaction center of defluorination [Qu et al., 2010, 2014]. Due to the inductive effect of carboxylate terminal group of PFOA, the C-F bond close COOH is readily attacked by a nucleophile like e_{aq}^- and eliminates fluoride ion, to form successively $C_7F_{14}HCOOH$ and

$C_7F_{13}H_2COOH$. The $C_6F_{13}^{\bullet}$ radicals, $^{\bullet}COOH$ radicals and CH_2 carbene are generated from $C_7F_{13}H_2COOH$. The reaction between $C_6F_{13}^{\bullet}$ radicals and $^{\bullet}COOH$ radicals perhaps occurs to form shorter chain intermediate, $C_6F_{13}COOH$, which is further degraded in the same manner. Meanwhile, CH_2 carbenes, as the reactive species, are transformed into CH_3 radical and subsequently recombined with $^{\bullet}COOH$ radical to form CH_3COOH. Also, CF_3H and C_2F_6 are found among the final products, and the former is stable specie that has high global-warming potentials.

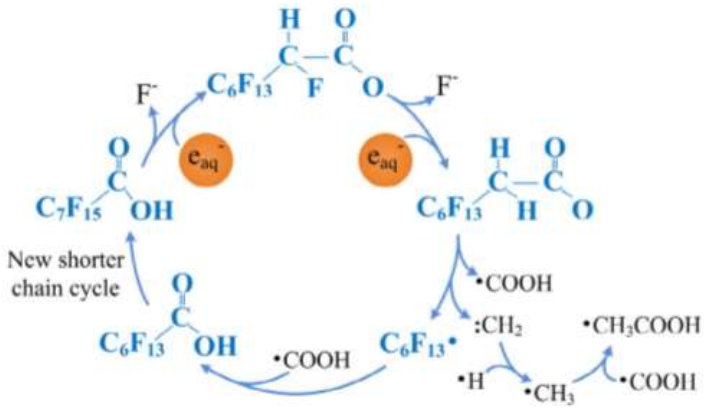

Figure 1.8. Possible photoreductive defluorination Pathways of PFOA

Another reaction of interest here is the UV-photolysis of isopropanol at high pH (> 12). This reaction results in the formation of a 2-hydroxyprop-2-yl radical, which can led to the decomposition of PFSAs [Knepper et al., 2011]. Also, titanium citrate can react with the cobalt in vitamin B_{12} to produce Co(I), which is a strong reducing agent [Ochoa-Herrera et al., 2008]. Another method of reductive degradation using UV/sulfite process (Eq. 1.10) under N_2 atmosphere [Song et al., 2013].

$$SO_3^{2-} + h\nu \rightarrow SO_3^{\bullet-} + e_{aq}^- \qquad (1.10)$$

Previously, a study investigated defluorination kinetics with PFAS headgroup by aquated electrons (e_{aq}^-) generated from the UV photolysis (λ = 254 nm) of iodide. It was proved that ionic headgroup ($-SO_3^-$ vs $-CO_2^-$) has a significant effect on the reduction kinetics, and extent of defluorination (F index = $-[F^-]$produced/[PFC]degraded). PFSAs reduction kinetics and F index increase linearly with increasing chain length. In contrast, PFCAs chain length appears to have a negligible effect on the observed kinetics and the F index [Park et al., 2011].

Compared with other redox technologies, photochemical degradation offers an easier operation under mild conditions, and achieves the higher decomposition and defluorination kinetics [Wang et al., 2017]. However, these technologies suffer from some disadvantages such as high consumption of chemical reagent, non-environmentally friendly process, high treatment cost or time-consuming [Dong et al., 2011 and Zhou et al., 2014]. Development of advanced water treatment technologies with low-cost and high efficiency to treat the PFAS contaminated wastewater is desirable.

Photocatalysis: Photocatalysis is a method of using light energy to power a reaction with the aid of a catalyst and has been used for the decomposition of many organic contaminants [Merino et al., 2016]. Photocatalytic decomposition happens when light exposure produces an energy difference between the valence band and the conduction band of the catalyst. Many semiconductors have been explored as photocatalysts for redox processes including CdS, SnO_2, WO_3, SiO_2, ZnO, Nb_2O_3, Fe_2O_3 , but nano TiO_2 photocatalyst is well known among the metal oxides for its high efficiency, low cost, physical and chemical stability, widespread availability, suitable band position, nontoxicity, biocompatibility, and noncorrosive property [Carp et al., 2004; Herrmann et al., 2007].

In general, TiO_2 naturally forms in four main phases: rutile, anatase, brookite, and TiO_2(B). The relative stability of the four titania phases depends on particle size, with rutile being the thermodynamically stable form in bulk titania but anatase being the most stable phase at sizes below 14 nm. Brookite and TiO_2(B) are metastable forms that are not commonly observed in minerals and difficult to synthesize in pure form. Anatase and rutile are the most common phases for TiO_2. Typically, the structural difference come from the connectivity of the TiO_6^{2-} octahedral units, which share edges and corners in different ways depending on the crystal phase. Anatase forms from octahedra share four edges, while two edges are shared in rutile; and three edges are shared in brookite as shown in Figure 1.9.

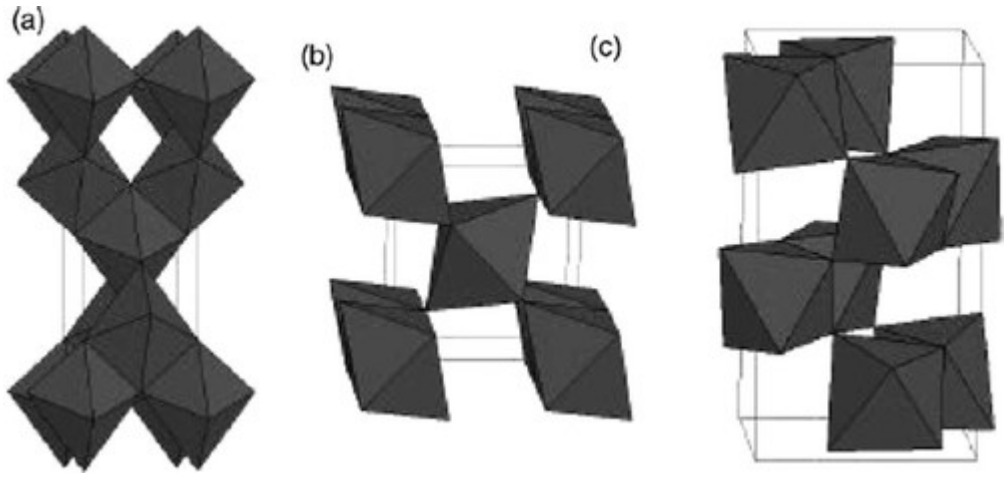

Figure 1.9. Connectivity of TiO_6^{2-} octahedral units in (a) anatase, (b) rutile, and (c) brookite.

Anatase is the widely studied polymorph, showing superior photochemical performances due to the high electron mobility, electron affinity, and transmittance for visible light [Lou et al., 2008; Chen et. al., 2013; Cargnello et al., 2014].

Properties also vary with the shapes of the nanomaterial change. The movement of electrons and holes in semiconductor nanomaterial is primarily governed by the well-known quantum confinement, and the transport properties related to photons, and the size and geometry of the materials [Xiaobo et al., 2007].

Commercially available Evonik (formerly Degussa) AEROXIDE® P-25 (denoted as P25), a benchmark material widely used for photocatalysis study. It is mixed-phaseTiO_2 containing anatase (majority) and rutile. Brookite has been rarely studied due to the challenges of obtaining in pure phase [Chen et al. 2007; Jiang et al. 2018].

Generally, there are five essential key steps in the heterogenous photocatalysis on the surface of TiO_2, namely, the (1) photoexcitation (light absorption and charge carriers generation), (2) diffusion, (3) trapping, (4) recombination, and (5) oxidation [Gaya et al., 2008; Chong et al., 2010; Foo et al., 2010].

Upon irradiation of TiO_2 with light energy equivalent to or greater than its band gap energy (anatase, ~3.2 eV), the electron is excited from the valence band (VB) to the conduction band (CB). The photoexcitation induces interband transition with the formation of conduction band electrons (e^-) and valence band holes (h^+). The e^-/h^+ pairs are photogenerated at a femtosecond time, however, the charge carriers can easily recombine either in the bulk or at the surface with the release of energy in form of light or heat. Free charge carriers that migrate to the semiconductor surfaces escaping recombination may be trapped before the interfacial charge transfer [Hoffmann et al. 1995; Kohtani et al, 2017]. It was reported that these surface-trapped electrons and holes recombine much more slowly than they do in the bulk [Furube et al., 2001]. The process is listed as follows: [Choi et. al., 2014]

1. Charge carrier generation

$$TiO_2 + h\nu \rightarrow TiO_2 (e_{CB}^- + h_{VB}^+) \quad (1.11)$$

2. Charge carrier trappings

$$e_{CB}^- + > Ti^{IV} OH \rightarrow \{> Ti^{III}OH\} \text{ (shallow trapping)} \quad (1.12)$$

$$e_{CB}^- + > Ti^{IV} \rightarrow > Ti^{III} \text{ (deep trapping)} \quad (1.13)$$

$$h_{VB}^+ + > Ti^{IV} OH \rightarrow \{> Ti^{III}OH^{\bullet}\} (h_{tr}^+) \quad (1.14)$$

3. Charge carrier recombination

$$e_{CB}^- + \{Ti^{III}OH^{\bullet}\} \rightarrow Ti^{IV} OH \quad (1.15)$$

$$h_{tr}^+ + \{Ti^{III}OH\} \rightarrow Ti^{IV} OH \quad (1.16)$$

$$h_{tr}^+ + Ti^{III} \rightarrow Ti^{IV} \quad (1.17)$$

4. Interfacial charge transfer to the surface adsorbed acceptor (A) or donor (D) molecules:

$$Ti^{III}OH + A \rightarrow \{> Ti^{IV} OH\} + A^{\bullet -} \quad (1.18)$$

$$\{Ti^{IV} OH^{\bullet}\}^+ + D \rightarrow \{> Ti^{IV} OH\} + D^{\bullet +} \quad (1.19)$$

Another study also highlighted the important consequences of surface trapped holes (h_{tr}) and electrons (e_{tr}) to the photooxidation of organic compounds. [Schneider et al., 2014] In the absence of electron scavengers, the photoexcited electron recombines with the valence band hole in nanoseconds with simultaneous dissipation of heat energy. However, the presence of electron scavengers is vital for prolonging the recombination and successful functioning of photocatalysis. In most applications, photocatalytic degradation reactions are carried out in presence of water, air, the target contaminant and the photocatalyst. Generally, the positive hole reacts with the surface OH^- groups on the TiO_2 particle to produce surface adsorbed hydroxyl radicals ($^{\bullet}OH_{ads}$). Other hand, oxygen prevents the recombination of electron hole pair, while allowing the formation of superoxide radicals anion ($O_2^{\bullet -}$). This $O_2^{\bullet -}$ radical can be further protonated to form the

hydroperoxyl radicals ($HO_2^{\bullet}$) and subsequently H_2O_2. (Eq. 1.20) The $HO_2^{\bullet}$ radical formed was also reported to have scavenging property and thus, the coexistence of these radical species can doubly prolong the recombination time of the h_{tr} in the entire photocatalysis reaction. Photogenerated holes and the formed reactive oxygen species (e.g., $HO_2^{\bullet}$) can participate in the degradation of organic pollutants [Fujishima et al., 2000; Zhao et al., 2003; Banerjee et al., 2014] (Eq. 1.20-1.23). Since the heterogenous photocatalysis reaction mostly occurs on the photon activated surface of TiO_2

$$(O_2)_{aq} + e_{CB}^- \rightarrow O_2^{\bullet-} + H^+ \rightarrow HO_2^{\bullet} + e_{CB}^- + H^+ \rightarrow H_2O_2 \quad (1.20)$$

$$Ti^{3+} + H_2O_2 \rightarrow Ti^{4+} + HO^{\bullet} + HO^- \quad (1.21)$$

$$H_2O_2 + O_2^{\bullet-} \rightarrow O_2 + HO^{\bullet} + HO^- \quad (1.22)$$

$$H_2O_2 + h\nu \rightarrow 2HO^{\bullet} \quad (1.23)$$

$$O_s^- + H_{aq}^+ + h_{VB}^+ \rightarrow 2HO_s^{\bullet} \quad (1.24)$$

The effect of excess oxygen in the reaction environment was investigated in a study, and suggested degradation by PFOA oxidation mechanism which is β-scissions routes mediated by COF_2 elimination [Sansotera et al., 2015]. The heterogeneous photocatalytic decomposition of PFOA by TiO_2 under UVC in presence of oxalic acid as a hole-scavenger showed accelerated PFOA decomposition under nitrogen atmosphere [Wang et al., 2017]. Figure 1.10 shows the proposed decomposition mechanism of PFOA by TiO_2 under UV (a) without oxalic acid and (b) with oxalic acid The electron paramagnetic resonance (EPR) measurements confirmed the existence of carbonyl radicals ($CO_2^{\bullet-}$) in the photocatalytic process, which was a result of the reaction between oxalic acid and photogenerated hole. These findings indicated that PFOA decomposition was primarily induced by $CO_2^{\bullet-}$ radicals.

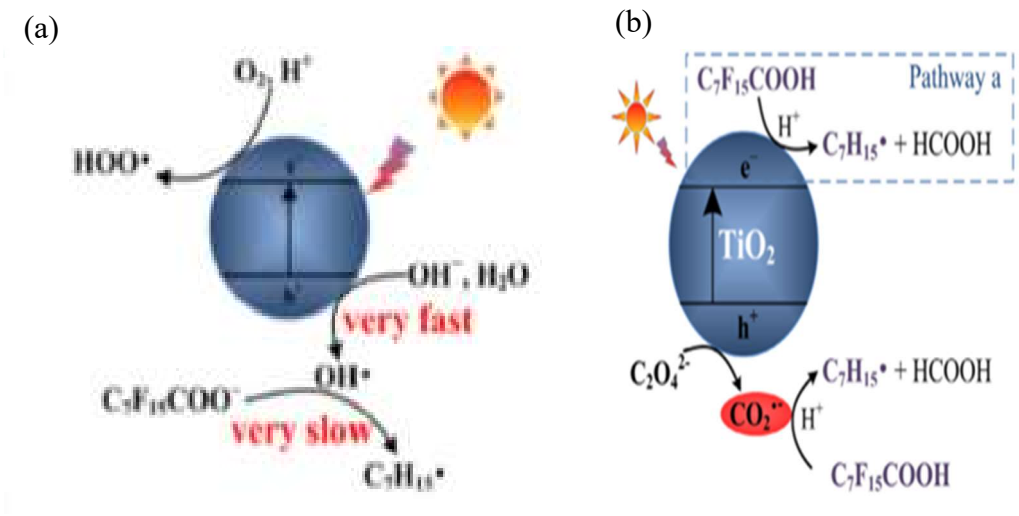

Figure 1.10. Proposed decomposition mechanism of PFOA by TiO_2 under UV (a) without oxalic acid and (b) with oxalic acid (Wang et al., 2017)

TiO_2 has a wide range of application in photocatalytic field. Studies in wastewater treatment by TiO_2 are still in the stage of laboratory experiments because of some technical barriers: 1) wide band gap (anatase, ~3.2 eV), which requires UV irradiation for photocatalytic activation [Yin et al., 2003; Zaleska, 2008; Chong et al., 2010], 2) low adsorption capacity to hydrophobic contaminants, 3) high aggregation tendency, and 4) difficulty of separation and recovery [Bhattacharyya et al., 2004; Gao et al., 2011; Cui et al., 2013]

Generally, the photogenerated holes of TiO_2 react with the OH^- groups to yield surface adsorbed $^{\bullet}OH$. Because PFAS is inert to $^{\bullet}OH$, pure TiO_2 appears to be the less effective in PFAS degradation [Fujishima et al., 2000 and Dong et al. 2015]. Fluoride anions generated from the PFAS degradation may modify TiO_2 surface, limiting the performances of TiO_2 for degradation [Sansotera et al. 2014, Gatto et al. 2015].

To achieve better photoactivity of TiO_2 under visible light, improvement of photocatalyst by optimizing catalyst synthesis such as a defined crystal structure, smaller particle sizes, and high affinity to various organic pollutants, is important [Lightcap et al., 2010; Makarova et al., 2000]. Mass transfer limitation must be minimized as photocatalytic degradation mainly occurs on the surface of TiO_2. If there is poor affinity towards organic pollutants (especially the hydrophobic organic pollutants), it resulted islow photocatalytic degradation rates. Many studies have been carried out to eliminate the limitations of TiO_2 photocatalysis of PFAS. Metal doped TiO_2 can be explained by a new energy level produced in TiO_2 by the dispersion of metal nanoparticles in the matrix [Dong et al., 2015]. Figure 1.11 shows mechanisms of metal doped TiO_2 photocatalysis, where Electrons can be excited from the defect state to the TiO_2 conduction band by photons with at lower energy than without doped metal. An additional benefit of transition metal doping is the improved trapping of electrons to inhibit electron hole recombination during irradiation. Decrease of charge carriers recombination results in enhanced photoactivity. Here, the metal nanoparticles act as a mediator in storing and shuttling photogenerated electrons from the TiO_2 surface to an acceptor. Increasing photocatalytical activity was reported with iron and niobium co doped TiO_2 prepared in sol-gel process, because of co-doping both on the physico-chemical properties and surface interfacial charge transfer mechanisms [Estrelan et al., 2010]. A study showed that the rate constant values of PFOA decomposition for the TiO_2/UV, TiO_2-Fe/UV, and TiO_2-Cu/UV systems were 0.0001, 0.0015, and 0.0031 min^{-1}, respectively [Meng et al. 2012]. Photodegradation of PFOA by Pb modified TiO_2 catalyst (TiO_2-Pb/UV) is faster than that of TiO_2/UV system and gives better performance than TiO_2-Cu/UV and TiO_2-Fe/UV [Chen et al., 2016]. Decomposition of perfluorooctanoic acid (PFOA) in aqueous solution by using noble metallic nanoparticles modified TiO_2 (TiO_2-M, M = Pt, Pd, Ag) was investigated [Li et al., 2015].

The pseudo-first-order rate constant for Pt, Pd, Ag modified TiO_2 were 12.5, 7.5 and 2.2 times higher than that for TiO_2 respectively. Increasing photocatalytic activity was reported with iron and niobium co doped TiO_2 because of co-doping improves both physico-chemical properties and surface interfacial charge transfer mechanism [Estrelan et al., 2010].

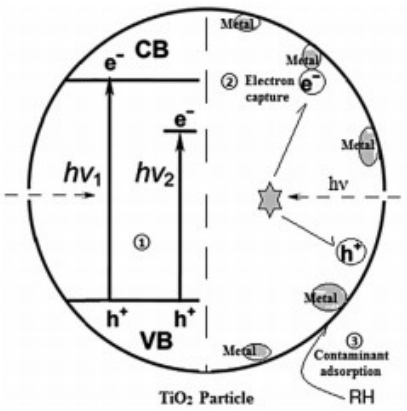

Figure 1.11. Mechanisms of metal-doped TiO_2 photocatalysis: (1)narrowing band gap (hv1: pure TiO_2; hv2: metal-doped TiO_2); (2) retarding electron hole recombination; and (3)enhancing adsorption of contaminants (RH).

A study showed a great improvement of photocatalytic decomposition of PFOA using a composite TiO_2/rGO (95:5) catalyst compared to the TiO_2 photocatalysis. [Beatriz et al., 2018] The photocatalytic enhancement of TiO_2/rGO composites can be attributed to three aspects. First, many π–π conjugated double bonds are present on the graphene surface, so the organic molecules in the solution can be well enriched into graphene [Yu et al., 2019]. Therefore, the HRs and photogenerated holes generated by TiO_2 on graphene surface have a good degradation effect on organic matter. Second, the photogenerated electrons and holes generated by TiO_2 can be effectively separated, thereby suppressing carrier recombination. Third, introduction of rGO on TiO_2 increase UV adsorption of the catalyst .

1.6 Goal and Objective

As the occurrence of short chain PFAS continues to rise in the environment, there is an urgent need to develop an effective and cost-efficient treatment technology in ambient condition. The primary goal of this work is to develop powerful destructive TiO_2 photocatalytic and photochemical treatment approaches toward PFAS in water avoiding future environmental liability issues to protect public health and ecosystem and elucidate the complex reaction mechanisms.

Objective 1

TiO_2 based photocatalytical process is considered as the most promising approach because of its outstanding physicochemical properties, low cost, suitable band position, nontoxicity, and biocompatibility. Previously, only long chain PFCAs were center of research. It is completely unknown how this photocatalytic technology works for other PFAS such as PFSAs and short chain PFCAs. Short chain PFAS are more hydrophilic and water soluble than long chain one. This may cause poor adsorptivity of short chain PFAS on TiO_2. As decomposition efficiency is function of PFAS adsorption, it can be hypothesized that short chain PFAS degrade at a lower rate compared to the long chain one. So, first objective is to identify if there is any correlation of carbon chain length or functional group or structure to PFAS decomposition in TiO_2 photocatalysis method. As overall photocatalytic efficiency is determined by the adsorption of PFAS on TiO_2/H_2O interface, photogenerated charge carrier dynamics and applied photon energy; it is important to known about the adsorption pattern and reaction mechanism of PFAS. To understand the underlying mechanism and efficient photocatalysis process design, it is important to determine the effect of pH and electron/ hole scavenger on photocatalytic reaction kinetics. Nine PFAS are selected in this study. Tasks of this study are listed below:

Task 1: Determine and compare PFAS adsorptivity on TiO_2 surface

Task 2: Determine direct photolytical decomposition and defluorination of PFAS.

Task 3: Determine photocatalytic removal and defluorination of PFAS. Evaluate the effect of carbon number and functional group on adsorption rate.

Task 4: Compare adsorptive, photolytic, and photocatalytic removal of PFAS and identify removal mechanism. Determine contribution of TiO_2 in photocatalytical removal process.

Task 5: Determine reaction intermediate short chain products and their production/decomposition pattern to predict possible reaction pathways.

Task 6: Investigate TiO_2/water interface chemistry and control the homogeneous and heterogeneous reactions at the TiO_2 surface using scavenger.

Task 7: Evaluate the effects of various operating parameters e.g., solution pH etc.

Table 1.2. PFASs tested in this study

PFAS #	Functional group	Name of PFASs	Structure	C# *
P1	Carboxylic acid (CA)	Perfluorobutanoic acid (PFBA)	$CF_3(CF_2)_2COOH$	C3
P2		Perfluoroheptanoic acid (PFHpA)	$CF_3(CF_2)_5COOH$	C6
P3		Perfluorooctanoic acid (PFOA)	$CF_3(CF_2)_6COOH$	C7
P4		Perfluorononanoic acid (PFNA)	$CF_3(CF_2)_7COOH$	C8
P5	Sulfonic acid (SA)	Perfluorobutane sulfonic acid (PFBS)	$CF_3(CF_2)_3SO_3H$	C4
P6		Perfluorohexane sulfonic acid (PFHxS)	$CF_3(CF_2)_5SO_3H$	C6
P7		Perfluorooctane sulfonic acid (PFOS)	$CF_3(CF_2)_7SO_3H$	C8
P8		6:2 Fluorotelomer sulfonic acid (6:2 FTS)	$CF_3\ (CF_2)_5\ (CH_2)_2SO_3H$	C8
P9	Ether	Hexafluoropropylene oxide dimer (GenX)	$CF_3CF_2CF_2OCFCF_3COOHNH_3$	C5

Table 1.3. Utilization of short-chain PFAS as alternatives to long-chain PFASs

Name	Long-Chain Benchmark and Usage
PFBA	Replacing PFOA and 6:2 fluorotelomer-based polymers used in fluorinated finish and impregnation, and oil, water, and dirt repellents.
PFBS	Replacing PFOS in strain repellent.
PFHpA	Selected for comparison purpose. Also, replacing 6:2 fluorotelomer-based polymers used in fluorinated finish and impregnation, and oil, water, and dirt repellents.
PFHxS	Replacing PFOS in AFFFs.
PFNA	Selected for comparison purpose with PFOS for same C#
GenX	Replacing PFOA

As calculated C-C and C-F bond dissociation energy (BDE) of long chain PFAS, PFCAs and polyfluorinated PFAS are lower than their counter part, decomposition trends can be hypothesized as Table 1.4.

Table 1.4. Comparison matrix among PFASs and expecting decomposition trends

Matrix #	Variables (fixed ones)	Targets	C#	Decomposition kinetics (expecting trends)
M1	Alkyl chain length (carboxylic acid; perfluoro)	P1, P2, P3, P4	C3, C6, C7, C8	P4>P3>P2>P1 (Longer, easier to decompose)
M2	Alkyl chain length (sulfonic acid; perfluoro)	P5, P6, P7	C4, C6, C8	P7>P6>P5 (Longer, easier to decompose)
M3	Functional group (C6; perfluoro)	P2, P6	C6,	P2>P6 (CA≥SA);
M5	Functional group (C8; perfluoro)	P4, P7	C8	P4>P7 (CA≥SA);
M6	GenX vs PFOA	P3, P9	C5 and C7	Unknown
M7	Per vs poly (PFOS vs 6:2 FTS)	P7, P8	C8	P8>P7

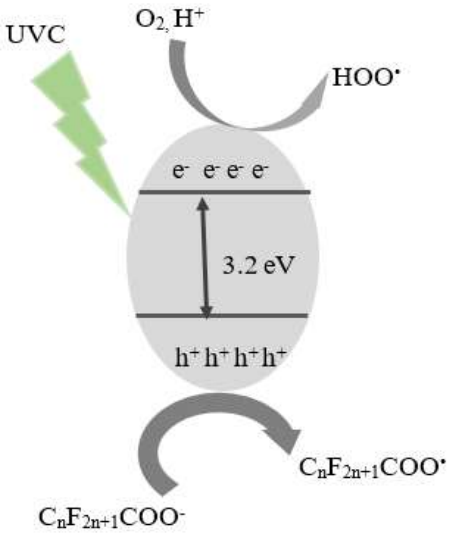

Figure 1.12. PFAS removal by TiO_2 under UVC

Objective 2

Based on previous research, TiO_2 photocatalysis process suffers from technical barriers that impede its commercialization, i.e., photogenerated hydroxyl radicals are inert to cleave C-F bond, high electron hole recombination, and low adsorption capacity etc. resulting poor degradation kinetics. To improve TiO_2 photocatalysis process, an integrated system is accessed in this work which were never studied before for PFAS remediation from aqueous media. The potential of enhancing photodegradation kinetics of PFCAs and PFSAs by coupling oxidant/reductant with TiO_2/UV system is studied expecting synergistic effect, and then determine contribution of TiO_2 and oxidant/reductant in overall degradation rate due to the presence of various reactive species such as SRs other than just HRs. The complex reaction mechanism was elucidated.

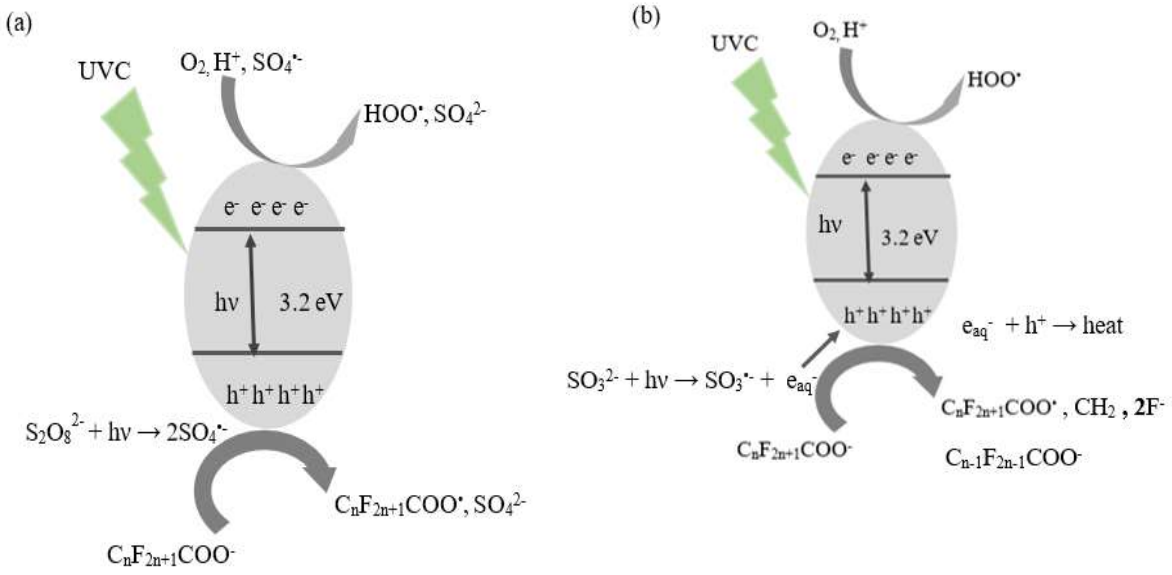

Figure 1.13. Possible PFAS removal by (a) TiO_2/UVC/PS and (b) TiO_2/UVC/sulfite

Objective 3

Metal doping into TiO_2 could enhance the photoactivity by decreasing band gap energies and increasing oxygen vacancies into catalyst. Meanwhile, rGO modified TiO_2 catalyst can offer enhanced photocatalytic activity due high UV absorption capacity, excellent thermal and electrical conductivity. The delocalized conjugated π structures in rGO allow charge carriers to achieve high mobility and relatively slow down charge recombination. In order to overcome limitation of TiO_2 and enhance photocatalytic activity to decompose PFAS, we proposed TiO_2-Pb/rGO ternary system to leverage the advantages of doping metal and introducing rGO to TiO_2. Previous study reported decomposition efficiency of PFAS as TiO_2-Pb> TiO_2-Cu > TiO_2-Fe > pristine TiO_2 , therefore, Pb is selected as doping metal. It is hypothesized that an appreciable improvement of photocatalytic reactivity of TiO_2-Pb/rGO with various PFAS is possible in comparison to TiO_2, TiO_2-Pb, TiO_2/rGO, and TiO_2-Fe/rGO. As, physical adsorption and chemical reaction could be

achieved in a single process, an effort is given to identify if incorporation of Pb and rGO enhance PFAS adsorptivity to offer adsorption mediated chemical decomposition.

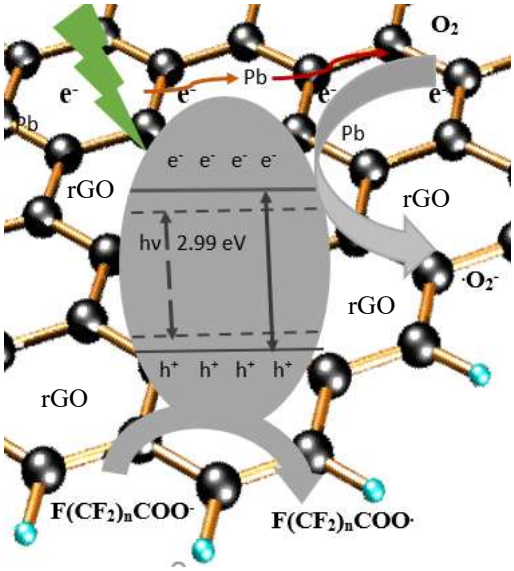

Figure 1.14. Possible PFAS removal by TiO_2-Pb/rGO under UVC

CHAPTER 2

Analytical Methodology

2.1 Sample Cleanup (Solid Phase Extraction) for LC-MS Analysis

For LC-MS analysis, samples are diluted 10 times prior to solids phase extraction. In addition, PFAS standard solution of 0.2 to 2.5µM are prepared for external calibration. Potential interferences from the collected samples were removed by solid phase extraction techniques. First, the vacuum manifold was loaded with Agilent LMS Bond-Elut cartridges (25mg, 1ml). The cartridges were conditioned by eluting 1 mL of methanol and then rinsed/equilibrated with 1 mL Milli-Q water with care taken not to allow the cartridges to dry up (and lose efficiency). Next, 1 mL of the dilued sample (previously collected from the reactor) was injected onto the cartridge and passed through at a flow rate of about 1 mL/min. This relatively slow flow rate was necessary to ensure that the target compound was completely adsorbed onto the cartridge. After loading the sample, the cartridge is rinsed (to remove any impurities that could interfere with analysis) with 1 mL water and then finally, PFAS is eluted from the sample matrix using 1 mL of methanol at a rate of 1 ml/min. This helps to concentrate the samples and make them easier to analyze.

Figure 2.1. Solid Phase Extraction Apparatus

2.2 Analytical Techniques

2.2.1 HPLC techniques:

An Agilent 1200 series High Performance Liquid Chromatography (HPLC) system consisting of quaternary pump, vacuum degasser, autosampler and suppressed conductivity detector was employed to monitor PFASs concentration reduction with time in water. Typically, the system involves an HPLC unit and a conductivity detector (CDD-10AVP) from Shimadzu Scientific manufacturer as Agilent 1200 series was only supported by UV detector. So, the signal from this CDD-10AVP was transmitted to Agilent's ChemStation Software using an Agilent 35900E A/D interface (Agilent Technologies). Chromatographic separation was carried out using Agilent C18 column with a particle size of 3 μm, diameter of 4.6 mm and length of 450 mm maintaining room temperature.

Figure 2.2. HPLC equipped with conductivity detector and quaternary pump.

Mobile phase use in this method is milli-Q water (A), HPLC grade Acetonitrile (B) and a solution of 9 mM NaOH and 100 mM H_3BO_3 (Boric Acid) (D). Injection volume used in this method was 100µl. The background conductivity of the bromate buffer was diminished using a Thermo Scientific AMMS-300 Anion Micromembrane suppressor (DIONEX/Thermo Fisher). The suppressor was regenerated by running 10 mN sulfuric through its membranes using nitrogen pressure.

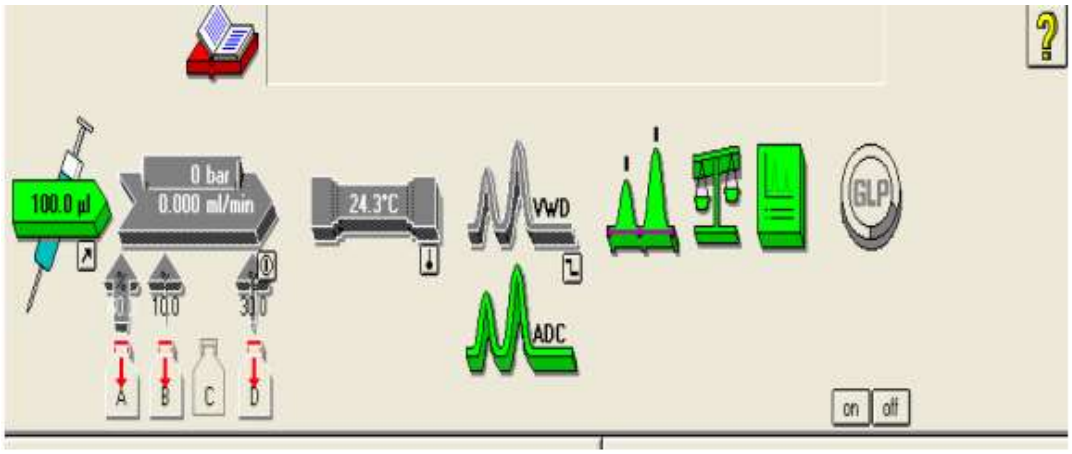

Figure 2.3. Flow diagram of the HPLC process from the ChemStation software

2.2.2 LC-MS analysis

Concentration of PFAS and possible aqueous phase reaction intermediate decomposition products were analyzed using a Shimadzu Nexera X2 LC (Nakagyo-ku, Kyoto, Japan) coupled with a Shimadzu 8040 triple quadrupole MS. MS detection is operated in the negative electrospray ionization (ESI) mode. Mobile phase was a mixture of LC/MS grade ACN with 0.1% formic acid and LC/MS grade water with 0.1% formic acid at a flow rate of 0.3 mL/min. Binary gradient was used where ACN contribution was increased from 30% to 90% over 6 min, held at 90% for 3 min, and ramped down back to 30% over 3 min. Separation was carried out using an Agilent Zorbax Eclipse C18 (50 mm x 3 mm x 1.8 µm particle size) column at 30^0C. Sample injection volume was 10 µL. Multiple reaction monitoring mode (MRM) was used to identify and quantify PFAS and targeted byproducts formed during the reaction. The sample was electro sprayed at a flowrate of 0.20 ml/min for mass spectrometric analysis. The electrospray potential was -4.5 kV and cone voltage were set at 20V. The heated capillary temperature used are set at 150^0C. Nitrogen is used as a collision gas (0.34 MPa). The full scan (m/z =50-500) mass spectra were obtained.

Figure 2.4. LC-MS/MS instrumentation

For quantification of the target analyte such as PFOS and PFOA and expected byproducts such as short-chain PFAS, multiple reaction monitoring (MRM) scans were conducted in a negative electrospray ionization mode. Confirmation of expected reaction intermediates was undertaken using targeted analysis. Monitored ion transitions of PFOSand other selected PFAS were conducted as shown in Table 2.1 [Bruton and Sedlak, 2017]

Table 2.1: Monitored transitions of selected PFAS in LC/MS equipment

Compound	**PrecursorIon**	**Quantifier ProductIon**	**ProductIon Qualifier**
PFOA	413	369	169
PFOS	499	80	99
PFHpA	363	319	169
PFNA	463	419	219
[^{13}C8] PFOA	421	376	N/A
[^{13}C8] PFOS	507	99	N/A
[^{13}C4] PFHpA	367	322	N/A
[^{13}C9] PFNA	472	427	N/A
[^{13}C4] PFBA	217	172	N/A
[^{13}C5] PFPeA	268	223	N/A
[^{13}C5] PFHxA	318	273	N/A

2.2.3 Fluoride Intellical F121 electrode probe

Aqueous fluoride ions (F^-) were measured by an Intellical ISE F121 electrode mounted to a Hach HQ 440D base (Loveland, CO) as shown in Fig. 14. The Fluoride Electrode is an ion-selective Sensor based on the potentiometric measuring principle, determines, and monitors the concentration of the anion Fluoride. Ion-selective electrodes (ISE) consist of an ion-specific half-cell and a reference half-cell. The ion-specific cell gives a potential against the reference cell depending on the specific ion concentration. When the specific ion concentration (the sample or an ion standard) changes, the potential changes as well. The relationship between the potential measured with the ISE and the ion concentration in the measured solution is expressed using the Nernst equation. Samples of 0.5 mL were diluted with 0.5 mL ISA stock solution (one pillow per 5 mL) prior to analysis.

Figure 2-5: Fluoride Intellical F121 electrode probe coupled to a Hach HQ 440D base.

Fluoride electrode was calibrated using six different standards and calibration plot is shown below:

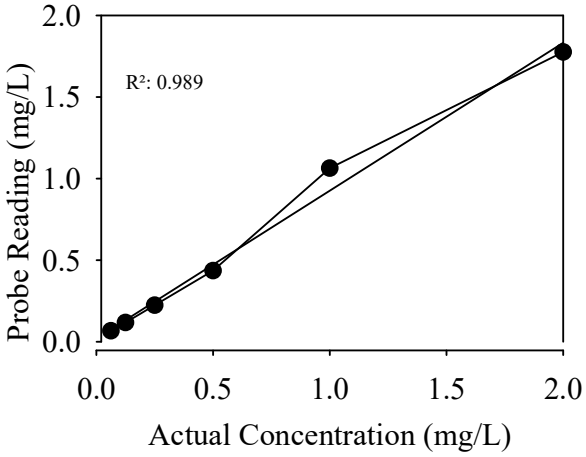

Figure 2-6. Fluoride measurement comparison between standard concentration and measured concentration

2.2.4 Total organic carbon measurements

The total organic carbon was analyzed using a Shimadzu TOC-Vcsh shown in Figure 2.7 in combination with a Shimadzu autosampler and nitrogen analyzer. Due to the high volume of samples required for the analysis, sacrificial batch reactors were kept for the various time intervals. Samples were placed in 20 mL autosampler vials. Samples from the reactor were collected and vacuum filtered through a 0.45 μm Whatman filter. All blanks, standards and unknown samples were acidified with HCl before analysis. Total organic carbon itself was indirectly measured using the TC - TIC method. In other words, total carbon (TC) and inorganic carbon (TIC) for each were measured individually and then the difference represents the TOC given that TOC + TIC = TC. Samples were analyzed by acidifying the samples and then measuring the resultant carbon dioxide using the instrument's in-built nondispersive infrared (NDIR) detector. TC was calibrated using potassium hydrogen phthalate standards ranging from 0.3 mg/L – 10 mg/L and then was measured by thermal oxidation (at 680^0C)

followed by determination of the resultant carbon dioxide by NDIR. Instrument was operated in the total carbon mode due to the absence of any inorganic carbon in the samples.

Figure 2.7. Total organic carbon instrument

2.3 Physical characterization of the catalysts

2.3.1 UV Spectrophotometer

Light adsorption of the catalysts was determined using UV-vis spectrophotometer (Shimadzu UV-2550). Scanning wavelength range was 300 nm to 800 nm, and scanning rate was set at 120 nm/min.

Figure 2-8: Shimadzu 2550 UV-visible spectrophotometer.

2.3.2 X-ray Diffractometer

Phase identification of the commercial TiO_2 crystal structure was also carried out using Bruker D8 X-Ray Diffraction equipped with a monochromator which produced CuKα radiation at wavelength 1.5 A^0. The voltage was set at 40 KV and scanning rate was 2^0/min. The scanning range was from 10 to 80^0. The sample was spread on a glass slide specimen holder, then placed at the center of the instrument and illuminated by the beam of the Xray. The X-ray tube and the detector move in a synchronized motion and the signal coming from the sample was recorded in the graph. The peaks observed was related to the atomic structure of the sample.

Figure 2.9. X-ray diffractometer

2.3.3 Scanning electron microscopic (SEM)

Scanning Electron Microscope (SEM) model Hitachi S-3000N (Hitachi, Tokyo), was used in combination with an energy dispersive X-ray spectroscopy (EDX) to determine elemental composition of TiO_2-Pb/rGO.

Figure 2.10. Scanning Electron Microscope with EDX

2.3.4 Horiba SZ-100

The size of TiO_2 and TiO_2-Pb/rGO particles in water were measured using a Horiba SZ-100 instrument (Figure 16) using dynamic light scattering (DLS) for particle size and Zeta potential analysis. DLS is commonly used and has proven to be very effective for measuring the size of particles, when they are dispersed in suspension. [Wu and Choi, 2016]. The method used in this study for the particle size analysis was adapted from the one developed by Wu and Choi [Wu and Choi, 2016] Based on light scattering of the particles, their hydrodynamic diameter is calculated by using the Stoke-Einstein equation. Particle size was measured at the 173° detection angle for 2 minutes. Particles were dispersed using a sonicator (Misonix S-4000) for 30 min prior to analysis.

Figure 2.11. Particle size analyzer Horiba SZ100

2.4 Calculations

The TOC removal efficiency was calculated Eq. (2.6) as follows:

$$\text{TOC removal (\%)} = C_t/C_0 \times 100 \quad (2.6)$$

Where C_0 is the TOC before the reaction and C_t is the TOC of the solution at any given time t (minutes).

The defluorination efficiency for each sample was calculated based on the following equation.

$$\text{Defluorination (\%)} = CF^- /(0.688 \times C_0) \quad (2.7)$$

C_0 was the initial concentration of PFOA; and CF^- was the concentration of the F^- at any given time. 0.668 represents the ratio between the molecular weight of all fluorine atoms in PFOA (15 × 19 g/mol = 285 g/mol) and the total molecular weight of PFO

2.5 References

[1] Administrative Record, 1–11.3M, Letter to US EPA, (2000) Re: Phase-out Plan for POSF-based Products (226-0600), US EPA

[2] Arvaniti, O., Hwang, Y., Andersen, H., Stasinakis, A., Thomaidis, N., Aloupi, M. (2015). Reductive Degradation of Perfluorinated Compounds in Water using mg-Aminoclay Coated Nanoscale Zero Valent Iron. Chemical Engineering Journal, 262, 133-139.

[3] Bao, Y., Niu, J., Xu, Z., Gao, D., Shi,J., Sun, X., Huang, Q. (2014). Removal of Perfluorooctane Sulfonate (PFOS) and Perfluorooctanoate (PFOA) from Water by Coagulation: Mechanisms and Influencing Factors. Journal of Colloid and Interface Science, 434, 59-64.

[4] Banerjee, S., Dionysiou, D, Pillai, S., (2015). Self-cleaning applications of TiO_2 by photo-induced hydrophilicity and photocatalysis, Applied Catalysis B: Environmental. 176–177, 396-428

[5] Bautista, P., Mohedano, A., Casas, J., Zazo, J., Rodriguez, J., (2008). An Overview of the Application of Fenton Oxidation to Industrial Wastewaters Treatment., Journal of Chemical Technology and Biotechnology, 83 (10), 1323-1338.

[6] Benford, D., Boer, D., Carere, A. Domenico, D., Johansson, N., Schrenk, D., Schoeters, G., Voogt, D., Dellatte, E., (2008). Opinion of the Scientific Panel on Contaminants in the Food Chain on Perfluorooctane Sulfonate (PFOS), Perfluorooctanoic Acid (PFOA) and their Salts. EFSA Journal, 653, 131.

[7] Bhattacharyya, A., Kawi, S. Ray, M., (2004). Photocatalytic degradation of Orange II by TiO_2 catalysts supported on adsorbents. Catal. 98, 431-439

[8] Brillas, E., Mur, E., Sauleda, R., Sanchez, L., Peral, J., Domenech, X., Casado, J., (1998). Aniline Mineralization by AOP's: Anodic Oxidation, Photocatalysis, Electro-Fenton and Photoelectro-Fenton Processes. Applied Catalysis B: Environmental, 16 (1),31-42.

[9] Baer, D. R., Tratnyek, G, P., Qiang, Y., Amonette, J.E., Linehan, J., Sarathy, V., Nurmi, T.J., Wang, C., Antony, J., (2012). Synthesis, Characterization, and Properties of Zero-Valent Iron Nanoparticles. Environmental Applications of Nanomaterials: Synthesis, Sorbents and Sensors, 49-86.

[10] Bahnemann, D.; Cunningham, J.; Fox, M.A.; Pelizzetti, E.; Pichat, P.; Serpone, N., (1994). Photocatalytic treatment of waters. In Aquatic and Surface Photochemistry. Lewis Publishers, 261-316

[11] Bigg, T., Judd., S.J., (2000). Zero-Valent Iron for Water Treatment. Environmental Technology, 21 (6), 661-670.

[12] Bruton, T.A., Sedlak. D.L., (2017). Treatment of aqueous film-forming foam by heat-activated persulfate under conditions representative of in situ chemical oxidation. Environ. Sci. Technol., 51(23). 13878-13885.

[13] Cai. M.G., Zhao, Z., Yin, Z.G., Ahrens, L., Huang, P., Yang, H., He, Z.F., Sturm, R., Ebinghaus, R., Xie, Z. Y., (2012). Occurrence of perfluoroalkyl compounds in surface waters from the north pacific to the arctic ocean. Environ. Sci. Technol., 46, 661–668.

[14] Carter, K. E., and Farrell, J. (2008). Oxidative Destruction of Perfluorooctane Sulfonate using Boron-Doped Diamond Film Electrodes. Environmental Science & Technology, 42 (16), 6111-6115.

[15] Cargnello, M., Gordon, T.R., Murray, C.B., (2014). Solution-phase synthesis of titanium dioxide nanoparticles and nanocrystals. Chem.Rev.,114, 9319–9345.

[16] Chang, K., Das, D.J., Ehresman, M.E., Ellefson, G.S., Gorman, J.A., Hart, P.E., Noker, Y.M., Tan, P.H., Lieder, C., Lau, G.W., Olsen, J.L., (2008) Butenhoff, Comparative pharmacokinetics of perfluorobutyrate in rats, mice, monkeys, and humans and relevance to human exposure via drinking water, Toxicol. Sci., 104, 40–53.

[17] Cao, B.B., Wang, H.S., Yu, L.L., Wang, S.H., Yuan, J. Chen, (2010) Photochemical decomposition of perfluorooctanoic acid in aqueous periodate with VUV and UV light irradiation, J. Hazard. Mater., 179, 1143–1146.

[18] Çeçen, F., Aktas, O, (2011). Activated Carbon for Water and Wastewater Treatment: Integration of Adsorption and Biological Treatment. John Wiley & Sons.

[19] Cerofolini, G.F., Bandosz, T.J., (1999). Adsorption and its Applications in Industry and Environmental Protection. Studies in Surface Science and Catalysis.

[20] Chen, J., Zhang, P., (2006). Photodegradation of Perfluorooctanoic Acid in Water Under Irradiation of 254 Nm and 185 Nm Light by use of Persulfate. Water Science and Technology, 54 (11-12), 317-325.

[21] Chen, M. J., Lo, S.L., Lee, Y.C., Huang. C.C. (2015). Photocatalytic Decomposition of Perfluorooctanoic Acid by Transition-Metal Modified Titanium Dioxide. Journal of Hazardous Materials, 288, 168-175.

[22] Chen, M.J.; Lo, S.L.; Lee, J. Kuo, Wu, C.H., (2016). Decomposition of perfluorooctanoic acid by ultraviolet light irradiation with Pb-modified titanium dioxide, J. Hazard. Mat., 303, 111–118.

[23] Chen, D.; Caruso, R. A, (2013). Recent progress in the synthesis of spherical titania nanostructures and their applications. Adv. Funct. Mater.23, 1356–1374.

[24] Chong, M.N., Jin, B., Chow, C.W.K., Saint, C., (2010). Recent developments in photocatalytic water treatment technology: a review. Water Res., 44, 2997-3027

[25] Cheng, J.H., Liang, X. Y, Yang, S.W., Hu, Y.Y., (2014) "Photochemical defluorination of aqueous perfluorooctanoic acid (PFOA) by VUV/Fe3+ system, Chem.Eng.J. 239, 242–249

[26] Choi, H., Agarwal, S. and Al-Abed, S., (2008). Adsorption and Simultaneous Dechlorination of PCBs on GAC/Fe/Pd: Mechanistic Aspects and Reactive Capping Barrier Concept. Environmental Science & Technology 43 (2): 488-493.

[27] Choi, H., Al-Abed, S., (2009). PCB Congener Sorption to Carbonaceous Sediment Components: Macroscopic Comparison and Characterization of Sorption Kinetics and Mechanism. Journal of Hazardous Materials, 165 (1), 860-866.

[28] Cui, J., He, T., Zhang, X., (2013). Synthesis of Fe_3O_4@SiO_2@Ption-TiO_2 hybrid composites with high efficient UV–visible light photoactivity" Catal. Commun., 40, 66-70

[29] Dillert, R., Bahnemann, D., Hidaka, H., (2007). Light-Induced Degradation of Perfluorocarboxylic Acids in the Presence of Titanium Dioxide. Chemosphere, 67 (4), 785-792.

[30] Dogliotti, L., Hayon, E., (1967). Flash photolysis of persulfate ions in aqueous solutions. Study of the sulfate and ozonide radical anions. J. Phys. Chem. 71, 2511-2516.

[31] Dorr, I., Moshe, T.B., Berkowitz, B., (2009). Use of Nanoparticles for Degradation of Water Contaminants in Oxidative and Reductive Reactions. ACS Publications, 1027, 23-37

[32] Dong, H., Zeng, G., Tang, L., Fan, C., Zhang, C., He, X., He, Y., (2015). An overview on limitations of TiO2-based particles for photocatalytic degradation of organic pollutants and the corresponding countermeasures, Water Res., 79, 128–146.

[33] Du, Z., Deng, S., Bei, Y., Huang, Q., Wang, B., Huang, J., Yu, G. (2014). Adsorption Behavior and Mechanism of Perfluorinated Compounds on various adsorbents—A Review. Journal of Hazardous Materials, 274, 443-454.

[34] Eilperin, J. (2005). Compound in Teflon a Likely Carcinogen. Washington Post, 4.

[35] Fujii, S., Polprasert, C., Tanaka, S. P. H., YONG. 2007. "New POPs in the Water Environment: Distribution, Bioaccumulation and Treatment of Perfluorinated Compounds-a Review Paper." Journal of Water Supply: Research and Technology. AQUA, 56 (5), 313-326.

[36] Fei, C., McLaughlin, J.K., Tarone, R.E., Olsen, J., (2007). Perfluorinated chemicals and fetal growth: a study within the Danish National Birth Cohort. Environ. Health Perspect. 115, 1677.

[37] Fei, Y., Bai, X., Yang, C., Xu, L., Ma, J., (2019). Reduced Graphene Oxide–P25 Nanocomposites as Efficient Photocatalysts for Degradation of Bisphenol A in Water. Catalyst, 9 (7), 607

[38] Fujishima, A., Rao, T.N., Tryk, D.A., (2000). Titanium dioxide photocatalysis. J. Photochem. Photobiol. C 1, 1–21.

[39] Furube, A., Asahi, T., Masuhara, H., Yamashita, H., Anpo, M., (2001), Direct observation of a picosecond charge separation process in photoexcited platinum loaded TiO_2 particles by femtosecond diffuse reflectance spectroscopy. Chem. Phys. Lett., 336, 424-430

[40] Foo, K.Y., Hameed, B.H., (2010). Decontamination of textile wastewater via TiO_2/activated carbon composite materials Adv. Colloid Interface Sci., 159, 130-143

[41] Gao, X., Chorover, J., (2012). Adsorption of Perfluorooctanoic Acid and Perfluorooctanesulfonic Acid to Iron Oxide Surfaces as Studied by Flow-through ATR-FTIR Spectroscopy. Environmental Chemistry., 9 (2), 148-157.

[42] Gaya, U.I., Abdullah, A.H., (2008). Heterogeneous photocatalytic degradation of organic contaminants over titanium dioxide: a review of fundamentals, progress and problems. J. Photochem. Photobiol., 9 (1), 1-12.

[43] Gatto, S., Sansotera, S., Persico, F., Gola, M., Pirola, C., Panzeri, W., Navarrini, W., Bianchi, C., (2015). Surface Fluorination on TiO2 Catalyst Induced by Photodegradation of Perfluorooctanoic Acid. Catalysis Today, 241, 8-14.

[44] Ghauch, A. (2008). Rapid Removal of Flutriafol in Water by Zero-Valent Iron Powder. Chemosphere, 71(5), 816-826.

[45] Giri, R.R., Ozaki, H., Morigaki, Taniguchi, T., Takanami, R., (2011). UV Photolysis of Perfluorooctanoic Acid (PFOA) in Dilute Aqueous Solution. Water Science and Technology, 63 (2), 276-282.

[46] GAC RSSCT (2017). Removal of Short Chain PFAS Compounds

[47] Giesy, J.P., Kannan, K., (2001). Global distribution of perfluorooctane sulfonate in wildlife. Environ. Sci. Technol. 35, 1339–1342.

[48] Gump B., Wu, Q., Dumas, A.K., Kannan, K., (2011). Perfluorochemical (PFC) exposure in children: associations with impaired response inhibition. Environ. Sci. Technol., 45, 8151–8159

[49] Gladitz, M., (2014). Science and Technology Against Microbial Pathogens: Research, Development and Evaluation, edited by Antonio Mendez-Vilas. Singapore: World Scientific Publishing Co Pte Ltd.

[50] Hansen, K.J., Johnson, H. Eldridge, J., Butenhoff, J., Dick, L., (2002). Quantitative Characterization of Trace Levels of PFOS and PFOA in the Tennessee River. Environmental Science & Technology, 36 (8), 1681-1685.

[51] Hansen, M. C., Børresen, M.H., Schlabach, M., Cornelissen, G., (2010). Sorption of Perfluorinated Compounds from Contaminated Water to Activated Carbon. Journal of Soils and Sediments, 10 (2), 179-185.

[52] Hayward, Oldham, D., Maurice, B., Trapnell, W., (1964). Chemisorption, Butterworths London.

[53] Hebert, G. N., Odom, M., Craig, P., Dick, D., Strauss, S., (2002). Method for the Determination of Sub-Ppm Concentrations of Perfluoroalkyl sulfonate Anions in Water, J.Environ.Monit., 4 (1), 90-95.

[54] Henrik, B.S., Stel, J.M., Marijn, V.D., Christian, E., Pim, D.V., Kraak, M.H.S., (2015), Acute and chronic toxicity of short chained perfluoroalkyl substances to daphnia magna. Environ. Pollut., 198, 47–53.

[55] Health Risk Assessment Unit, PFBS and Drinking Water, Minnesota Department of Health, 2017. http://www.health.state.mn.us/divs/eh/risk/guidance/gw/ pfbsinfo.pdf.

[56] Hogue, C. (2005). Dupont, EPA Settle. Chemical & Engineering News, 83 (10).

[57] Hogue, C. (2005). PFOA Called Likely Human Carcinogen. Chemical and Engineering News, 83 (27), 5.

[58] Hogue, C. (2006). Pledges on PFOA-Eight Companies Agree to Cut Releases of Perfluorochemicals. Chemical and Engineering News, 10.

[59] Hori, H., Hayakawa, E., Einaga, H., Kutsuna, S., Koike, K., Ibusuki, T., Kiatagawa, H. , Arakawa, R. (2004). Decomposition of Environmentally Persistent Perfluorooctanoic Acid

in Water by Photochemical Approaches. Environmental Science & Technology, 38 (22), 6118-6124.

[60] Hori, H., Yamamoto, A., Hayakawa, E., Taniyasu, S., Yamashita, N., Kutsuna, S., Kiatagawa, H., Arakawa, R. (2005). Efficient Decomposition of Environmentally Persistent Perfluorocarboxylic Acids by use of Persulfate as a Photochemical Oxidant. Environmental Science & Technology, 39 (7), 2383-2388.

[61] Hori, H., Hayakawa, E., Yamashita, N., Taniyasu, S., Nakata, F., Kobayashi, Y., (2004). High-Performance Liquid Chromatography with Conductimetric Detection of Perfluorocarboxylic Acids and Perfluoro sulfonates. Chemosphere, 57 (4), 273-282.

[62] Hori, H., Takano, Y., Koike, K., Takeuchi, K., Einaga, H., (2003). Decomposition of environmentally persistent trifluoroacetic acid to fluoride ions by a homogeneous photocatalyst in water, Environ. Sci. Technol., 37, 418– 422.

[63] . Hoffmann, M., Martin, S.T., Choi, W., Bahnemann, D.W., (1995). Environmental application of semiconductor photocatalysis, Chem.Rev., 95, 69–96.

[64] Hoffman, K., Webster, T.F., Weisskopf, M.G., Weinberg, J., Vieira, V., (2010), Exposure to Polyfluoroalkyl Chemicals and Attention Deficit Hyperactivity Disorder in U.S. Children Aged 12-15 Years. Environmental Health Perspectives., 118(12), 1762-1767

[65] Jiang, M., Manawan, T, Feng, R, Qian, T.; Zhao, G., Zhou, F., Kong, Q., Wang, S., Dai, J.H., (2018). Anatase and rutile in Evonik Aeroxide P25: Hetero junction or individual nanoparticles? Catal. Today, 300, 12–17.

[66] Joo, Hee, S., Cheng, F., (2006) Nanotechnology for Environmental Remediation. Springer Science & Business Media.

[67] Joshi, R., Mukherjee, T., (2006). Carbonate radical anion-induced electron transfer in bovine serum albumin, Radiat. Phys. Chem., 75, 760–767.

[68] Karanfil, T., Kilduff , J.E., (2000). Role of granular activated carbon surface chemistry on the adsorption of organic compounds. Priority pollutants Environ. Sci. Technol., 34, 3217-3224

[69] Kohtani, S., Kawashima, A., Miyabe, H., (2017) Reactivity of trapped and accumulated electrons in titanium dioxide photocatalysis. Catalysts, 7, 303.

[70] Key, B., Robert, D., Howell, D., Criddle, C., (1997). Fluorinated Organics in the Biosphere. Environmental Science & Technology, 31 (9), 2445-2454.

[71] Kissa, E., (1994). Fluorinated Surfactants: Synthesis, Properties. Applications M. Dekker http://books.google.com/books?id=vA9tAAAAMAAJ

[72] Knepper, T. P., Lange, F. (2011). Polyfluorinated Chemicals and Transformation. Products. The Handbook of Environmental Chemistry, 17

[73] Kuang, Y., Wang, Q., Chen, Z., Megharaj, M., Naidu, R.. (2013). Heterogeneous Fenton-Like Oxidation of Monochlorobenzene using Green Synthesis of Iron Nanoparticles. Journal of Colloid and Interface Science, 410, 67-73.

[74] Kudo, N., Kawashima, Y., (2003). Toxicity and Toxicokinetics of Perfluorooctanoic Acid in Humans and Animals. The Journal of Toxicological Sciences, 28 (2), 49-57.

[75] Kudo, N., Suzuki-Nakajima, E. Mitsumoto, A., Kawashima, Y., (2006). Responses of the Liver to Perfluorinated Fatty Acids with Different Carbon Chain Length in Male and Female Mice: In Relation to Induction of Hepatomegaly, Peroxisomal B-Oxidation and Microsomal 1-Acylglycerophosphocholine Acyltransferase. Biological and Pharmaceutical Bulletin, 29 (9), 1952-1957.

[76] Knox, S., Jackson, T., Javins, B., Frisbee, S., Shankar, A., Ducatman, M., (2011). Metabolism, Implications of early menopause in women exposed to perfluorocarbons. J. Clin. Endocrinol. Metab., 96, 1747–1753.

[77] Kjølholt, J., Jensen, A., Warming, M., (2015). Short-chain Polyfluoroalkyl Substances (PFAS), T.D.E.P. Agency, Copenhagen, Denmark.

[78] Lange, F.T, Schmidt, C., Brauch, H.J. (2007). Perfluoroalkyl carboxylates and–sulfonates. Water Sci Technol, 56(11),151-8.

[79] Lau, C., Anitole, K., Hodes, C., Lai, D., Hutchens, P., Seed, J., (2007), Perfluoroalkyl Acids: A Review of Monitoring and Toxicological Findings. Toxicological Sciences: An Official Journal of the Society of Toxicology, 99 (2), 366-394.

[80] Lee, Y., Lo, S., Chiueh, P., Liou, Y., Chen, M., (2010). Microwave-Hydrothermal Decomposition of Perfluorooctanoic Acid in Water by Iron-Activated Persulfate Oxidation. Water Research, 44 (3), 886-892.

[81] Li, S., Yan, W., Zhang, W., (2009), Solvent-Free Production of Nanoscale Zero-Valent Iron (nZVI) with Precision Milling. Green Chemistry, 11 (10), 1618-1626.

[82] Li, X., Chen, S., Quan, X., Zhang, Y., (2011), Enhanced Adsorption of PFOA and PFOS on Multiwalled Carbon Nanotubes Under Electrochemical Assistance., Environmental Science & Technology, 45 (19), 8498-8505.

[83] Li, X., Zhang, P., Jin, L., Shao, T., Li, Z., Cao, J., (2012). Efficient Photocatalytic Decomposition of Perfluorooctanoic Acid by Indium Oxide and its Mechanism. Environmental Science & Technology, 46 (10), 5528-5534.

[84] Lightcap, I.V, Kosel, T.H., Kamat, P.V., (2010), Anchoring semiconductor and metal nanoparticles on a two-dimensional catalyst mat. storing and shuttling electrons with reduced graphene oxide Nano Lett., 10, 577-583

[85] Liang, C., Lai. M., (2008). Trichloroethylene Degradation by Zero Valent Iron Activated Persulfate Oxidation. Environmental Engineering Science, 25 (7), 1071-1078.

[86] Liao, Z., Farrell, J., (2009). Electrochemical Oxidation of Perfluorobutane Sulfonate using Boron-Doped Diamond Film Electrodes. Journal of Applied Electrochemistry, 39 (10), 1993-1999.

[87] Lien, H., Zhang., W., (2007). Nanoscale Pd/Fe Bimetallic Particles: Catalytic Effects of Palladium on Hydro dichlorination. Applied Catalysis B: Environmental 77 (1): 110-116.

[88] Washington (2016), Lifetime Health Advisories and Health Effects Support Documents for Perfluorooctanoic Acid and Perfluorooctane Sulfonate, Federal Information & News Dispatch, Inc.

[89] Lin, H., Wang, Y., Niu, J., Yue, Z., Huang, Q., (2015). Efficient Sorption and Removal of Perfluoroalkyl Acids (PFAAs) from Aqueous Solution by Metal Hydroxides Generated in Situ by Electrocoagulation. Environmental Science & Technology, 49 (17), 10562-10569.

[90] Lindstrom, A., Mark, B., Strynar, J., Libelo, E.L., (2011), Polyfluorinated Compounds: Past, Present, and Future. Environmental Science and Technology, 44 (19), 7954-7961.

[91] Li, M.; Yu, Z. Liu, Q. Sun, L., Huang, W., (2016). Photocatalytic decomposition of perfluorooctanoic acid by noble metallic nanoparticles modified TiO_2, Chem. Eng. J., 286, 232–238.

[92] Li, F., Duan, J., Tian, S., Ji, H., Zhu, Y., Wei, Z., Zhao, D., (2020) Short-chain per- and polyfluoroalkyl substances in aquatic systems: Occurrence, impacts and treatment, Chemical Engineering Journal, 380, 122506

[93] Makarova, O.V., Rajh, T., Thurnauer, M.C., Surface modification of TiO_2 nanoparticles for photochemical reduction of nitrobenzene, Environ. Sci. Technol., 34, 4797-4803

[94] Melzer, D. Rice, N., Depledge, M.H., Henley, W.E., Galloway,T.S., (2010). Association between serum perfluorooctanoic acid (PFOA) and thyroid disease in the US National Health and Nutrition Examination Survey, Environ. Health Perspect., 118, 686.

[95] Meng, H.L, Cui, C.; Shen, H.L, (2012).Synthesis and photocatalytic activity of TiO2@CdS and CdS@TiO2 double-shelled hollow spheres. Journal of Alloys and Compounds, 527, 30-35

[96] Merino, N., Qu, Y., Deeb, R., Hawley, E., Hoffmann, M., Mahendra, S., (2016). Degradation and Removal Methods for Perfluoroalkyl and Polyfluoroalkyl Substances in Water. Environmental Engineering Science, 33 (9), 615-649.

[97] Mitchell, S., Ahmad, M., Teel, A., Watts, R., (2013). Degradation of Perfluorooctanoic Acid by Reactive Species Generated through Catalyzed H2O2 Propagation Reactions. Environmental Science & Technology Letters, 1 (1), 117-121.

[98] Moody, C., Field. J., (1999). Determination of Perfluoro carboxylates in Groundwater Impacted by Fire-Fighting Activity. Environmental Science & Technology, 33 (16), 2800-2806.

[99] Moody, C., Kwan, W., Martin, J., Muir, D., Mabury, S. (2001). Determination of Perfluorinated Surfactants in Surface Water Samples by Two Independent Analytical

Techniques: Liquid Chromatography/Tandem Mass Spectrometry and 19F NMR. Analytical Chemistry, 73 (10), 2200-2206.

[100] Moody, C., Field, J. (2000). Perfluorinated Surfactants and the Environmental Implications of their use in Fire-Fighting Foams. Environmental Science & Technology, 34 (18), 3864-3870.

[101] Nassi, M., Sarti, E., Pasti, L., Martucci, A., Marchetti, N., Cavazzini, A., Renzo, F., Galarneau, A. (2014). Removal of Perfluorooctanoic Acid from Water by Adsorption on High Surface Area Mesoporous Materials. Journal of Porous Materials, 21 (4), 423-432.

[102] Neta, P., Huie, R.E., Ross, A.B. (1988). Rate Constants for Reactions of Inorganic Radicals in Aqueous Solution. Journal of Physical and Chemical Reference Data, 17, 1027.

[103] Nfodzo, P., Choi. H. (2011). Sulfate Radicals Destroy Pharmaceuticals and Personal Care Products. Environmental Engineering Science, 28 (8), 605-609.

[104] Nfodzo, P., Choi, H., (2011). Triclosan Decomposition by Sulfate Radicals: Effects of Oxidant and Metal Doses. Chemical Engineering Journal, 174 (2-3), 629-634.

[105] O'Hagan, D. (2008). Understanding Organofluorine Chemistry. an Introduction to the C–F Bond. Chemical Society Reviews, 37 (2), 308-319.

[106] Pramanik, B.K. Pramanik, S.K., Suja, F., (2015). A comparative study of coagulation, granular- and powdered-activated carbon for the removal of perfluorooctane sulfonate and perfluorooctanoate in drinking water treatment, Environ. Technol. 36, 2610–2617.

[107] Panchangam, S. C., Lin, A.Y., Shaik, Lin. C.F. (2009). Decomposition of Perfluorocarboxylic Acids (As) by Heterogeneous Photocatalysis in Acidic Aqueous Medium. Chemosphere, 77 (2), 242-248.

[108] Park, H., Vecitis, C.D., Cheng, J., Choi, W., Mader, B. T., Hoffmann, M. R. (2009). Reductive Defluorination of Aqueous Perfluorinated Alkyl Surfactants: Effects of Ionic Headgroup and Chain Length. The Journal of Physical Chemistry A, 113 (4), 690-696.

[109] Park, H., Vecitis, C.D., Cheng, J., Choi, W., Mader, B. T., Hoffmann, M. R., (2011). Reductive Degradation of Perfluoroalkyl Compounds with Aquated Electrons Generated from Iodide Photolysis at 254 Nm. Photochemical & Photobiological Sciences, 10 (12), 1945-1953.

[110] Park, S., Zenobio, J., Lee, L.S. (2018). Perfluorooctane Sulfonate (PFOS) Removal with Pd0/nFe0 Nanoparticles: Adsorption Or Aqueous Fe-Complexation, Not Transformation? Journal of Hazardous Materials, 342, 20-28.

[111] Pignatello, J. J., Oliveros, E., MacKay, A. (2006). Advanced Oxidation Processes for Organic Contaminant Destruction Based on the Fenton Reaction and Related Chemistry. Critical Reviews in Environmental Science and Technology 36 (1): 1-84.

[112] Poboży, Ewa, Król, E., Wójcik, L., Wachowicz, M., Trojanowicz, M. (2011). HPLC Determination of Perfluorinated Carboxylic Acids with Fluorescence Detection. Microchimica Acta, 172 (3-4): 409-417.

[113] Post, G.B., Cohn, P.D., Cooper, K.R., (2012)**,** Perfluorooctanoic acid (PFOA), an emerging drinking water contaminant: a critical review of recent literature**.** Environ. Res., 116, 93-117

[114] Pramanik, B.K., Pramanik, S.K., Suja, F. (2015). A comparative study of coagulation, granular- and powdered-activated carbon for the removal of perfluorooctane sulfonate and perfluorooctanoate in drinking water treatment, Environ. Technol. 36, 2610–2617.

[115] Qu, Y., Zhang, C., Li, F., Bo, X., Liu, G., Zhou, Q. (2009). Equilibrium and Kinetics Study on the Adsorption of Perfluorooctanoic Acid from Aqueous Solution onto Powdered Activated Carbon. Journal of Hazardous Materials 169 (1): 146-152

[116] Qu, Y., Zhang, C.J., Chen, P., Zhou, Q., Zhang, W.X. (2014). Effect of Initial Solution pH on Photo-Induced Reductive Decomposition of Perfluorooctanoic Acid. Chemosphere 107: 218-223.

[117] Qu, Y., Zhang, C., Li, F., Chen, J., Zhou, Q. (2010). Photo-Reductive Defluorination of Perfluorooctanoic Acid in Water. Water Research 44 (9): 2939-2947.

[118] Quinn, J., Geiger, C., Clausen, C., Brooks, K., Coon, C., O'Hara, S., Krug, T., Major, D., Yoon, W., Gavaskar, A. (2005). Field Demonstration of DNAPL Dehalogenation using Emulsified Zero-Valent Iron. Environmental Science & Technology 39 (5): 1309-1318.

[119] Qiana, R., Zonga, H., Schneiderc, J., Zhoua, G., Zhaoa, T., Lid, Y., Yange, J., Bahnemannf, D.W., Pana, J.H., (2019). Charge carrier trapping, recombination and transfer during TiO_2 photocatalysis: An overview. Catalysis Today 335, 78–90

[120] Rayne, S., Forest, K. (2009). Perfluoroalkyl Sulfonic and Carboxylic Acids: A Critical Review of Physicochemical Properties, Levels and Patterns in Waters and Wastewaters, and Treatment Methods. Journal of Environmental Science and Health Part *A,* 44 (12), 1145-1199.

[121] Reisch, M. S., (2015). DuPont Loses First PFOA Trial in Ohio. Chemical and Engineering News, C&EN, 93 (40): 20-21.

[122] Ritter, S., (2010). Fluorochemicals go short, Chem. Eng. News 88 (5), 12–17.

[123] Rozwadowski, M., Siedlewski,J., Wojsz, R., (1979). Sorption of polar substances on active carbons**,** Carbon, 17, 411-417

[124] Rosenfeldt, E. J., Linden, K.G. (2004). Degradation of Endocrine Disrupting Chemicals Bisphenol A, Ethinyl Estradiol, and Estradiol during UV Photolysis and Advanced Oxidation Processes. Environmental Science & Technology 38 (20): 5476-5483.

[125] Ruiz, B. G., Ribao, P., Diban, N., Rivero, M.J., Ortiz, I., Urtiaga, A., (2018). Photocatalytic degradation and mineralization of perfluorooctanoic acid (PFOA) using a composite TiO_2-rGO catalyst, J. Hazard. Mat. 344, 950–957.

[126] Sansotera, M.; Persico, F. Pirola, C., Navarrini, W., Michele, A.D., Bianchi, C.L. (2014). Decompositionofperfluorooctanoicacidphotocatalyzedbytitaniumdioxide: chemical modification of the catalyst surface induced by fluoride ions. Appl. Catal. B, 148, 29–35.

[127] Saito, N., Harada, K., Inoue, K., Sasaki, K., Yoshinaga, T., Koizumi, A., (2004). Perfluorooctanoate and Perfluorooctane Sulfonate Concentrations in Surface Water in Japan. Journal of Occupational Health, 46 (1), 49-59.

[128] Scott, B. F., Moody, C.A., Spencer, C., Small, J.M., Muir, C.D., Mabury, S.A. (2006). Analysis for Perfluorocarboxylic Acids/Anions in Surface Waters and Precipitation using GC− MS and Analysis of PFOA from Large-Volume Samples. Environmental Science & Technology, 40 (20), 6405-6410.

[129] Schneider, J., Matsuoka, M., Takeuchi, M., Zhang, J., Horiuchi, Y., Anpo, M., Bahnemann, D.W. (2014). Understanding TiO_2 Photocatalysis: Mechanisms and Materials. Chem. Rev., 114, 9919−9986

[130] Serpone, N., Lawless, D, Khairutdinov, R., (1995). Size effects on the photophysical properties of colloidal anatase TiO2 particles: size quantization versus direct transitions in this indirect semiconductor? The journal of Physical Chemistry, 99 (45), 16646–16654

[131] Shahid U., (2013), Improved analytical methods for perfluoroalkyl acids (PFAAs) and their precursors – a focus on human dietary exposure. PhD thesis, Stockholm University

[132] Skutlarek, D., Exner, M., Farber, H., (2006). Perfluorinated Surfactants in Surface and Drinking Waters. Environ Sci Pollut Res Int., 13 (5), 299-307.

[133] Stein, C. R., Savitz, D.A., Dougan, M., (2009). Serum Levels of Perfluorooctanoic Acid and Perfluorooctane Sulfonate and Pregnancy Outcome. American Journal of Epidemiology 170(7), 837-846.

[134] Seyedali, A., Aziz. Raman, A., Parthasarathy, R., Sajjadi, B., (2016). Sonochemical reactors: Review on features, advantages and limitations. Renewable and Sustainable Energy Reviews, 63, 302-314,

[135] Song, C., Chen, P., Wang, C., Zhu, L., (2012). Photodegradation of Perfluorooctanoic Acid by Synthesized TiO2–MWCNT Composites Under 365 Nm UV Irradiation. Chemosphere, 86 (8), 853-859.

[136] Song, Z., Tang, H., Wang, N., Zhu, L. (2013). Reductive Defluorination of Perfluorooctanoic Acid by Hydrated Electrons in a Sulfite-Mediated UV Photochemical System. Journal of Hazardous Materials, 262, 332-338.

[137] Sue, Y., Zhang, S., Saito, F., Sato, T., (2003). Preparation of visible light-activated titania photocatalyst by mechanochemical method, Chem. Lett., 32, 358-359

[138] Tang, C.Y., Fu, Q. S., Gao, D., Criddle, C.S., Leckie, J.O. (2010)., Effect of solution chemistry on the adsorption of perfluorooctane sulfonate onto mineral surfaces. Water Research, 44 (8), 2654-2662.

[139] Tang, C. Y., Fu, Q.S., Robertson, A., Criddle, C.S., Leckie, J.O. (2006). Use of Reverse Osmosis Membranes to Remove Perfluorooctane Sulfonate (PFOS) from Semiconductor Wastewater. Environmental Science & Technology, 40 (23), 7343-7349.

[140] Taniyasu S., Yamashita, N., Yamazaki, E., Petrick, G., Kannan, K., (2012). The environmental photolysis of perfluorooctane sulfonate, perfluorooctanoate, and related fluorochemicals, Chemosphere, 90, 1686–1692.

[141] Teng, Jiuwei, Shuze Tang, and Shiyi Ou. 2009. "Determination of Perfluorooctanesulfonate and Perfluorooctanoate in Water Samples by SPE-HPLC/Electrospray Ion Trap Mass Spectrometry. Microchemical Journal, 93 (1), 55-59.

[142] Thompson, J., Eaglesham, G., Reungoat, J., Poussade, Y., Bartkow, M., Lawrence, M., Mueller, J.F., (2011). Removal of PFOS, PFOA and Other Perfluoroalkyl Acids at Water Reclamation Plants in South East Queensland Australia. Chemosphere, 82 (1): 9-17.

[143] Thi, L.A.P., Do, H.T., Lee, Y.C., Lo, S.L. (2013). Photochemical decomposition of perfluorooctanoic acids in aqueous carbonate solution with UV irradiation. Chem. Eng. J., 221, 258–263.

[144] Tzabar, N., Grossman, G., (2012). Analysis of an activated-carbon Sorption Compressor operating with gas mixtures. Cryogenics, 52, 491-499

[145] Ochoa. H., Lourdes, V. (2008). Removal of Perfluorooctane Sulfonate (PFOS) and Related Compounds from Industrial Effluents. The University of Arizona.

[146] Ochiai, T., Iizuka, Y., Nakata, K., Murakami, T., Tryk, A.D. Fujishima, A., Koide, Y., Morito, Y., (2011). Efficient Electrochemical Decomposition of Perfluorocarboxylic Acids by the use of a Boron-Doped Diamond Electrode. Diamond and Related Materials, 20 (2), 64-67.

[147] Ochiai, T., Moriyama, H., Nakata,K., Murakami, T., Koide, Y., Fujishima, A.. (2011). Electrochemical and Photocatalytic Decomposition of Perfluorooctanoic Acid with a Hybrid Reactor using a Boron-Doped Diamond Electrode and TiO2 Photocatalyst. Chemistry Letters, 40 (7), 682-683.

[148] Urtiaga, A., González, C.F., Sonia Gómez-Lavín, and Inmaculada Ortiz. 2015. Kinetics of the Electrochemical Mineralization of Perfluorooctanoic Acid on Ultra nanocrystalline Boron Doped Conductive Diamond Electrodes. Chemosphere, 129, 20-26.

[149] U.S. EPA, (2018). Technical Fact Sheet: Draft Toxicity Assessments for GenX Chemicals and PFBS. https://www.epa.gov/sites/production/files/2018-12/

[150] Wang, S. Yanga, Q., Chena, F., Suna, J., Luoa, K., Yaoa, F., Wanga, X., Wanga, D., Lia, X., Zenga, G., (2017). Photocatalytic degradation of perfluorooctanoic acid and perfluorooctane sulfonate in water: A critical review. Chemical Engineering Journal, 328, 927-942

[151] Wang, Y., Zhang, P., Pan, G., Chen, H., (2008). Ferric Ion Mediated Photochemical Decomposition of Perfluorooctanoic Acid (PFOA) by 254 Nm UV Light. Journal of Hazardous Materials, 160 (1), 181-186.

[152] Wang, Y., Zhang, P., (2011). Photocatalytic decomposition of perfluorooctanoic acid (PFOA) by TiO_2 in the presence of oxalic acid, J. Hazard. Mater., 192 (2011) 1869–1875.

[153] Wagner, I.., Strehlow, H., (1982). Flash photolysis in aqueous periodate-solutions, Phys. Chem., 86, 297–301.

[154] Wu, S., Choi, H. (2016). Interpreting Unique Colloidal Response of TiO_2 Nanomaterials to Controlled Sonication for Understanding of their Assembly Configuration in Water. Water Science and Technology: Water Supply 16 (6), 1768-1775.

[155] Vecitis, C. D., Park, H., Cheng, J., Mader, B.T., Hoffmann, M.R., (2008). Kinetics and Mechanism of the Sonolytic Conversion of the Aqueous Perfluorinated Surfactants, Perfluorooctanoate (PFOA), and Perfluorooctane Sulfonate (PFOS) into Inorganic Products. The Journal of Physical Chemistry, 112 (18), 4261-4270.

[156] Vecitis, C. D., Park, H., Cheng, J., Mader, B.T., Hoffmann, M.R., (2009). Treatment Technologies for Aqueous Perfluorooctane sulfonate (PFOS) and Perfluorooctanoate (PFOA). Frontiers of Environmental Science & Engineering in China, 3 (2), 129-151.

[157] Wang, T., Wang, Y.W., Liao, C.Y., Cai, Y.Q., Jiang, G.B., (2009). Perspectives on the inclusion of perfluorooctane sulfonate into the Stockholm Convention on persistent organic pollutants, Environ. Sci. Technol., 43, 5171–5175.

[158] Xiao, F., Simcik, M.F., Gulliver, J.S., (2013). Mechanisms for Removal of Perfluorooctane Sulfonate (PFOS) and Perfluorooctanoate (PFOA) from Drinking Water by Conventional and Enhanced Coagulation. Water Research, 47 (1), 49-56.

[159] Yamamoto, T., Noma, Y., Sakai, S., Shibata, Y., (2007). Photodegradation of Perfluorooctane Sulfonate by UV Irradiation in Water and Alkaline 2-Propanol. Environmental Science & Technology, 41 (16), 5660-5665.

[160] Yamase, T., Kurozumi, T., (1983) Photoreduction of polymolybdates(VI) in aqueous solutions containing acetic acid, J. Chem. Soc. Dalton Trans. 1983, 2205–2209.

[161] Yu, Q., Zhang, R., Deng, S., Huang, J., Yu, G. (2009). Sorption of Perfluorooctane Sulfonate and Perfluorooctanoate on Activated Carbons and Resin: Kinetic and Isotherm Study. Water Research, 43 (4), 1150-1158.

[162] Zaleska, A., (2008). Doped-TiO_2: a review, Recent Pat. Eng., 2, 157-164

[163] Zhang, Z., Chen, J., Lyu, X., Yin, H., Sheng, G. (2014). Complete Mineralization of Perfluorooctanoic Acid (PFOA) by Γ-Irradiation in Aqueous Solution. Scientific Reports, 4, 7418.

[164] Zhou, K.F., Zhu, Y.H., Yang, X.L., Jiang, X., Li, C.Z., (2011). Preparation of graphene-TiO_2 composites with enhanced photocatalytic activity. New J. Chem., 35, 353–359.

[165] Zhang, Z., Wang, C., Zakaria, R., Ying, J.Y., (1998). Role of particles size in nanocrystalline TiO_2-based photocatalysts, J. Phys. Chem. B, 102, 10871–10878.

CHAPTER 3

Dependency of photocatalytic and photochemical decomposition of PFAS on their chain lengths, functional groups, and structural properties

3.1. Introduction

Per- and polyfluoroalkyl substances (PFAS) with chemically inert C-F bonds have been widely used in various industries thanks to their many useful properties such as both water and oil repelling property [Fujii et al., 2007]. PFAS are designed to contain different functional groups and carbon chain lengths, which imparts unique physicochemical properties and affects their affinity and reactivity [Buck et Al., 2011]. Historically, two PFAS groups, namely perfluorocarboxylic acids (PFCAs; $C_nF_{2n+1}COOH$) and perfluorosulfonic acids (PFSAs; $C_nF_{2n+1}SO_3H$) are most known. In particular, long chain PFSAs containing ≥6 carbons such as perfluorooctanesulfonic acid (PFOS) and PFCAs containing ≥ 8 carbons such as perfluorooctanoic acid (PFOA) have been popularly used [USEPA, 2017; Trojanowicz et al., 2018].

The occurrence, fate, and transformation of long chain PFAS, mainly PFOA and PFOS, have been relatively well documented [Rahman et al., 2014]. Unfortunately, but as well expected, PFAS with extraordinarily stable C-F bonds (dissociation energy of 533 kJ/mol) are rarely decomposed in the environment, presenting a huge challenge for environmental remediation [Rayne et al. 2009, Duan et al., 2020]. The challenge becomes serious especially for PFOA and PFOS as two presenting perfluoroalkyl substances due to their highly oxidized states and complete substitution of C-H bonds with C-F bonds. United States Environmental Protection Agency released a drinking water health advisory for PFOA and PFOS and limits their concentration to 70 parts per trillion in drinking water separately or in combination [USEPA, 2017].

Long chain PFAS have been phased out by manufacturers and end-users and switched to short chain surrogates which are characterized with the presence of hetero atoms and/or vulnerable C-H bonds along with short chain length, including perfluorobutane sulfonic acid (PFBS), hexafluoropropylene oxide dimer acid (HFPO-DA), and 6:2 fluorotelomer sulfonic acid (6:2 FTS) [Renner et al, 2006; Danish Ministry , 2011; Xiao et al., 2017]. For example, ammonium salt of HFPO-DA (also known as GenX) with a hetero atom O in the middle of an alkyl chain has replaced PFOA [DuPont Marketing, 2010]. The most common alternative to PFOS is 6:2 FTS with 4 C-H bonds as one of polyfluoroalkyl substances [Ritter et al., 2010]. Such alternatives and short chain PFAS recently started being detected in water [Cai et al., 2012]. Short chain PFAS can spread faster in the environment due to their high mobility [Hoisaeter et al., 2019]. Although less information is available regarding their adverse health impact, short chain PFAS are assumed to be as toxic as long chain PFAS [Wang et al., 2015].

Considering the chemical stability of PFAS, photocatalytic, photochemical, sonochemical, electrochemical, radiochemical, thermochemical, subcritical, and plasma treatment processes have been studied for destroying PFAS in water [Chen et al., 2006; Tang et al., 2012; Dong et al., 2015; Chen et al., 2015; Chen et al., 2016; Wang et al., 2017; Fujishima et al., 2000]. Those advanced oxidation processes introduce powerful radicals such as hydroxyl (HRs; $^{\bullet}OH$) and sulfate radicals (SRs; $SO_4^{\bullet-}$) to decompose PFAS, along with other decomposition mechanisms [Chen et al., 2006; Tang et al., 2012]. Especially titanium dioxide (TiO_2)-based photocatalysis has shown effective degradation and defluorination of PFAS and other halogenated chemicals under ultraviolet (UV) irradiation [Fujishima et al., 2000; Dong et al., 2015; Chen et al., 2015; Chen et al., 2016]. Long chain PFAS, especially PFCAs, have been the centre of the research (but limited information is still available) while the reactivity of emerging short chain PFAS and their treatability by TiO_2

photocatalysis are less known [Wang et al., 2017]. In general, short chain and polyfluoro ones are expected to be relatively easier to decompose than counter parts, i.e., long chain and perfluoro ones, due to the presences of overall less C-F bonds and more C-H bonds. However, previous work reported that short chain PFAS are as nearly resistant to chemical oxidation as PFOA and PFOS [Park et al., 2009].

In the context that the photocatalytic decomposition of emerging short chain PFAS should be revealed and compared with that of conventional long chain PFAS, this present study reports the reactivity of 9 PFAS, including 4 PFCAs, 3 PFSAs, GenX, and 6:2 FTS and specifically the dependency of the photocatalytic decomposition of PFAS on their chain lengths, functional groups, and structural properties. In addition, various chemical oxidants and reductants, such as hydrogen peroxide, PS, and sulfite, which can also be activated by UV to generate secondary reactive species, were introduced to induce the photochemical decomposition of PFAS and thus to combine it with the photocatalytic decomposition of PFAS, expecting a synergistic effect. Reactive species and reaction byproducts were identified to elucidate the decomposition mechanism of PFAS.

As a result, this study would provide comprehensive information on the dependency of photocatalytic and photochemical decomposition of PFAS on their chain lengths, functional groups, and structural properties and thus help to establish powerful destructive chemical treatment approaches toward PFAS in water.

3.2. Materials and Methods

3.2.1. Chemicals

Perfluorooctanoic acid (PFOA; C8F15O2H; CAS 335-67-1), Perfluorooctanesulfonic acid (PFOS; C8F17SO3K; CAS 2795-39-3), Perfluorobutanesulfonic acid (PFBS; C4F9SO3K; CAS 2940-49-3), perfluorononanoic acid (PFNA; $C_9F_{17}O_2H$; CAS 375-95-1), and perfluorobutanoic acid (PFBA; C_3F_7COOH; CAS 375-22-4) were obtained from Sigma-Aldrich (St. Louis, MO). Perfluoroheptanoic acid (PFHpA; $C_7F_{13}O_2H$; CAS 375-85-9), 6:2 FTS (1H,1H,2H,2H-perfluorooctane sulfonic acid; $C_8H_5F_{13}O_3S$; CAS 27619-97-2), and GenX (undecafluoro-2-methyl-3-oxahexanoic acid; $C_6HF_{11}O_3$; CAS 13252-13-6) were purchased from Synquest Laboratories (Alachua, FL) while perfluorohexane sulfonic acid (PFHxS; $C_6F_{13}SO_3K$; CAS 3871-99-6) was obtained from Frontier Scientific (Logan, UT). Sodium persulfate (PS; $Na_2S_2O_8$), sodium sulfite (Na_2SO_3), sodium periodate ($NaIO_4$), sodium bromate ($NaBrO_3$), and sodium hydroxide (NaOH) were purchased from Sigma-Aldrich while hydrogen peroxide (H_2O_2), sodium hypochlorite (NaOCl), potassium iodide (KI), oxalic acid (OA; HO_2CCO_2H), formic acid (CH_2O_2), acetonitrile (ACN; C_2H_3N), and methanol (CH_4O) were purchased from Thermo Fisher Scientific (Waltham, MA). TiO_2 (Degussa Aeroxide P25) was obtained from Degussa Corp (Parsippany, NJ). Water used for all experiments was Milli-Q water produced by a Millipore Milli-Q filtration system (Billerica, Massachusetts).

Large molecule separation (LMS) solid phase extraction (SPE) cartridges (25 mg, 1 mL) were purchased from Agilent Technologies (Santa Clara, CA). Polyether sulfone syringe filters (0.22 μm pore size, 13mm) manufactured by Foxx Life Sciences (Salem, NH) were purchased through Thermo Fisher Scientific. Isotopically marked standards for parent and byproduct PFAS were obtained as mixtures in methanol from Wellington Laboratories (Guelph, ON, Canada).

3.2.2. Batch experiments

All reactions were carried out in a Pyrex glass beaker with effective volume of 21 mL containing PFAS at 10 mg/L. Concentration of TiO_2 was 0.66 g/L. A 15 Watt 17-inch length lamp capable of producing 254 nm (UVC) was used as a UV source. Preliminary experiments showed that longer wavelengths such as UVA and UVB are not so effective for either photolytic or photocatalytic decomposition of PFAS. The lamp was placed on the top of the reactor, exhibiting around 6.0 mW/cm^2 UV intensity which was measured by an Ophir starlite energy meter (P/N7Z01565).

No pH was adjusted. Initial pH at around 4.5 to 7.5 and ended at 2.5-7.0 depending on the reaction conditions. Temperature was kept at around 25 $^{\circ}C$ using cooling air flow around the reactor. A magnetic stirrer was used to agitate the reaction solution. The reactor was sealed using a clear plastic cover to prevent evaporation of PFAS solution during the experiment. In most cases, dissolved oxygen (DO) was not controlled at around 3.0 mg/L. Then in order to determine the effect of DO as electron acceptor, air or nitrogen gas was purged into water to achieve oxygen-rich and oxygen-poor conditions at above 5.0 mg/L and below 1.0 mg/L, respectively. For experiments using 4.0 mM of OA as a hole scavenger, reaction solution was purged with nitrogen gas for 30 min to achieve oxygen-poor condition in advance. Oxidants such as PS, bromate, hypochlorite, iodate, hydrogen peroxide and reductants such as sulfite and iodide were added at 4.0 mM to investigate their effects on the photochemical decomposition of PFAS. Consequently, many combinatorial experiments were conducted with/without UV, TiO_2, DO, oxidant, reductant, and scavenger. At each time interval of 2, 6, 10, 24, and 48 h, aqueous sample of 800 μL was collected and filtered with 0.22 μm syringe.

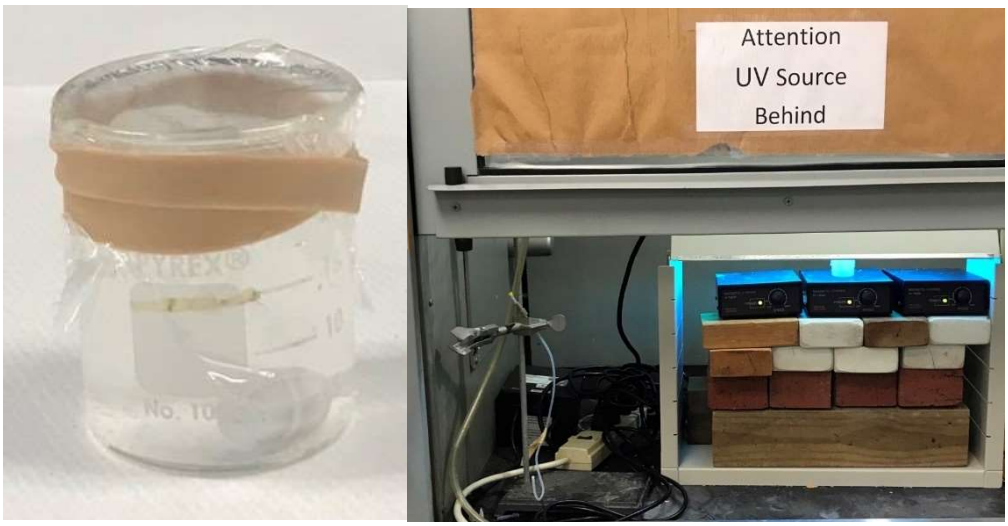

Figure 3.1. Batch TiO_2 photocatalytic experiment using pyrex glass beaker containing reaction solution sealed with plastic on magnetic stirrer under open UV source.

Some selected experiments especially with PFOA and PFOS were triplicated to notice the reproducibility of experimental results.

3.3 Results and Discussion

3.3.1. UV selection for photochemical, and photocatalytic study of PFAS

In our preliminary experiments (Figure 3.2), none of UVA, UVB, TiO_2/UVA, and TiO_2/UVB systems showed significant decomposition of PFAS (i.e., kinetically too slow) while only UVC and TiO_2/UVC exhibited certain decomposition of some PFAS, especially, long chain PFAS. Use of UVC is beneficial to electron excitation and spatial charge separation and most importantly it can cause photolysis of organic chemicals to initiate their decomposition [Furube et al., 2001; Dong et al., 2015]. This agrees with a previous study concluding that UVA and UVB absorption by PFOA in water was negligible and thus UVC and vacuum UV were effective [Chen et al., 2006].

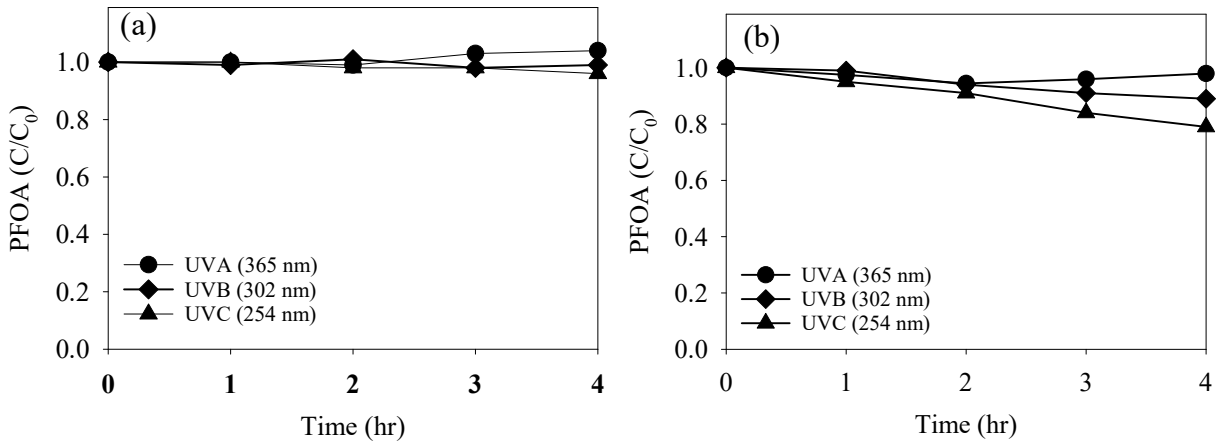

Figure 3.2. Effect of UV wavelength on **(**a**)** photolytic and (b) photocatalytical removal of PFOA (10 mg/L PFAS, initial pH around 4.5 (no pH control), and temperature 25 °C).

Although TiO_2 under UVA, UVB, or UVC irradiation can generate various reactive species such as electrons, holes, and radicals, which might be potentially involved in PFAS decomposition, only TiO_2/UVC system worked. In cases that removal of PFAS was observed, TiO_2/UVC generally showed better performance than UVC alone. We believe that there might have been UVC photolysis initiated TiO_2 photocatalysis to synergistically decompose PFAS.

In addition to photolytical and photocatalytical removal, the effect of UV wavelength in photochemical decomposition of PFOA using PS is also evaluated as seen in Figure 3.3. It shows PFOA decomposition rate at around 19%, 46% and 60% with UVA, UVB and UVC respectively.

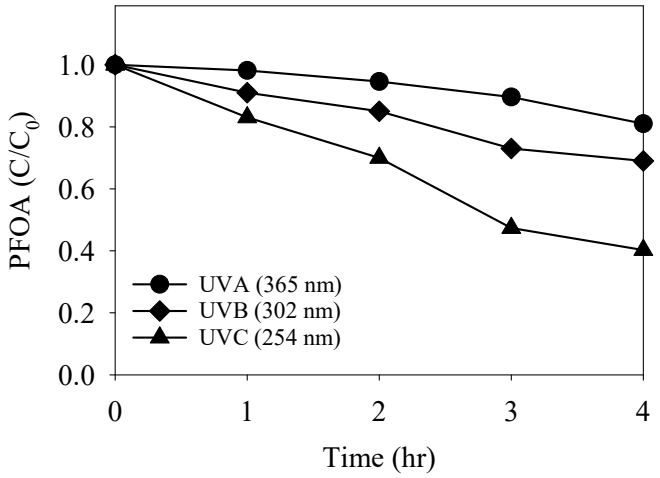

Figure 3.3. Effect of UV wavelength on photochemical removal of PFOA (10 mg/L PFAS, 4 mM PS, initial pH around 4.5 (no pH control), and temperature 25 °C).

In general, PS has strong UV absorption from deep region to visible light, therefore, it is effectively photolyzed to strong oxidizing SRs in reaction solution under all UV tested. Compared to direct photolysis and photocatalysis, addition of PS significantly enhanced PFOA degradation for all UVA, UVB and UVC irradiation. However, degradation kinetics of PFOA followed the trend as UVC> UVB>UVA, which indicates that concentration of sulfate radical formed from PS depends on UV wavelength.

As a result, UVC was used for the photolytic and photocatalytic decomposition of PFAS in this present study. Some selected experiments especially with PFOA and PFOS were triplicated to notice the reproducibility of experimental results.

3.3.2. TiO_2 photocatalyst characterization

Since the properties of P25 TiO_2 have been well documented, we briefly characterized it for confirmation purpose (Figure 3.4). It was mixture of anatase (note the diffraction peaks at 25.2 and 48.1°) and rutile (27.4, 55.0, 62.6, and 68.8°) at around 7:3 ratio.

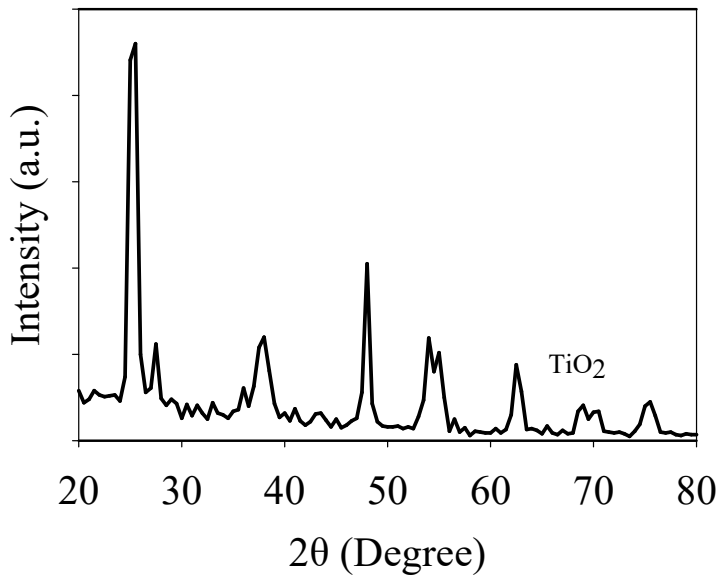

Figure 3.4. XRD peaks of TiO_2 photocatalyst

Mean size of completely segregated TiO_2 particles was measured at 29.4 nm using Horiba SZ100 nanosizer (Figure 3.5), while size of agglomerated TiO_2 particles was well above tens µm.

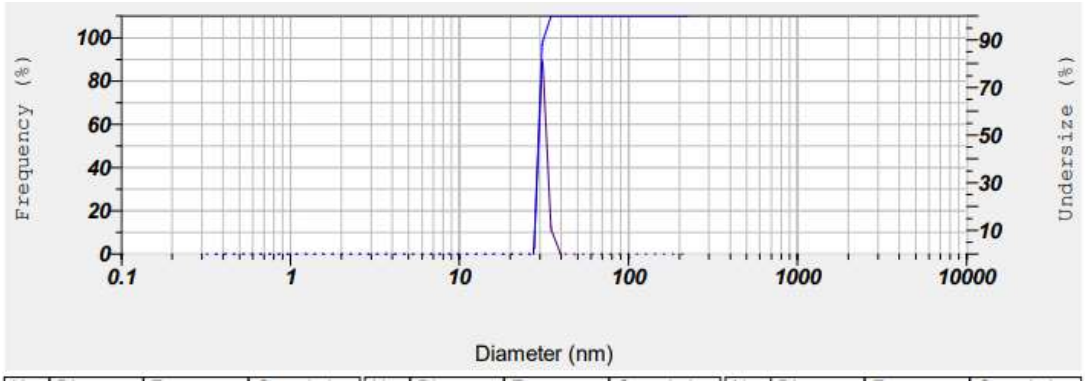

Figure 3.5: Particle size distribution of TiO_2 photocatalyst

Its UV absorption spectra spanned up to 379 nm as shown in Figure 3.6, which is equivalent to bandgap energy of 3.27 eV [Yin et al., 2003]. The surface area and pore volume of TiO_2 was 50 m^2/g and 0.173 cm^3/g, respectively.

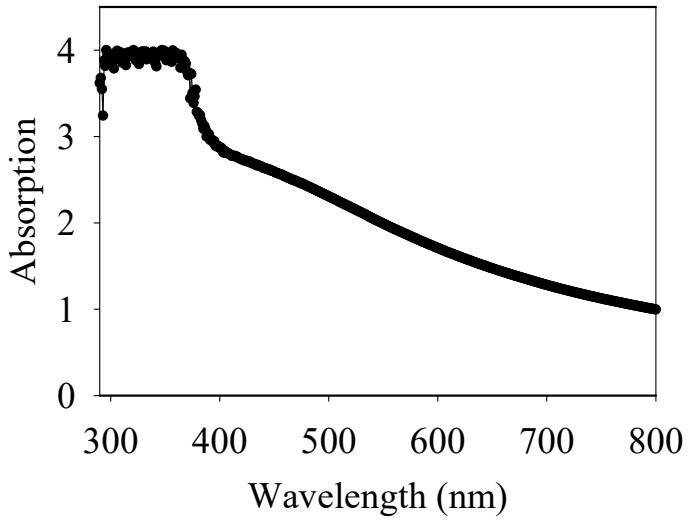

Figure 3.6. UV-vis spectra of TiO_2 photocatalyst

3.3.3. Adsorptive, photolytic, and photocatalytic removal of PFAS

Removal of PFAS via adsorption to TiO_2 and photolysis by UVC in comparison is shown in Figure 3.7(a) and Figure 3.7(b), respectively (please also note Figure 3.8 for individual PFAS). Unlike typical adsorption behavior of organic chemicals onto adsorbents, which is initial significant removal followed by quick equilibrium within several hr. [Lawal et al., 2018] adsorption of PFAS onto TiO_2 proceeded gradually even after 24 hr. (Figure 3.7(a)).

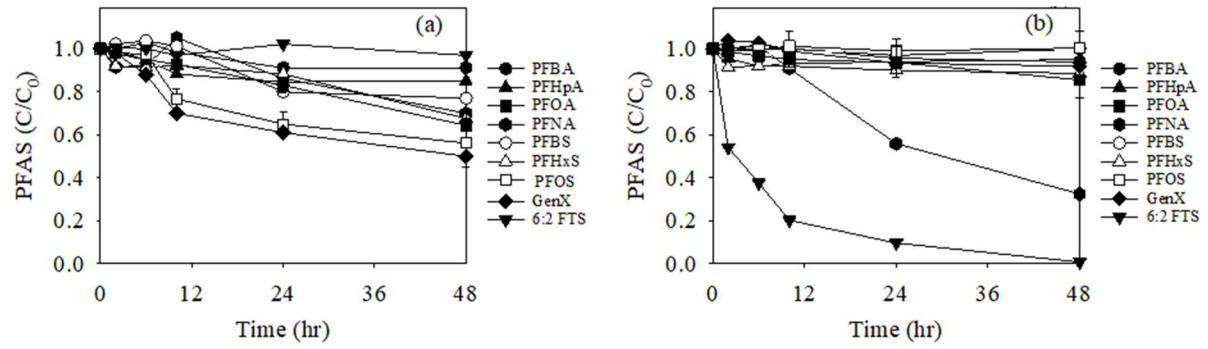

Figure 3.7. Removal of PFAS by (a) TiO_2 and (b) UVC (10 mg/L PFAS, 0.66 g/L TiO_2, initial pH varied around 4.5 to 7.5 and final pH 4.0-7.0 (no pH control), and temperature 25 °C). The error bars are the standard deviation of triplicated results for some selected experiments.

PFAS removal by adsorption ranged at 9-30% for PFCAs, 23-45% for PFSAs, 5 % for 6:2 FTS, and 50% for GenX after 48 h. Adsorption tendency was in order of PFOS > PFHxS > PFBS > 6:2 FTS within sulfonic group and GenX > PFOA ≈ PFNA > PFHxA > PFBA within carboxylic group. Within similar alkyl chain length, PFSAs were removed faster than PFCAs [Maimaiti et al., 2018; Zhao et al., 2014]. In general, adsorption process is driven by hydrophobic interaction between nonpolar tail of PFAS and hydrophobic site of adsorbents, implying that hydrophobic PFAS are beneficial to adsorption [Senevirathna et al., 2010]. The finding that long chain PFAS, except for PFNA, were removed better is supported by the fact that alkyl chain of typical PFAS is hydrophobic while their functional groups are hydrophilic, which makes long chain PFAS relatively more hydrophobic and less water-soluble than short chain PFAS [Deng et al., 2012].

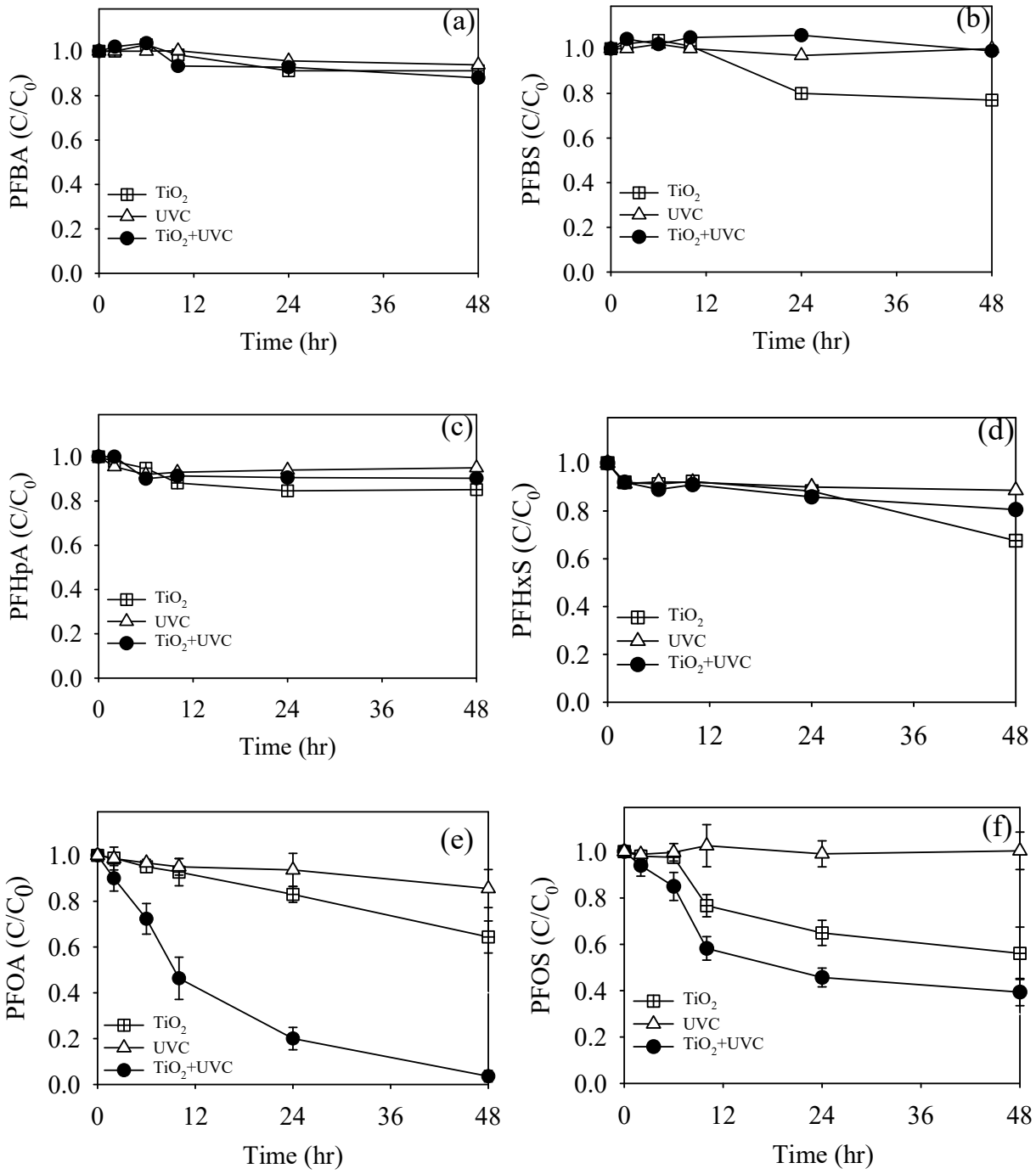
(a)
PFBA (C/C0)
Time (hr)
TiO2
UVC
TiO2+UVC
(b)
PFBS (C/C0)
(c)
PFHpA (C/C0)
(d)
PFHxS (C/C0)
(e)
PFOA (C/C0)
(f)
PFOS (C/C0)

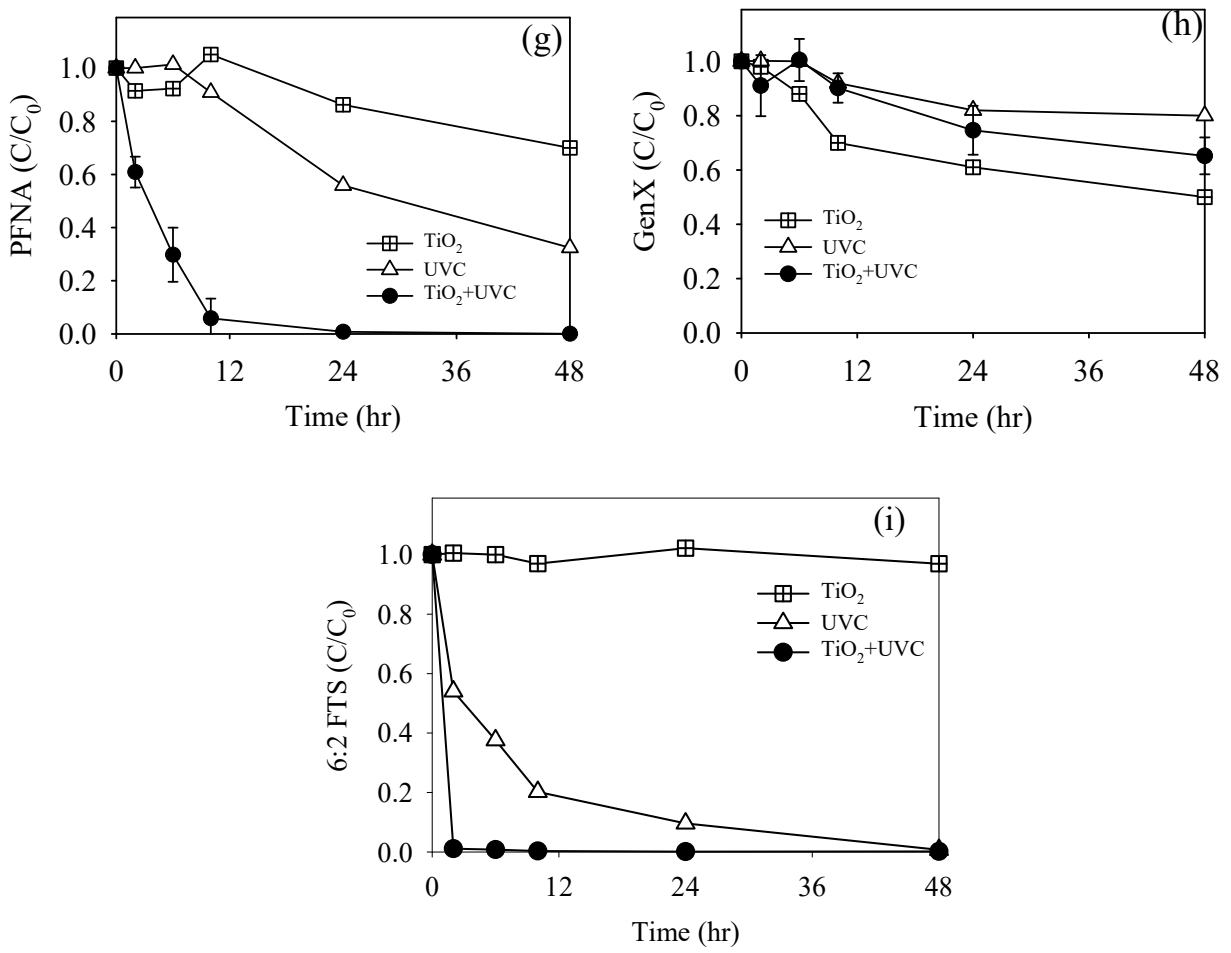

Figure 3.8. Removal of various PFAS by TiO_2, UVC, and TiO_2/UVC: (a) PFBA, (b) PFBS, (c) PFHpA, (d) PFHxS, (e) PFOA, (f) PFOS, (g) PFNA, (h) GenX, and (i) 6:2 FTS (10 mg/L PFAS, 0.66 g/L TiO_2, initial pH around 4.5-7.5 and final pH 3.0-7.0 (no pH control), and temperature 25 $^{\circ}$C). The experiments for (e) PFOA and (f) PFOS were triplicated, and (g) PFNA and (h) GenX were duplicated. The error bars are the standard deviation of triplicated results for some selected experiments.

Meanwhile, PFCAs exhibited photolysis under UVC to a certain extent (Figure 3.7(b)). For example, decomposition of PFOA and PFNA was achieved at around 15% and 68%, respectively. However, photolysis of PFSAs was negligible for 48 h. All 6:2 FTS, as a

representative of polyfluoroalkyl substances, was removed, confirming that polyfluoroalkyl substances are more susceptible to photolysis than perfluoroalkyl substances (note that 6:2 FTS also contains sulfonic group). Consequently, photolytic decomposition of PFAS under UVC was found to rely on their alkyl chain length and functional group and the presence of C-H bonds.

Results of main photocatalytic experiments with TiO_2/UVC are shown in Figure 3.9 (a). The observed removal of PFAS can be ascribed to adsorption, photolysis, and/or photocatalysis. Removal of PFAS by TiO_2/UVC, in particular long chain PFCAs and 6:2 FTS, was much enhanced compared to their removal by TiO_2 or UVC alone.

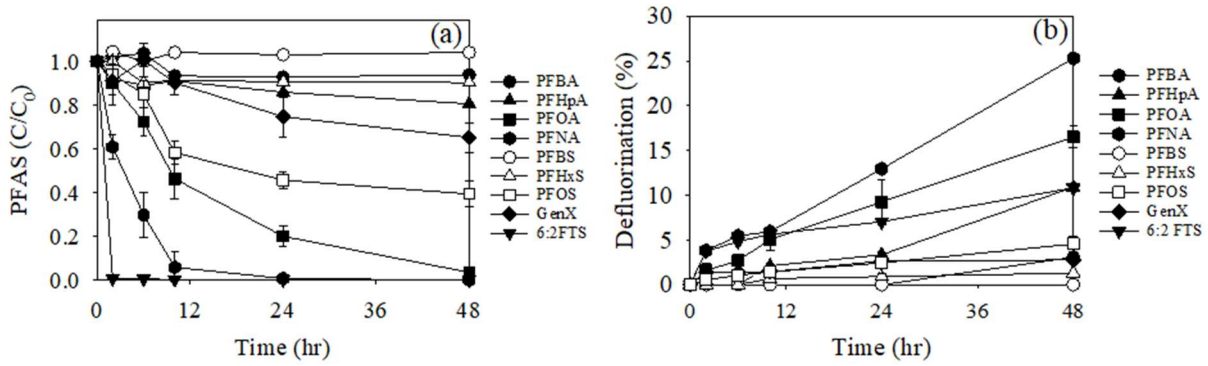

Figure 3.9. (a) Removal and (b) defluorination of PFAS by TiO_2/UVC (10 mg/L PFAS, 0.66 g/L TiO_2, initial pH around 7.5 to final pH 3.0-6.0 (no pH control), and temperature 25 °C). Defluorination % is simply calculated, based on observed F^- ion concentration in water in comparison to maximum F^- ion concentration when all fluorines are detached.

Assuming 1st order removal kinetics, rate constants (k) were calculated and summarized in Table 3.1. For PFCAs, k ranged at 0.0021-0.144 hr^{-1}; for PFSAs, k at 0.0002-0.0252 hr^{-1}; for Gen X, k at 0.0105 hr^{-1}; and for 6:2 FTS, k at 2.25 hr^{-1}. Apparently, PFNA and 6:2 FTS removal seemed not to follow 1st order.

Table1 3.1

First order removal rate constant (k) of PFAS by TiO_2/UVC*

Group	PFCAs				PFSAs			Others	
PFAS	PFBA	PFHpA	PFOA	PFNA	PFBS	PFHxS	PFOS	GenX	6:2 FTS
k(1/hr)	0.0027	0.0021	0.063	0.144	0.0002	0.0045	0.0252	0.0105	2.25

*$C=C_0 \times e^{-kt}$, where C_0 is initial concentration (mg/L) at t=0, k is 1st order rate constant (1/hr), and t is reactoin time (hr).

In general, polyfluoro one, 6:2 FTS was removed much faster than perfluoro ones; longer chain PFAS were removed faster, e.g., PFNA > PFOA > PFHpA within PFCAs and PFOS > PFHxS > PFBS within PFSAs [Park et al., 2009; Qu et al., 2016]; and PFOA as C8 was removed faster than PFOS. Although poor adsorption of 6:2 FTS and PFNA to TiO_2 was observed, they were significantly removed by TiO_2/UVC in comparison to UVC only (note Figure 3.8) and LC/MS analysis proved significant chemical decomposition of those PFAS. Unlike a general expectation that adsorption-mediated decomposition of PFAS is beneficial to fast removal of PFAS, removal of GenX and short chain PFSAs by adsorption onto TiO_2 was slightly higher than that by photocatalysis under TiO_2/UVC. 6:2 FTS and long chain PFCAs such as PFNA were removed mostly via chemical decomposition mechanism while GenX and PFSAs were removed mostly via physical adsorption mechanism. Short chain PFCAs could not be removed by TiO_2/UVC via either chemical decomposition or physical adsorption mechanism.

3.3.4. Effects of chain length and functional group

As shown in Figure 3.9(a), overall removal increased in order of 6:2 FTS > PFNA > PFOA > PFOS >> GenX > PFHpA≈ PFHxS ≈ PFBA > PFBS. In general, PFSAs and short chain PFAS

were removed much less. Bentel and co-workers explained decomposition tendency of PFAS with their bond dissociation energy (BDE) calculated using density functional theory, proposing that the α-position C-F BDE for PFCAs and the primary and secondary C-F BDE for long chain PFAS are generally lower than their counter parts [Bentel et al., 2019]. Even though both GenX and PFOA contain the same carboxylic head group, GenX (37% removal) was much more refractory than PFOA (95% removal) under the experimental conditions most probably due to the presence of a hetero atom in the middle of the alkyl chain of GenX [Bao et al., 2018]. For similar chain length of PFNA vs. PFOS or PFOA vs. PFOS, removal rates were different because of the different functional groups. Carboxylic group was more vulnerable to attack by holes and HRs than sulfonic group. 6:2 FTS, a non-fully fluorinated one with 4 C-H bonds, was removed much faster than its homologue PFOS, a fully fluorinated one.

Figure 3.9(b) shows defluorination of PFAS by TiO_2/UVC. Defluorination here describes detachment of fluorines caused by various reactions in a wide concept. Previous studies concluded that adsorption of fluoride ion onto TiO_2 surface is not significant. [Park et al., 2004] As expected, defluorination of PFAS was much slower than their removal. Defluorination ranged at around 3.1-25.3% for PFCAs, 0-5.4% for PFSAs, 2.8% for GenX, and 10.8% for 6:2 FTS. PFCAs were defluorinated faster than PFSAs and defluorination increased with increase in their carbon chain length.

3.3.5. Evolution of reaction byproducts

Only in the cases showing significant defluorination, apparent reaction byproducts were observed. Figure 3.10 shows evolution of reaction byproducts simply found in the aqueous phase. Shorter

chain PFAS were formed as identifiable PFAS through the targeted LC/MS analysis. Under the tested condition, short chain PFCAs with carbon number less than 5 were rarely identified.

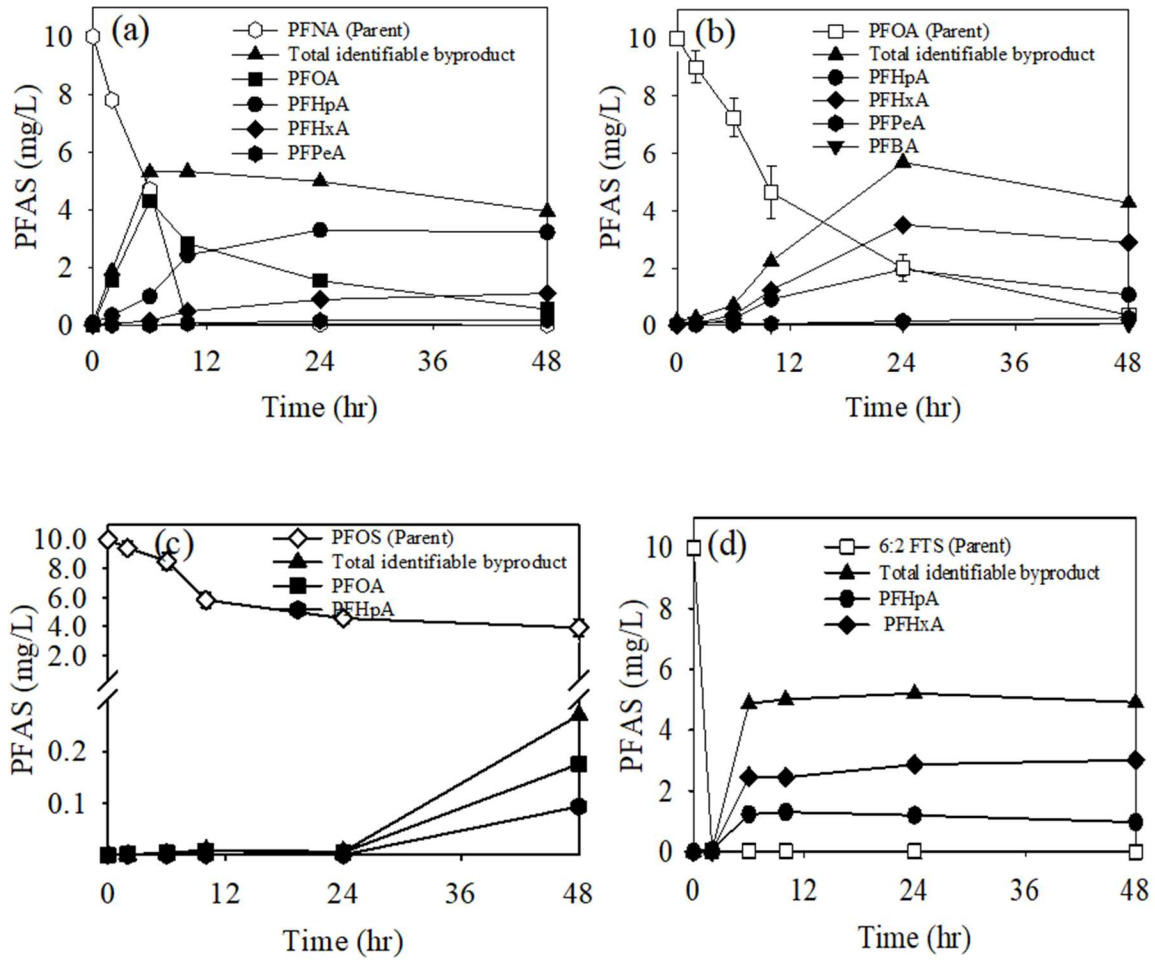

Figure 3.10. Evolution of aqueous short chain byproducts formation during decomposition of PFAS by TiO_2/UVC: (a) PFNA, (b) PFOA, (c) PFOS, and (d) 6:2 FTS (10 mg/L PFAS, 0.66 g/L TiO_2, initial pH around 7.5 to final pH 3.0-6.0 (no pH control), and temperature 25 $^{\circ}$C).

As seen in Figure 3.11, the longest PFNA (C9) was decomposed to PFOA (C8), PFHpA (C7), PFHxA (C6), and PFPeA (C5), which are all PFCAs.

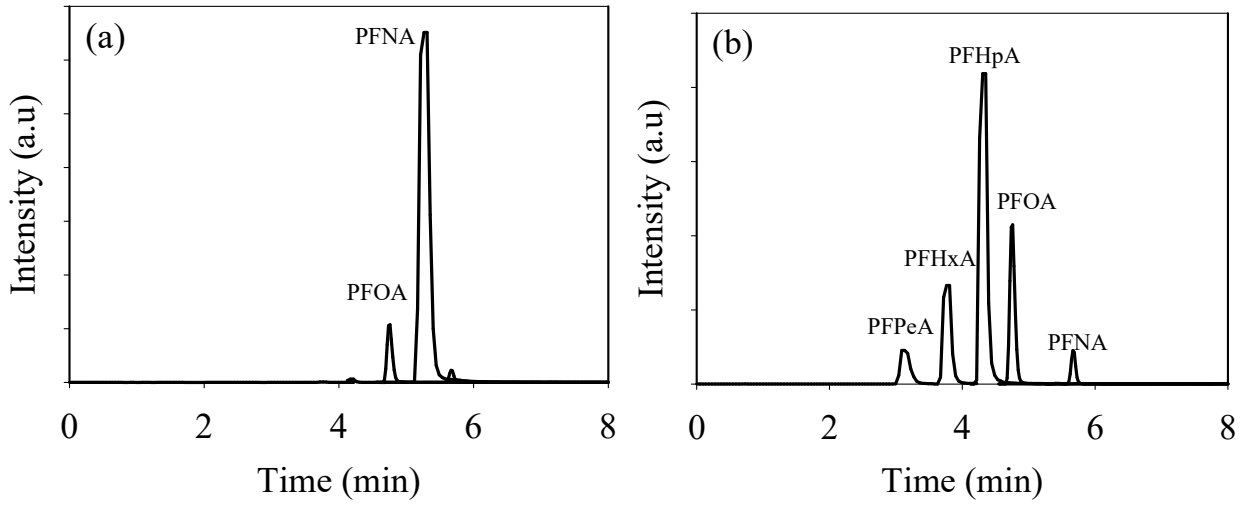

Figure 3.11: LC/MS chromatogram based on targeted analysis, showing identifiable aqueous byproducts formed during decomposition of PFNA by TiO_2/UVC: (a) O mins sample (control), (b) 48 hrs. sample (10 mg/L PFAS, 0.66 g/L TiO_2, initial pH around 7.5 (no pH control), and temperature 25 $^{\circ}$C).

Similarly, decomposition of PFOA led to the formation of subsequent short chain PFCAs. Meanwhile, PFOS (C8) was decomposed to PFOA (C8) and other shot chain PFCAs such as PFHpA (C7) (i.e., no short chain PFSAs). The presence of various peaks in the chromatogram is shown in Figure 3.12.

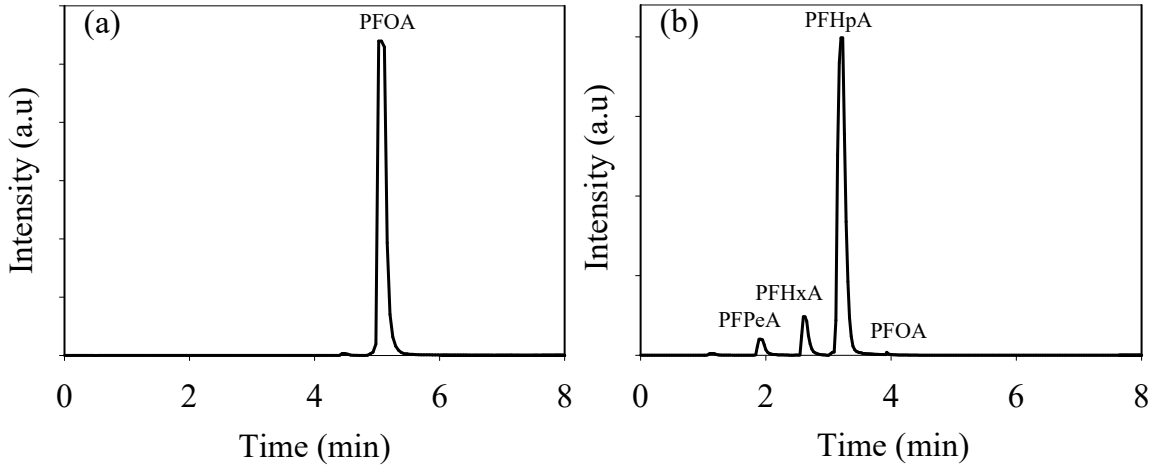

Figure 3.12: LC/MS chromatogram based on targeted analysis, showing identifiable aqueous byproducts formed during decomposition of PFOA by TiO_2/UVC: (a) O mins sample (control), (b) 48 hrs. sample (10 mg/L PFAS, 0.66 g/L TiO_2, initial pH around 7.5 (no pH control), and temperature 25 °C).

6:2 FTS (another sulfonic PFAS) was also decomposed to short chain PFCAs. Previous studies also reported the formation of shorter chain PFCAs during decomposition of both PFCAs and PFSAs [Park et al., 2016; Gu et al., 2017].

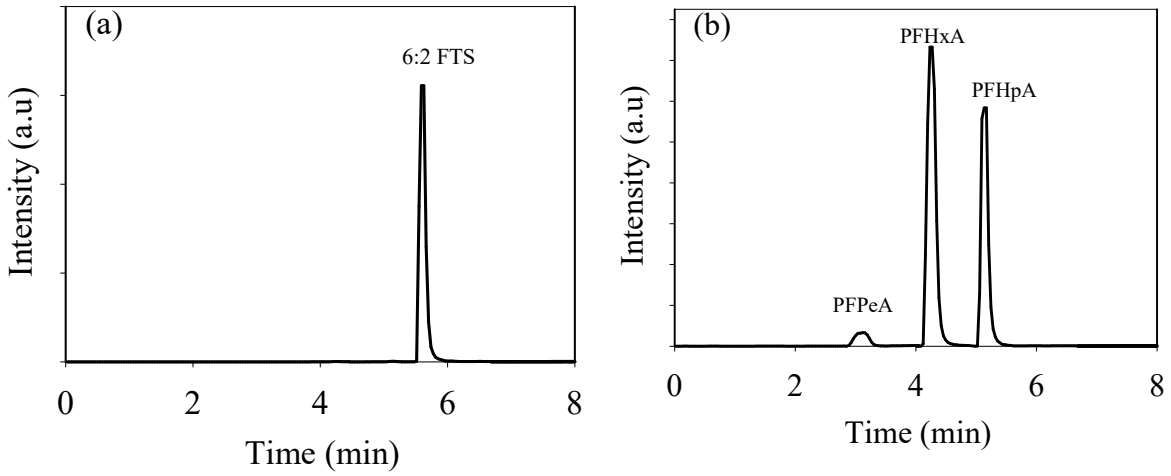

Figure 3.13. LC/MS chromatogram based on targeted analysis, showing identifiable aqueous byproducts formed during decomposition of 6:2 FTS by TiO_2/UVC: (a) O mins sample (control), (b) 48 hrs. sample (10 mg/L PFAS, 0.66 g/L TiO_2, initial pH around 7.5 (no pH control), and temperature 25 °C).

Primary reactive species such as electrons and holes are generated by TiO_2/UVC (Eq. 3.1). Then photocatalysis of PFAS, in particular PFCAs here, starts with ionization and formation of perfluoroalkyl anions (Eq. 3.2) which are oxidized to perfluoroperoxy radicals by holes (Eq. 3.3) [Dillert et al., 2007]. The unstable perfluoroperoxy radicals undergo photo-Kolbe decarboxylation

to form perfluoroalkyl radicals (Eq. 3.4) which are further oxidized to form one-CF_2-shortened PFCA (Eq. 3.5) [[Kutsuna et al, 2007; Panchangam et al., 2009]. This cycle repeats to from shorter chain PFCAs, and presumably, radicals generated such as HRs are also involved in the decomposition of PFCAs.

$$TiO_2 + h\nu \rightarrow e^- + h^+ \quad (3.1)$$

$$F(CF_2)_nCOOH \rightarrow F(CF_2)_nCOO^- + H^+ \quad (3.2)$$

$$F(CF_2)_nCOO^- + h^+ \rightarrow F(CF_2)_nCOO^\bullet \quad (3.3)$$

$$F(CF_2)_nCOO^\bullet \rightarrow F(CF_2)_n^\bullet + CO_2 \quad (3.4)$$

$$F(CF_2)_n^\bullet + O_2 \rightarrow F(CF_2)_{n-1}COO^- + 2F^- \quad (3.5)$$

In Figure 3.10, the discrepancy between parent PFAS removed from the aqueous phase (10 mg/L of $PFAS_0$ - $PFAS_t$) and total identifiable aqueous byproducts can be explained by various factors including mainly adsorption of PFAS and byproducts to TiO_2 surface and partially and possibly presence of non-identifiable byproducts, complete mineralization, and loss due to formation of volatile byproducts [Parenky et al., 2020]. Total identifiable byproducts explained nearly 40-50% of PFNA and 6:2 FTS completely removed for 48 h. Similarly, around 42% (4.2 mg/L) of removed PFOA in 48 h was turned into total identifiable byproducts and around 16% defluorination was observed. These all results implied significant photocatalytic decomposition of PFNA, 6:2 FTS, and PFOA. Meanwhile, significant removal of PFOS at 62% (from 10 mg/L to around 3.8 mg/L) was observed in 48 h while total identifiable aqueous byproducts (i.e., sum of C7-C8) accounted for only 2.7%. Among several reasons mentioned above, adsorption of PFOS to TiO_2 surface was thus proposed to explain the observed PFOS removal, which was also supported by low defluorination at around 5.4%. Figure 3-14 shows that there is no formation of reaction by products in photocatalytic removal of PFOS.

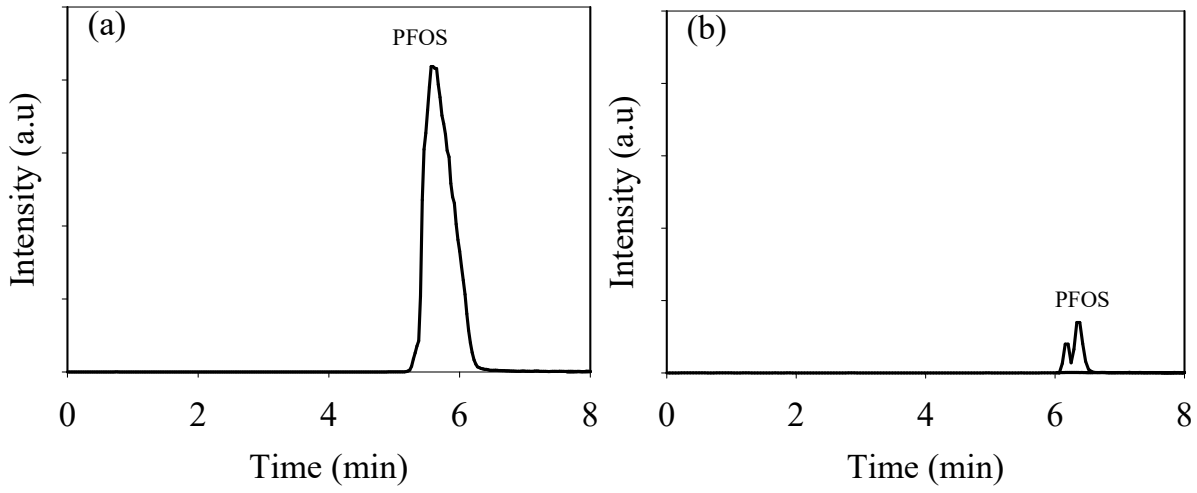

Figure 3.14: LC/MS chromatogram based on targeted analysis, showing identifiable aqueous byproducts formed during removal of PFOS by TiO_2/UVC: (a) O mins sample (control), (b) 48 hrs. sample (10 mg/L PFAS, 0.66 g/L TiO_2, initial pH around 7.5 (no pH control), and temperature 25 °C).

Long chain byproducts were present at higher levels for the tested time frame, which confirms the stepwise decomposition of PFAS, in particular PFCAs and PFSAs, via the photo-Kolbe decarboxylation proposed in Eqs. 3.1-3.5 while decomposition of 6:2 FTS might have started at C-H bonds via hydrogen abstraction reaction.

Figure 3.15 shows TOC removal in the aqueous phase containing PFOA and PFOS. If chemical reactions really occur to decompose organic chemicals, decrease in aqueous TOC is directly due to mineralization of organic chemicals (i.e., PFOA and, if any, reaction intermediates) completely into H_2O, CO_2, and many other simple inorganic species. In this case, TOC removal should be substantially slower than PFOA removal or disappearance in water, as typically observed [Eskandarian et al., 2016].

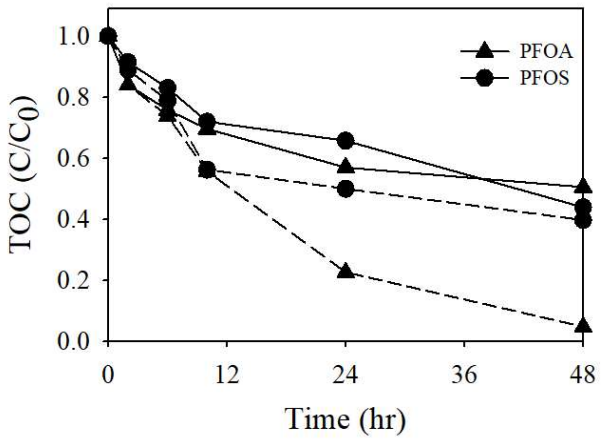

Figure 3.15. TOC removal of PFAS by TiO_2/UVC (10 mg/L PFAS, 0.66 g/L TiO_2, initial pH around 7.5 to final pH 3.0-6.0 (no pH control), and temperature 25 °C).

In Figure 3.15, TOC removal is compared with PFAS removal, which is extracted from Figure 3.9 and expressed with empty dots with dashed lines. Meanwhile, if adsorption occurs, decrease in aqueous TOC is simply due to mass transport of PFAS from water to solid TiO_2 materials. In this case, TOC removal in water should be theoretically the same as PFAS removal in water. In comparison between TOC removal in Figure 3.15 and PFOS removal in Figure 3.9, TOC removal kinetics were very similar to PFOS removal kinetics, and there was no significant retardation. The result indicates adsorption was dominant than chemical reaction for PFOS removal. However, the result is also possible for a case in which both adsorption and reaction occur at TiO_2 surface and reaction intermediates stay at the surface as adsorbed. On contrary to PFOS, PFOA removal on TiO_2 was significantly faster than TOC removal indicating chemical reaction dominant for PFOA removal.

3.3.6. Effects of reaction pH

Reaction conditions were adjusted to accelerate the PFOS removal kinetics and to elucidate the effects of operational parameters. As a result, PFOS removal by TiO_2 was examined at different pH. As shown in Figure 3.16, initial pH (7.5 neutral) was adjusted at 2.5 (acidic) and 10.5 (basic) using HCl and NaOH without using any buffer species.

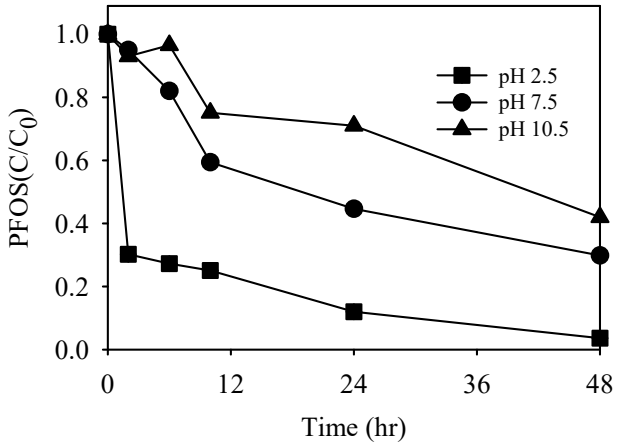

Figure 3.16: PFOS removal by TiO_2/UVC at different pH (10 mg/L PFAS, 0.66 g/L TiO_2, and temperature 25 °C).

TiO_2 showed better PFOS removal at acidic pH. PFOS removal was increased from 30% at neutral pH to 96% at pH 2.5, while basic pH 10.5 is not beneficial for PFOS removal. The same pH dependence of the removal rate was observed for the photocatalytic degradation by previous researchers, who explained with a surface complexation model involving increasing concentrations of PFAS surface complexes with decreasing pH [Qu et al., 2014]. However, it should be noted that the oxidative power of the valence band holes in TiO_2 is also pH-dependent and increases as the pH decreases. Consequently, the observed dependence of reaction rates on the pH can be rationalized in part by the fact that the pH value has an impact on the adsorption characteristics of the acid on the catalyst surface (electrostatic attraction between the positively

charged semiconductor particle and the negatively charged perfluorinated), on the formation of surface complexes, and on the oxidative power of the photocatalyst.

3.3.7. Effects of electron and hole scavengers

In order to study the removal mechanisms of PFAS by TiO_2/UVC, DO was controlled and OA was added as scavengers of photogenerated electrons and holes, respectively, as shown in Figure 3.17. DO levels were measured at above 5.0 mg/L for air purging and below 1.0 mg/L for N_2 purging. DO significantly affected decomposition and defluorination of PFOA and PFOS. PFOA was removed at 99% in DO-rich condition in 48 hr, while it was removed only at around 60% in DO-poor condition. Similarly, 99% of PFOS removal was decreased to around 27%.

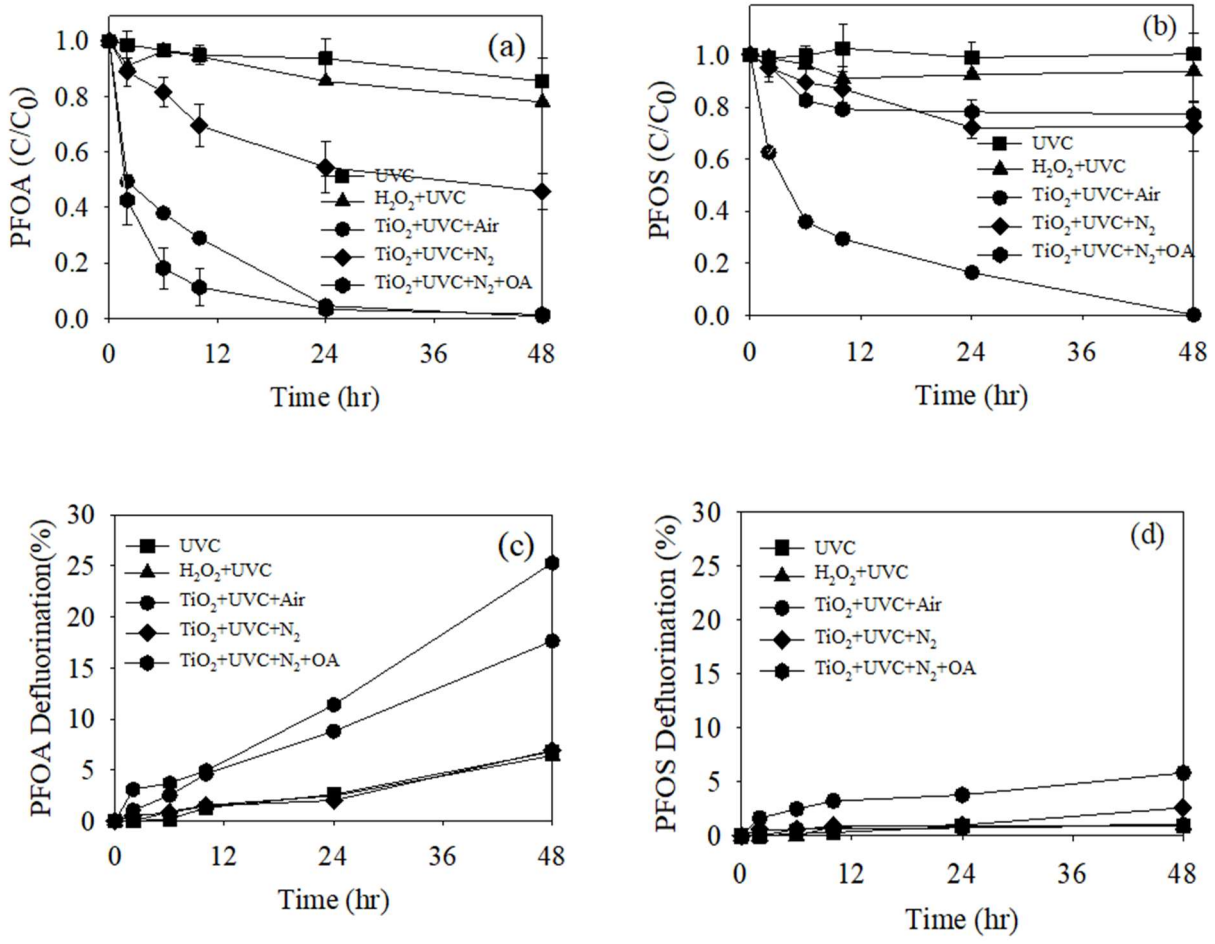

Figure 3.17. Removal of (a) PFOA and (b) PFOS and defluorination of (c) PFOA and (d) PFOS by TiO_2 /UVC in the presence of oxygen (air) as electron scavenger and oxalic acid (OA) as hole scavenger (10 mg/L PFAS, 0.66 g/L TiO_2, 1.5 g/L H_2O_2, 3 mM OA, air: initial DO at above 5 mg/L, N_2: initial DO at below 1 mg/L, no DO control for others: initial DO at around 3.0 mg/L, initial pH around 4.5-7.5 to final pH 3.0-7.0 (no pH control), and temperature 25 °C).

In general, oxygen prevents recombination of photogenerated electrons and holes and accepts electrons in the conduction band of TiO_2 to generate superoxide radical anions ($O_2^{\bullet-}$), which are strong reducing species and can be further protonated to form hydroperoxyl radical ($HO_2^{\bullet}$) and subsequently H_2O_2 (Eq. 3.6) [Sansotera et al., 2015]. However, previous studies reported that $O_2^{\bullet-}$ and $^{\bullet}OH$ are not so effective in decomposing PFAS [Maruthamuthu et al. 1995; Qiuying et al., 2019]. PFAS generally stay in an anionic form in water. Removal of PFAS via adsorption and/or decomposition was enhanced in DO rich condition presumably because TiO_2 surface becomes more positively charged when electrons are trapped by oxygen. Higher removal of PFOA and PFOS in DO-rich condition demonstrated greater defluorination. As expected, defluorination of PFOS was not significant at 5.8% and 2.6% in DO-rich and DO-poor conditions, respectively, proposing that adsorption of PFOS to TiO_2 was main mechanism for its removal which was significantly influenced by DO level. High electron and hole recombination in DO-poor condition reduces net positive charge of TiO_2 surface, which may substantially reduce PFOS removal via adsorption mechanism.

$$O_2 + e^- \rightarrow O_2^{\bullet-} \rightarrow HO_2^{\bullet} \rightarrow H_2O_2 \quad (3.6)$$

$$C_2O_4^{2-} + h^+ \rightarrow CO_2 + CO_2^{\bullet-} \quad (3.7)$$

$$H_2O_2 + h\nu \rightarrow 2^{\bullet}OH \quad (3.8)$$

Meanwhile, holes in the valance band of TiO_2 were assumed to be one of the main oxidizing species. OA was added as a hole scavenger in DO-poor condition. OA significantly enhanced PFOA removal from 60% to 100% while it did not affect PFOS removal at around 26%. In general, OA quickly donates electrons to photogenerated holes, resulting in formation of CO_2 and carbonyl radical ($CO_2^{\bullet-}$) in DO-poor condition (Eq. 3.7). This makes photogenerated electrons to be readily available for reaction with PFAS via reduction pathways. Previous work also indicated that carbonyl radicals, along with photogenerated electrons, induce quick PFOA decomposition [Wang et al., 2011]. However, poor removal of PFOS in Figure 3.17(b) and its low defluorination in Figure 3.17(d) indicated that carbonyl radicals and conduction band electrons are not effective in decomposing PFOS. In addition, addition of OA can reduce net positive surface charge of TiO_2, resulting in less PFOS adsorption and thus rather less PFOS removal observed.

Holes also react with OH^- to yield HRs which are strong oxidizing species. To confirm the effect of HRs on PFAS removal, HRs were generated by photolysis of H_2O_2 by UVC in the absence of TiO_2 (Eq. 3.8) [Liao et al., 1995]. Removal of PFOA and PFOS under the condition was not different from that under only UVC, indicating HRs alone were ineffective to decompose PFAS. Even UVC/TiO_2 was more effective than UVC/H_2O_2 (both systems commonly generate HRs), indicating some photogenerated electrons and holes formed around TiO_2 surface may be directly involved in PFAS decomposition and TiO_2 surface-mediated reaction may exhibit better PFAS removal. These all results implied that prevention of the recombination of photogenerated electrons and holes is most important for PFAS removal and the secondary reactive species such as radicals work together with the primary reactive species such as electrons and holes.

3.3.8. Effects of various oxidants and reductants

Addition of oxidants can enhance PFAS decomposition by generating reactive species under UV radiation and later by preventing recombination of electrons and holes in TiO_2/UV system. As shown in Figure 3.18(a), PFOA was chosen as a representative PFAS, and initially $NaBrO_3$, $NaIO_4$, H_2O_2, NaOCl, and $Na_2S_2O_8$ were selected as oxidants to produce bromate, iodate, hydroxyl, hypochlorite, and sulfate radicals under UVC, respectively [Ravichandran et al., 2006]. After 4 hr, PFOA removal was achieved at 0%, 2%, 5%, 14%, and 62% with $NaBrO_3$, $NaIO_4$, H_2O_2, NaOCl and $Na_2S_2O_8$, respectively, indicating PS producing SRs was most efficient.

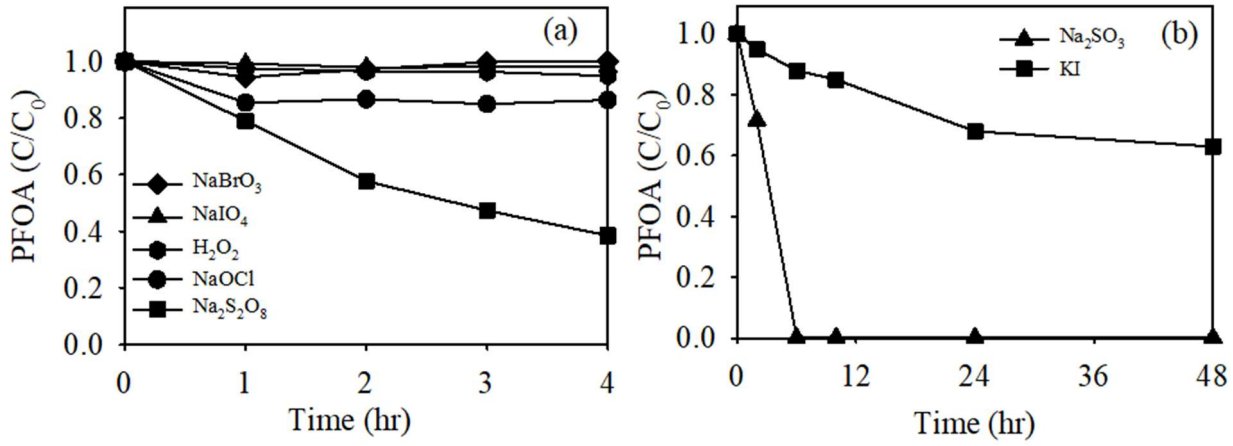

Figure 3.18. Removal of PFOA by (a) oxidants and (b) reductants under UVC irradiation (10 mg/L PFOA, 4.0 mM oxidant or reductant, initial pH 4.5 to final pH 3.0-5.0 (no pH control), and temperature 25 °C). Please note the different time scales.

Meanwhile, previous studies on phochemical decomposition of PFAS reported successful decomposition and defluorination of both PFCAs and PFSAs by using different reductants such as KI and Na_2SO_3 [Park et al., 2009; Song et al. ,2013]. As shown in Figure 3.9(b), the presence of Na_2SO_3 under UVC greatly improved PFOA removal, compared to KI.

Since PS was highly effective to remove PFOA, more detailed experiments were conducted to remove and defluorinate PFOA and PFOS, as shown in Figure 3.19. PS itself as an oxidant was not effective. In general, UV photolysis of PS produces highly reactive SRs. It is proposed that PFCAs are initially decomposed via decarboxylation reaction triggered by SRs, followed by HF elimination process, which produces one-CF_2-shortened perfluoroalkyl carboxylic acids in each step [Dogliotti et. al., 1967].

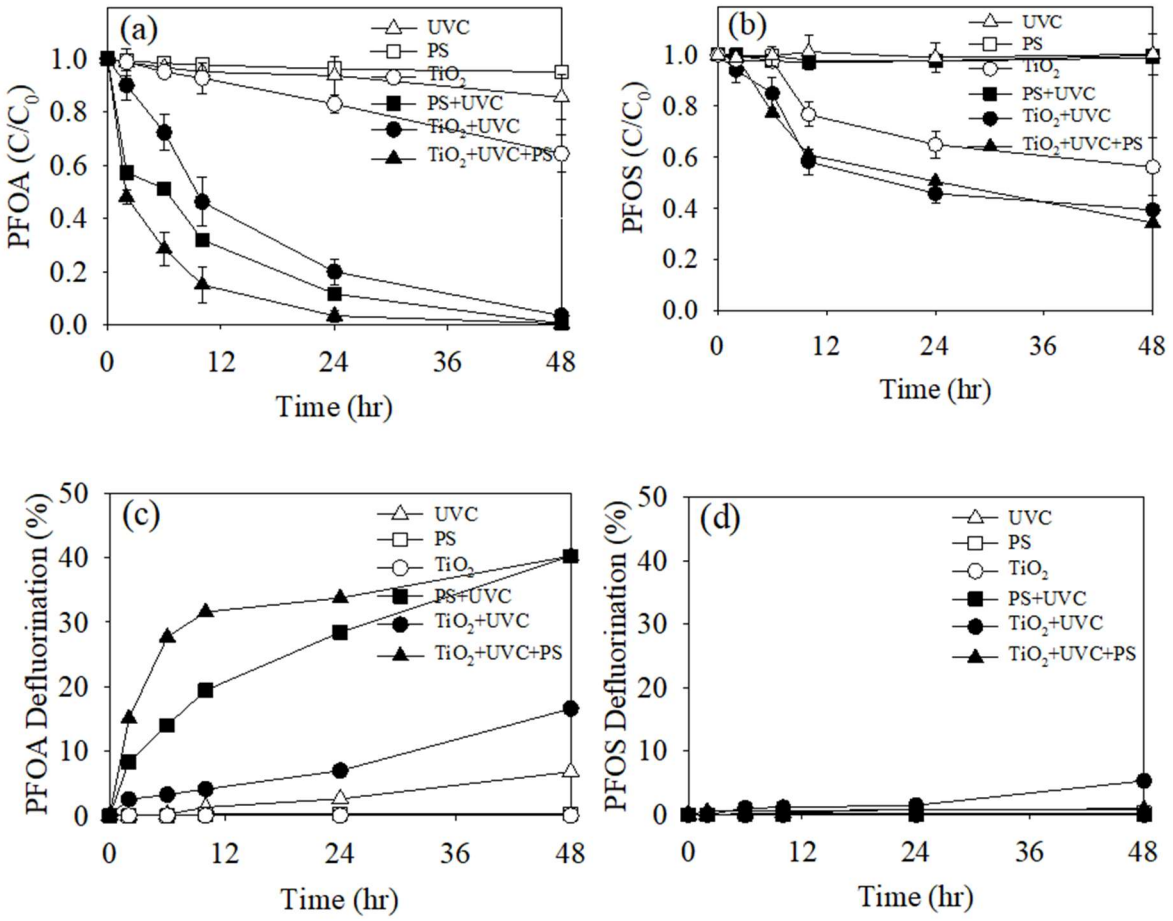

Figure 3.19. Removal of (a) PFOA and (b) PFOS and defluorination of (c) PFOA and (d) PFOS by TiO_2/UVC in the presence of PS as sulfate radical generator (10 mg/L PFAS, 0.66 g/L TiO_2, 4.0 mM PS, initial pH 4.5-7.5 to final pH around 2.5 (no pH control), and temperature 25 $^{\circ}$C).

PS/UVC producing mostly SRs was more effective to remove PFOA than TiO_2/UVC mostly producing HRs, and TiO_2/UVC/PS showed the best reactivity for PFOA. TiO_2/UVC/PS is assumed to produce various radicals such as HRs and SRs. SRs are better species than HRs for direct electron transfer reaction to decompose PFAS and reaction byproducts [Liang et al., 2009]. Degree of PFOA defluorination showed a very similar trend to that of PFOA removal. Continuous pH drops from 4.5 to 2.5 was observed in case of TiO_2/UVC/PS, resulting from presumably formation of acidic byproducts. Meanwhile, PS/UVC was not effective at all for PFOS removal while TiO_2/UVC showed comparable reactivity with PFOS to TiO_2/UVC/PS. The result indicated that SRs are ineffective for PFOS. This finding obtained was not in agreement with a previous study reporting that PFOS was decomposed faster than PFOA by PS/UV under adjusted pH 6-8 [Park et al., 2009]. The presence of PS did not help PFOS defluorination.

Then, removal of 3 PFCAs and 3 PFSAs with different chain lengths by TiO_2/UVC/PS was compared, as shown in Figure 3.20. Removal of PFSAs was confirmed to be negligible while both long and short chain PFCAs were successfully removed. Interestingly, short chain PFBA was removed faster than long chain PFOA and PFHpA in this TiO_2/UVC/PS case producing both HRs and SRs while the opposite result was obtained in the previous experiment with TiO_2/UVC producing mainly HRs. Consequently, SRs generated in this case along with HRs seemed to play an important role in decomposing PFCAs.

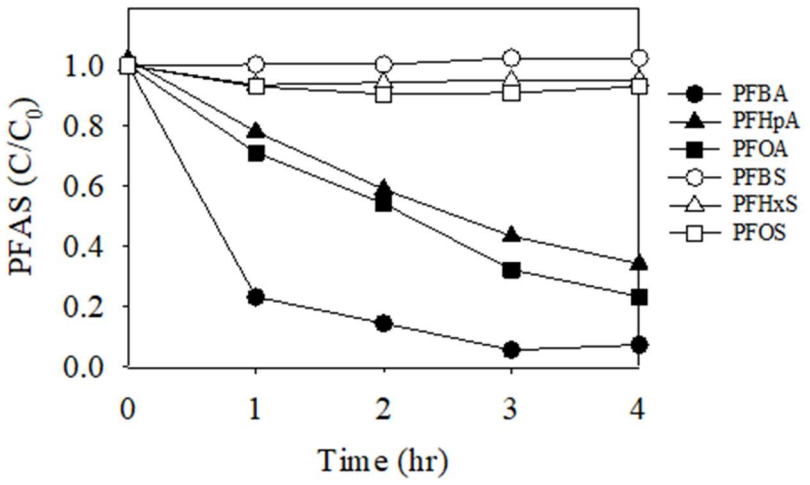

Figure 3.20. Removal of PFCAs and PFSAs by TiO_2/UVC/PS (10 mg/L PFAS, 0.66 g/L TiO_2, 4 mM PS, initial pH around 7.0 to final pH around 2.5 (no pH control), and temperature 25 °C).

Formation of short chain byproducts during decomposition of PFOA by TiO_2/UVC/PS is shown in Figure 3.21. Decomposition mechanism of PFCAs by TiO_2/UVC/PS was speculated to be very similar to that by TiO_2/UVC in Figure 3.9, i.e., gradual removal of CF_2 moieties and reformation of a carboxylic functional group [Hori et al., 2004].

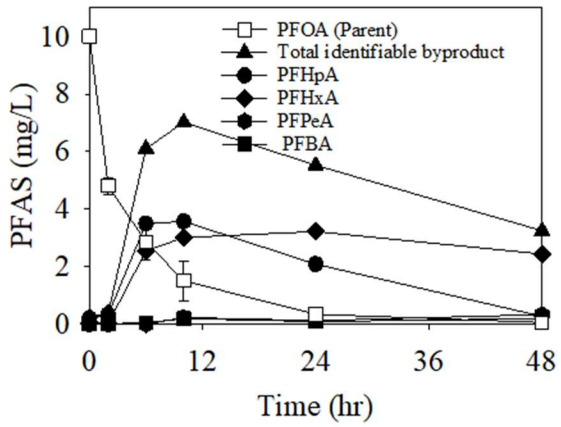

Figure 3.21. Evolution of aqueous short chain byproducts formation during decomposition of PFOA by TiO_2/UVC/PS (10 mg/L PFAS, 0.66 g/L TiO_2, 4.0 mM PS, initial pH around 4.5-7.5 to final pH around 2.5 (no pH control), and temperature 25 °C).

LC/MS chromatogram during removal of PFOA and PFOS by TiO_2/UVC/PS are shown in Figure 3.22. It shows the presence of short chain PFCAs during removal of PFOA, but that there is no formation of reaction by products during removal of PFOS.

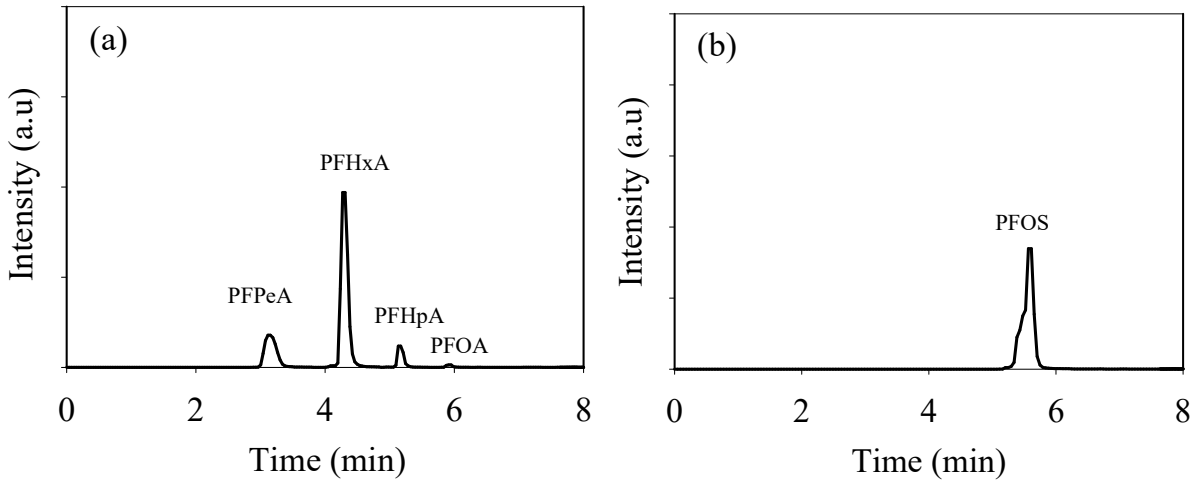

Figure 3.22: LC/MS chromatogram based on targeted analysis, showing identifiable aqueous byproducts formed during removal of (a) PFOA, (b) PFOS by TiO_2/UVC/PS (10 mg/L PFAS, 0.66 g/L TiO_2, initial pH around 7.5 (no pH control), and temperature 25 °C).

In comparison to addition of PS as an oxidant to TiO_2/UVC (Figure 3.20), sulfite as a reductant was introduced to TiO_2/UVC, as shown in Figure 3.23. Sulfite itself was not effective to remove PFOA and PFOS. Sulfite/UVC was most effective, followed by TiO_2/UVC/sulfite > TiO_2/UVC for PFOA and TiO_2/UVC > TiO_2/UVC/sulfite for PFOS. The observed decrease in the reactivity of sulfite with PFAS in the presence of TiO_2 might be explained partially with quenching of sulfite-mediated hydrated electrons by reactive species generated from TiO_2/UVC.

Interestingly, defluorination of both PFOA and PFOS was much more significant in cases of UVC/sulfite and TiO_2/UVC/sulfite, compared to TiO_2/UVC.

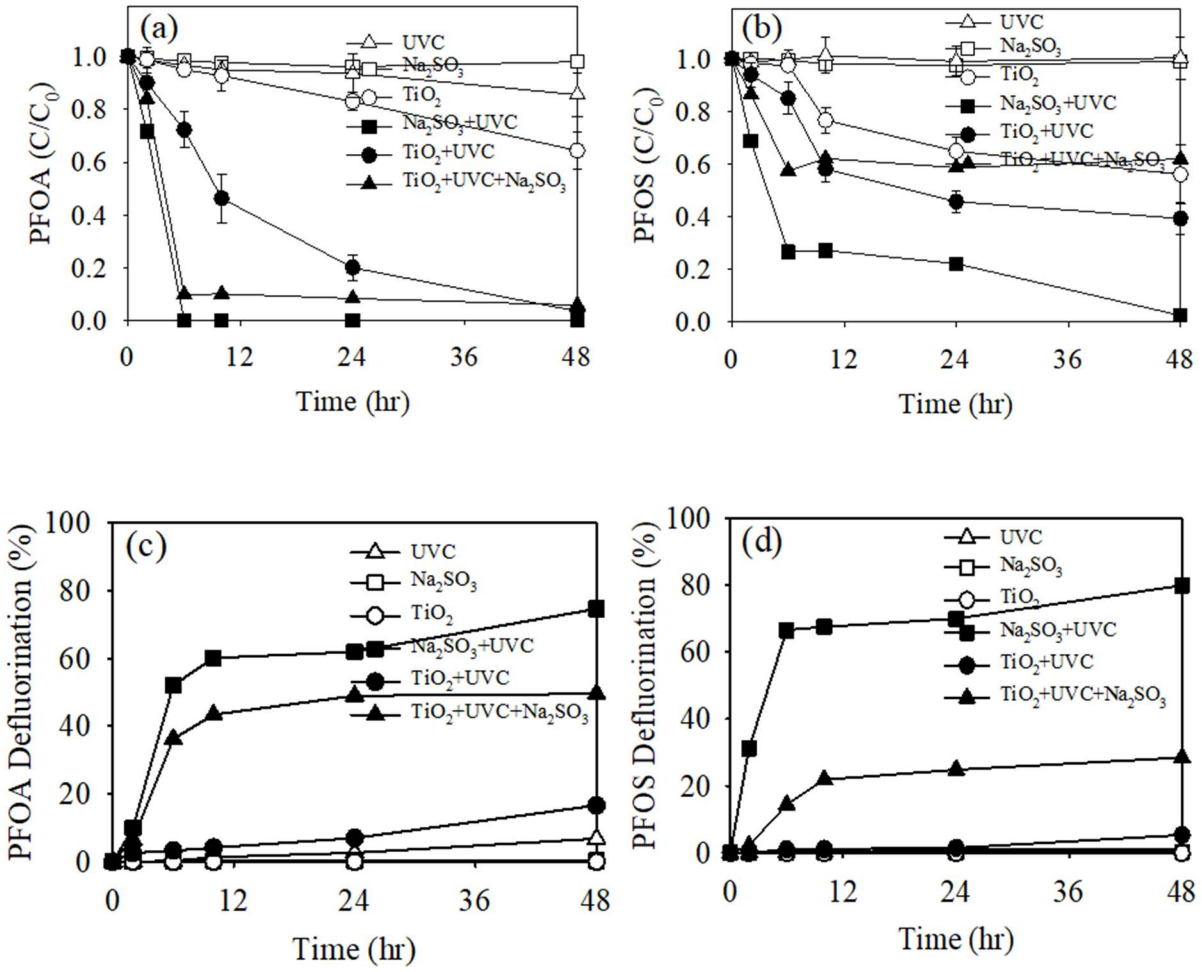

Figure 3.23. Removal of (a) PFOA and (b) PFOS and defluorination of (c) PFOA and (d) PFOS by TiO_2/UVC in the presence of sulfite (10 mg/L PFAS, 0.66 g/L TiO_2, 4.0 mM Na_2SO_3, initial pH around 4.5-7.5 to final pH around 6.0 (no pH control), and temperature 25 °C).

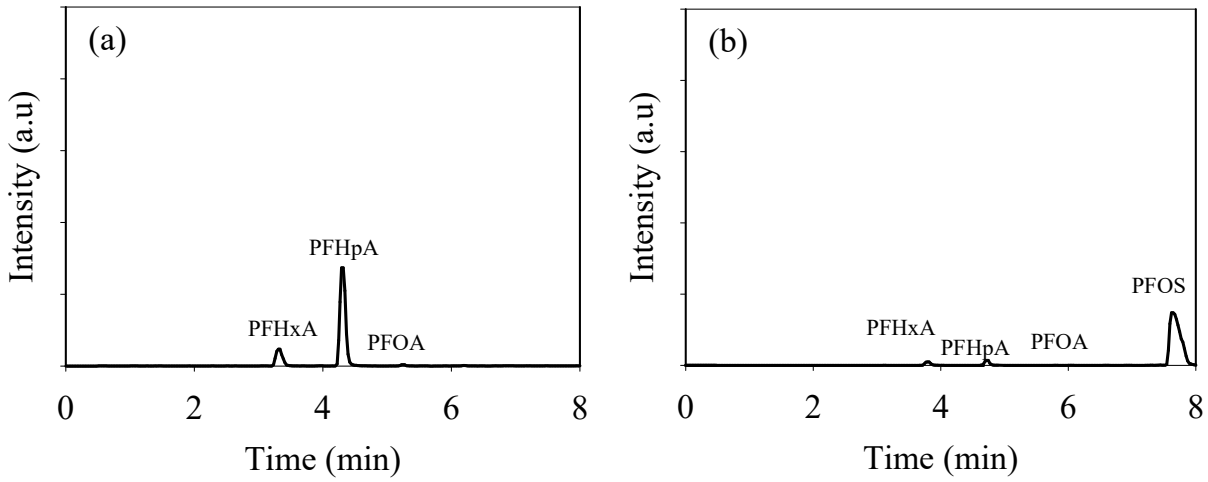

Figure 3.24: LC/MS chromatogram based on targeted analysis, showing identifiable aqueous byproducts formed during removal of (a) PFOA, (b) PFOS by TiO_2/UVC/Sulfite (10 mg/L PFAS, 0.66 g/L TiO_2, 4.0 mM Na_2SO_3, initial pH around 4.5-7.5 to final pH around 6.0 (no pH control), and temperature 25 °C).

Although PFOA was removed faster by UVC/sulfite than PFOS, defluorination of PFOS was slightly more significant. A previous study confirmed that sulfite radicals and hydrated electrons are produced (Eq. 3.9) via UV photolysis of sulfite [Fischer et al., 1996]. Considering the absence of adsorptive removal of PFOA and PFOS in the UVC/sulfite system, hydrated electrons generated from sulfite activated by UVC should have played a significant role in decomposing PFOA and PFOS. [Song et al., 2013] Important PFAS removal kinetics by PS system and sulfite system are extracted and summarized in Figure 3.25.

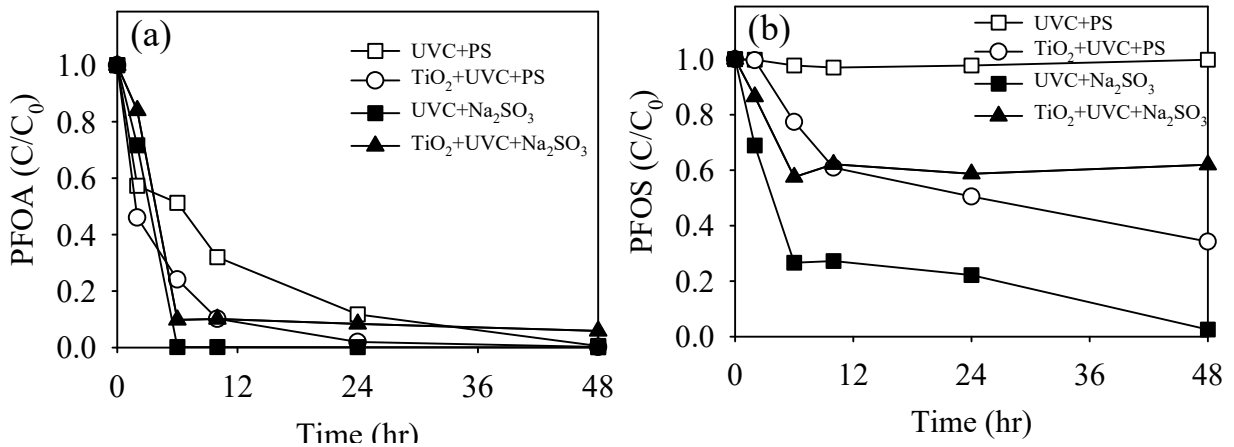

Figure 3.25. Removal of (a) PFOA and (b) PFOS via UVC and TiO_2/UVC in the presence of PS and sulfite (10 mg/L PFAS, 0.66 g/L TiO_2, 4.0 mM PS, 4.0 mM Na_2SO_3, initial around pH 4.5-7.5 to final pH 2.5-6.0 (no pH control), and temperature 25 °C).

Sulfite system, either UVC/sulfite or TiO_2/UVC/sulfite, was marginally better than PS system for PFOA removal, while sulfite system, especially UVC/sulfite, was much better than PS system for PFOS removal.

$$SO_3^{2-} + h\nu \rightarrow SO_3^{\bullet -} + e_{aq}^- \qquad (3.9)$$

3.3.9 Possible Mechanisms and Pathways of PFOA Decomposition:

Based on our observation, Eqs. 1-9, and literature, the decomposition mechanisms of PFCAs by different photocatalytic and photochemical methods are summarized in Figure 3.26.

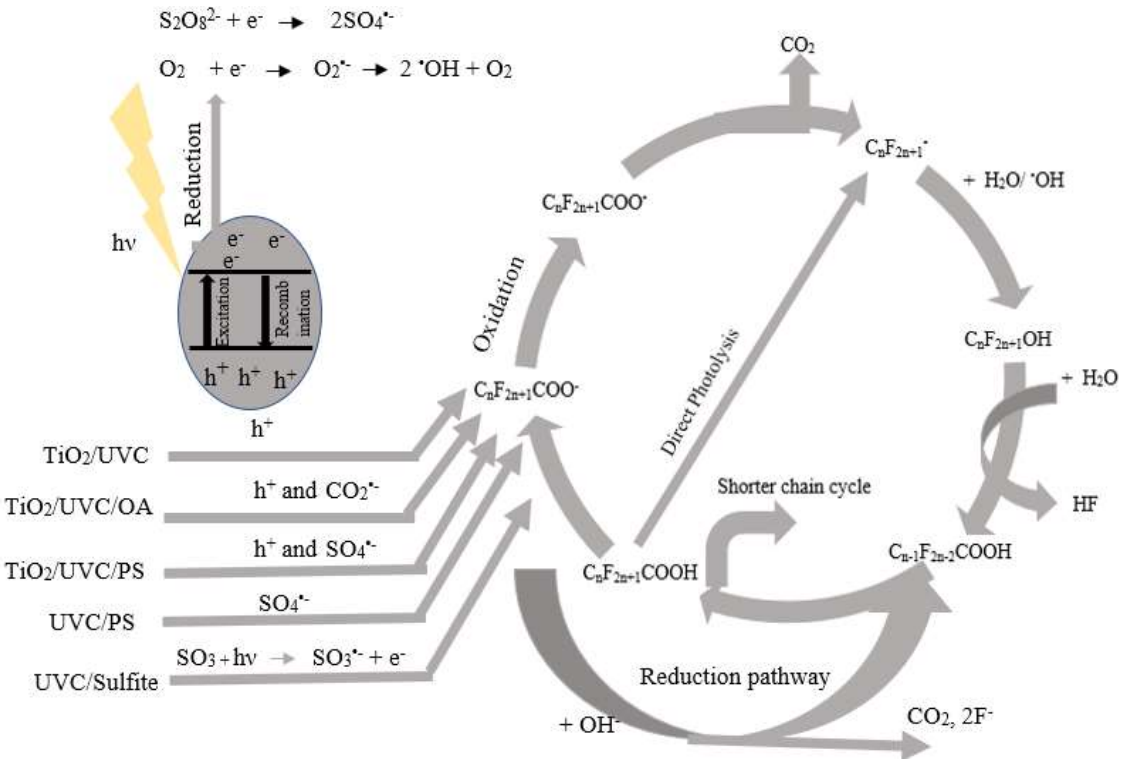

Figure 3.26. Proposed mechanisms for the photocatalytic and photochemical decomposition of PFCAs.

3.4. Conclusions

In the TiO_2/UVC system, overall PFAS removal increased in order of 6:2 FTS > PFNA > PFOA > PFOS >GenX >> PFHpA ≈ PFHxS ≈ PFBA > PFBS. A polyfluoroalkyl substance 6:2 FTS was removed faster than perfluoroalkyl ones. Longer chain PFAS were removed faster, e.g., PFNA > PFOA > PFHpA within PFCAs and PFOS > PFHxS > PFBS within PFSAs. PFOA as C8 was removed faster than PFOS. PFNA and 6:2 FTS were removed mostly via chemical decomposition mechanism while GenX and PFSAs were removed mostly via physical adsorption mechanism. Scavenger tests implied that prevention of recombination of photogenerated electrons and holes is most important for PFAS removal and the secondary reactive species such as radicals work together with the primary reactive species such as electrons and holes. SRs generated by PS seemed

to play a significant role in decomposing PFCAs. Sulfite activated by UVC worked significantly for defluorination of PFAS including even PFOS. Sulfite system was marginally better than PS system for PFOA removal while it was much better for PFOS removal. Although it is hard to explain some of the observed results, overall susceptibility of PFAS to the chemical reactions could be explained with their properties and the reactivity of reactive species produced in each system. With a best-working and affordable system, more in-depth chemistry aspects of this study as well as engineering inquiries such as TiO_2 property changes should be addressed in near future. This comprehensive study on the dependency of photocatalytic and photochemical decomposition of PFAS on their properties would help to establish powerful destructive chemical approaches toward PFAS in water.

3.5 References

[1] Bao Y., Deng, S., Jiang, X., Qu, Y., He, Y., Liu, L., Chai, Q., Mumtaz, M., Huang, J., Cagnetta, G., Yu, G., (2018). Degradation of PFOA substitute: GenX (HFPO−DA ammonium salt): oxidation with UV/persulfate or reduction with UV/sulfite; Environ. Sci. Technol., 52(20), 11728−11734.

[2] Bentel, M.J., Yu, Y., Xu, L., Li, Z., Wong, B.M., Men, Y., Liu, J., (2019). Defluorination of per- and polyfluoroalkyl substances (PFASs) with hydrated electrons: structural dependence and implications to PFAS remediation and management. Environ. Sci. Technol., 53 (7), 3718–3728.

[3] Buck, R.C., Franklin, J., Berger, U., Conder, J.M., Cousins, I.T., Voogt, P.D., Jensen, A.A.; Kannan, K., Mabury, S.A., Leeuwen, S.P. V., (2011). Perfluoroalkyl and polyfluoroalkyl substances in the environment: terminology, classification, and origins. Integr. Environ. Assess. Manag., 7 (4), 513–541.

[4] Cai, M.H., Zhao, Z., Yin, Z.G., Ahrens, L., Huang, P., Cai, M.G., Yang, H.Z., He, J.F., Sturm, R., Ebinghaus, R., Xie, Z.Y., (2012). Occurrence of perfluoroalkyl compounds in surface waters from the north pacific to the arctic ocean. Environ. Sci. Technol., 46 (2), 661–668.

[5] Chen, J., Zhang, P., (2006). Photodegradation of perfluorooctanoic acid in water under irradiation of 254 nm and 185 nm light by use of persulfate. Water Sci. Technol., 54, (11-12), 317-325.

[6] Chen, M.J., Lo, S.L., Lee, Y.C., Kuo, J., Wu, C.H., (2016). Decomposition of perfluorooctanoic acid by ultraviolet light irradiation with Pb-modified titanium dioxide. J. Hazard. Mater., 303, 111–118.

[7] Chen, M.J., Lo, S.L., Lee, Y.C, Huang, C.C., (2015). Photocatalytic decomposition of perfluorooctanoic acid by transition-metal modified titanium dioxide. J. Hazard. Mater., 288, 168–175.

[8] Danish Ministry of Environmental Protection Agency (2015). Short-chain Polyfluoroalkyl Substances (PFAS). Environmental Project No. 1707. https://cswab.org/wp-content/uploads/2018/05/Short-chain-PFAS-literature-review-Danish-EPA-2015.pdf

[9] Deng, S., Zhang, Q., Nie, Y., Wei, H., Wang, B., Huang, J.,Yu, G., Xing, B., (2012). Sorption mechanisms of perfluorinated compounds on carbon nanotubes. Environ. Pollut. 168, 138–144.

[10] Dillert, R., Bahenemann, D., Hidaka, H., (2007). Light-induced degradation of perfluorocarboxylic acids in the presence of titanium dioxide. Chemosphere, 67 (4) 785-792.

[11] Dogliotti, L., Hayon, E., (1967). Flash photolysis of persulfate ions in aqueous solutions. Study of the sulfate and ozonide radical anions. J. Phys. Chem., 71 (8), 2511-2516.

[12] Dong, H., Zeng, G., Tang, L., Fan, C., Zhang, C., He, X., He, Y., (2015). An overview on limitations of TiO_2-based particles for photocatalytic degradation of organic pollutants and the corresponding countermeasures. Water Res., 79, 128–146

[13] DuPont Marketing (2010). DuPont GenX Processing Aid for Making Fluoropolymer Resins.https://bladenonline.com/wpcontent/uploads/2017/06/Chemours_GenX_Brochure_Final_07July2010.pdf

[14] Eskandarian, Reza, M., Choi, H., Fazli, M., Rasoulifard, M.H., (2016). Effect of UV-LED Wavelengths on Direct Photolytic and TiO_2 Photocatalytic Degradation of Emerging Contaminants in Water. Chemical Engineering Journal, 300, 414-422

[15] Fischer, M., Warneck, P., (1996). Photodecomposition and photooxidation of hydrogen sulfite in aqueous solution. J. Phys. Chem., 100 (37), 15111–15117.

[16] Furube, A., Asahi, T., Masuhara, H., Yamashita, H., Anpo, M. (2001). Direct observation of a picosecond charge separation process in photoexcited platinum loaded TiO_2 particles by femtosecond diffuse reflectance spectroscopy. Chem. Phys. Lett., 336 (5-6), 424–430.

[17] Fujii, S., Tanaka, S., Lien, N.P.H, Qiu, Y., Polprasert, C., (2007). New POPs in the water environment: distribution, bioaccumulation and treatment of perfluorinated compounds—a review paper; J. Water Supply Res. Technol. AQUA, 56 (5), 313-326.

[18] Fujishima, A., Rao, T.N., Tryk, D.A., (2000). Titanium dioxide photocatalysis. J. Photochem. Photobiol. C: Photochem. Rev., 1 (1) 1–21.

[19] Gu, Y., Liu, T., Wang, H., Han, H., Dong, W., (2017), Hydrated electron based decomposition of perfluorooctane sulfonate (PFOS) in the VUV/sulfite system. Sci. Total Environ., 607–608 (2017) 541–548.

[20] Hoisaeter, A., Pfaff, A., Breedveld, G.D., (2019). Leaching and transport of PFAS from

aqueous film-forming foam (AFFF) in the unsaturated soil at a firefighting training facility under cold climatic conditions. J. Contam. Hydrol., 222, 112–122.

[21] Hori, H., Hayakawa, E., Einaga, H., Kutsuna, S., Koike, K., Ibusuki, T., Kiatagawa, H., Arakawa, R., (2004), Decomposition of environmentally persistent perfluorooctanoic acid in water by photochemical approaches. Environ. Sci. Technol., 38 (22), 6118–6124.

[22] Kutsuna, S., Hori, H., (2007). Rate constants for aqueous-phase reactions of SO^{4-} with $C_2F_5C(O)O^-$ and $C_3F_7C(O)O^-$ at 298 K. Int. J. Chem. Kinet., 39, 276-288.

[23] Lawal, W. A., Choi, H., (2018). Feasibility study on the removal of perfluorooctanoic acid by using palladium-doped nanoscale zerovalent iron. J. Environ. Eng., 144 (11), 04018115.

[24] Liang, C., Su, H.W., (2009). Identification of sulfate and hydroxyl radicals in thermally activated persulfate. Ind. Eng. Chem. Res., 48 (11), 5558–5562.

[25] Liao, C.H., Gurol, M.D., (1995). Chemical oxidation by photolytical decomposition of hydrogen peroxide. Environ. Sci. Technol., 29 (12), 3007-3014.

[26] Li, F., Duan, J., Tian, S., Ji, H., Zhu, Y., Wei, Z., Zhao, D., (2020). Short-chain per- and polyfluoroalkyl substances in aquatic systems: Occurrence, impacts and treatment. Chem. Eng. J, 380, 122506.

[27] Maimaiti, A., Deng, S., Meng, P., Wang, W., Wang, B., Huang, J., Wang, Y., Yu, G., (2018), Competitive adsorption of perfluoroalkyl substances on anion exchange resins in simulated AFFF-impacted groundwater. Chem. Eng. J., 348, 494–502.

[28] Maruthamuthu, P., Padmaja, S., Huie, R.E., (1995). Rate constants for some reactions of free radicals with haloacetates in aqueous solution. Int. J. Chem. Kinet., 27, 605–612.

[29] Park, H., Vecitis, C.D., Cheng, J., Choi, W., Mader, B.T., Hoffmann, M.R., (2009). Reductive defluorination of aqueous perfluorinated alkyl surfactants: effects of ionic

headgroup and chain length. J. Phys. Chem. A., 113 (4), 690–696.

[30] Park, H., Choi, W., (2004), Effects of TiO_2 surface fluorination on photocatalytic reactions and photoelectrochemical behaviors. J. Phys. Chem. B, 108 (13), 4086–4093.

[31] Park, S., Lee, L.S., Medina, V.F., Zull, A.,Waisner, S., (2016). Heat-activated persulfate oxidation of PFOA, 6:2 fluorotelomer sulfonate, and PFOS under conditions suitable for in-situ groundwater remediation. Chemosphere. 145, 376–383.

[32] Panchangam, S.C., Lin, A.Y., Shaik, K.L., Lin, F.C (2009). Decomposition of perfluorocarboxylic acids (PFCAs) by heterogeneous photocatalysis in acidic aqueous medium. Chemosphere, 77 (2), 242-248.

[33] Parenky, A.C., Gevaerd de Souza, N., Asgari, P., Jeon, J., Nadagouda, M.N., Choi, H., (2020). Removal of perfluorooctane sulfonic acid (PFOS) in water by combining zerovalent iron particles with common oxidants. Environ. Eng. Sci., 37 (7), 472-481.

[34] Qiuying, Y., Jiahui, J., Bin, S., Chencheng, D., Jun, L., Jinlong, Z., Mingyang, X., (2019). Singlet oxygen triggered by superoxide radicals in a molybdenum cocatalytic Fenton reaction with enhanced redox activity in the environment. Environ. Sci. Technol., 53(16), 9725–9733.

[35] Qu, R., Liu, J., Li, C., Wang, L., Wang, Z., Wu, J., (2016). Experimental and theoretical insights into the photochemical decomposition of environmentally persistent perfluorocarboxylic acids. Water Res. 104 (2016) 34-43.

[36] Qu, Y., Zhang, C., Chen, P., Zhou, Q., Zhang, W., (2014). Effect of initial solution pH on photo-induced reductive decomposition of perfluorooctanoic acid. Chemosphere, 107, 218-223.

[37] Rahman, M.F., Peldszus, S., Anderson, W.B., (2014). Behaviour and fate of perfluoroalkyl

and polyfluoroalkyl substances (PFASs) in drinking water treatment: a review. Water Res., 50, 318-340.

[38] Ravichandran, L., Selvam, K., Muruganandham, M., Swaminathan, M., (2006), Photocatalytic cleavage of C–F bond in pentafluorobenzoic acid with titanium dioxide-P25. J. Fluorine Chem., 127(9)1204-1210.

[39] Rayne, S., Forest, K. (2009). Perfluoroalkyl sulfonic and carboxylic acids: A critical review of physicochemical properties, levels and patterns in waters and wastewaters, and treatment methods. J. Environ. Sci. Heal. - Part A Toxic/Hazardous Subst. Environ. Eng., 44 (12), 1145–1199.

[40] Renner, R., (2006). The long and the short of perfluorinated replacements1 Environ. Sci. Technol., 40 (1), 12A–13A.

[41] Ritter, S.K., (2010). Fluorochemicals go short. Chem. Eng. News, 88 (5), 12–17.

[42] Sansotera, M., Persico, F., Rizzi, V., Panzeri, W., Pirola, C., Bianchi, C.L., Mele, A., Navarrini, W., (2015). The effect of oxygen in the photocatalytic oxidation pathways of perfluorooctanoic acid. J. of Fluorine Chem., 179, 159-168.

[43] Senevirathna, S.T.L.M.D., (2010) Development of effective removal methods of PFCs (perfluorinated compounds) in water by adsorption and coagulation; Japan, School of Engineering, Kyoto University., 39255785.

[44] Song, Z., Tang, H., Wang, N., Zhu, L., (2013). Reductive defluorination of perfluorooctanoic acid by hydrated electrons in a sulfite-mediated UV photochemical system; J. Hazard. Mater. 262, 332–338.

[45] Song, Z., Tang, H., Wang, N., Zhu, L., (2013). Reductive defluorination of perfluorooctanoic acid by hydrated electrons in a sulfite-mediated UV photochemical

system. J. Hazard. Mater., 262, 332–338.

[46] Tang, H., Xiang, Q., Lei, M., Yan, J., Zhu, L., Zou, J., (2012). Efficient degradation of perfluorooctanoic acid by UV-Fenton process. Chem. Eng. J., 184, 156– 162.

[47] Trojanowicz, M., Bojanowska-Czajka, A., Bartosiewicz, I., Kulisa, K., (2018). Advanced oxidation/reduction processes treatment for aqueous perfluorooctanoate (PFOA) and perfluorooctanesulfonate (PFOS): A review of recent advances. Chem. Eng. J., 336, 170–199. https://doi.org/10.1016/j.cej.2017.10.153

[48] U.S. EPA; Risk Management for Per- and Polyfluoroalkyl Substances (PFASs) under TSCA, (2017). https://www.epa.gov/assessing-and-managing-chemicals-undertsca/risk-managementand-polyfluoroalkyl-substances-pfass.

[49] USEPA; Drinking Water Health Advisories for PFOA and PFOS; (2017). https:// www.epa.gov/ground-water-and-drinking-water/drinking-water-healthadvisoriespfoa-and-pfos.

[50] Wang, Z., Cousins, I.T., Scheringer, M., Hungerbuehler, K., (2015). Hazard assessment of fluorinated alternatives to long chain perfluoroalkyl acids (PFAAs) and their precursors: status quo, ongoing challenges and possible solutions. Environ. Int., 75, 172–179.

[51] Wang, Y., Zhang, P., (2011). Photocatalytic decomposition of perfluorooctanoic acid (PFOA) by TiO_2 in the presence of oxalic acid. J. Hazard. Mater., 192 (3), 1869–1875.

[52] Wang, S., Yang, Q., Chen, F., Sun, J., Luoa, K., Yaoa, F., Wang, X., Wang, D., Lia, X., Zeng, G., (2017). Photocatalytic degradation of perfluorooctanoic acid and perfluorooctane sulfonate in water: A critical review. Chem. Eng. J., 328, 927-942.

[53] Xiao, F., (2017). Emerging poly- and perfluoroalkyl substances in the aquatic environment: A review of current literature. Water Res., 124, 482–495.

[54] Yin, S., Zhang, Q., Saito, F., Sato, T., (2003). Preparation of visible light-activated titania photocatalyst by mechanochemical method; Chem. Lett., 32 (4), 358–359.

[55] Zhao , L., Bian , J., Zhang , Y., Zhu , L., Liu, Z., (2014). Comparison of the sorption behaviors and mechanisms of perfluoro sulfonates and perfluorocarboxylic acids on three kinds of clay minerals. Chemosphere, 114, 51-58.

CHAPTER 4

Photocatalytic Degradation of Perfluorooctanoic Acid on Pb-doped TiO_2 Coated with Reduced Graphene Oxide

4.1. Introduction

Per- and polyfluoroalkyl substances (PFAS) with chemically inert C-F bonds (dissociation energy of 533 kJ/mol) have been widely used in various industries due to their useful properties such as both water and oil repelling property [Fujii et al., 2007]. According to toxicological studies, exposure to PFAS such as perfluorooctanoic acid (PFOA) can lead to liver damage, reproductive toxicity, and possibly cancer [Hinderliter et al., 2006; Potera et al., 2009]. Unfortunately, but as well-expected, PFAS are rarely decomposed in the environment, presenting a huge challenge for environmental remediation [Rayne et al., 2009; Li et al., 2020]. Various advanced oxidation processes have been studied in the last two decades for PFAS remediation in water such as photocatalytic, photochemical, sonochemical, electrochemical, radiochemical, thermochemical, and plasma treatment [Fujishima et al., 2000; Hori et al., 2005; Krusic et al., 2005; Moriwaki et al., 2005; Liao et al., 2009; Zhang et al., 2014; Obo et al., 2015].

Compared with others, photocatalytic approaches show much higher PFAS decomposition and defluorination [Wang et al., 2017]. TiO_2 is widely used as a photocatalyst because it is a readily available, inexpensive, and nontoxic compound with high chemical stability and photocatalytic reactivity [Dillert et al., 2007]. However, use of TiO_2 for photocatalytic decomposition of organic pollutants has been limited due to its relatively large band gap at 3.2 eV and fast recombination of photo-induced electron and hole pairs. Although TiO_2 photocatalysis produces hydroxyl radicals ($^{\bullet}OH$) with high oxidation potential of 2.80 eV as major oxidizing species, some PFAS

species such as PFOA have been reported to be inert to •OH because dissociation energy of C-F bonds (530 kJ mol^{-1}) in PFOA is much higher than that of C-C bonds (410 kJ mol^{-1}) [Dong et al., 2015]. As a result, TiO_2 photocatalysis has shown slow or negligible kinetics for decomposition of PFOA and others.

Significant efforts have been given to developing hybrid TiO_2 photocatalysts that can improve charge carrier separation, bandgap reduction or narrowing, and thus overall reactivity [Wang et al., 2017, Oppong et al., 2019]. For the photocatalytic decomposition of PFOA, many modifications have been reported, including lead (Pb)-doped TiO_2, copper (Cu)-doped TiO_2, iron (Fe)-doped TiO_2, platinum-doped TiO_2, TiO_2 coated with reduced graphene oxide (rGO), TiO_2 coated with multiwall carbon nanotubes, and TiO_2 immobilized onto activated carbon [Chen et al., 2016; Chen et al., 2015; Ruiz et al., Song et al., 2012; Swaminathan et al., 2010; Ravichandran et al., 2009]. Decomposition and defluorination efficiencies were generally reported in order of TiO_2-Pb > TiO_2-Cu > TiO_2-Fe > pristine TiO_2 [Chen et al., 2016]. The enhanced photoactivity of TiO_2-Pb was explained by electron trapping mechanism and oxygen (O_2) vacancies [Li et al., 2016; Bhattacharyya et al., 2020; Ismail et Al., 2007]. Meanwhile, TiO_2/rGO exhibited enhanced photocatalytic activity due to the unique two-dimensional structure of rGO such as large specific surface area, high ultraviolet (UV) absorption capacity, and excellent thermal and electrical conductivity [Dastjerdi et.al., 2010].

In order to leverage the advantages of doping TiO_2 with Pb and introducing rGO to TiO_2 such as excitation UV wavelength extension, electron-hole recombination prevention, and enhanced oxygen mobility, herein, we synthesized Pb-doped TiO_2 coated with rGO and evaluated its reactivity with PFAS. As a result, the objective of this study was to prove the enhanced photocatalytic reactivity of TiO_2-Pb/rGO with various PFAS in particular PFOA in comparison to

P25 as a bench marking TiO_2, TiO_2-Pb, TiO_2/rGO, and TiO_2-Fe/rGO. Three perfluorocarboxylic acids (PFCAs), three perfluorosulfonic acids (PFSAs), and one polyfluoroalkyl substance were examined. Reactive species, reaction byproducts, and fluoride ions were identified. To the best of our knowledge, this is the first study combining metal doping and rGO introduction for enhanced removal of PFAS. We also detailed possible decomposition mechanism of PFAS by the TiO_2-Pb/rGO system under UV at room temperature.

4.2. Materials and Methods

4.2.1. Chemicals

Perfluorooctanoic acid (**$C_8F_{15}O_2H$**; CAS 335-67-1), perfluorooctanesulfonic acid (PFOS; $C_8F_{17}SO_3K$; CAS 2795-39-3), perfluorobutanesulfonic acid (PFBS; $C_4F_9SO_3K$; CAS 2940-49-3), and perfluorobutanoic acid (PFBA; C_3F_7COOH; CAS 375-22-4) were obtained from Sigma-Aldrich (St. Louis, MO). Perfluoroheptanoic acid (PFHpA; $C_7F_{13}O_2H$; CAS 375-85-9) and 6:2 fluorotelomer sulfonate *(6:2* FTS; 1H,1H,2H,2H-perfluorooctane sulfonic acid; $C_8H_5F_{13}O_3S$; CAS 27619-97-2) were purchased from Synquest Laboratories (Alachua, FL) while perfluorohexanesulfonic acid (PFHxS; $C_6F_{13}SO_3K$; CAS 3871-99-6) was obtained from Frontier Scientific (Logan, UT). Lead nitrate ($Pb(NO_3)_2$) was obtained from Honeywell Fluka (Charlotte, NC) and rGO powder (Model# 5060512170122) was purchased from graphitene (Scunthorpe, United Kingdom). Ferric nitrate ($Fe(NO_3)_3{\cdot}9H_2O$), sodium azide (NaN_3), p-benzoquinone (p-BQ; $C_6H_4O_2$), and tert-butyl alcohol (TBA; $(CH_3)_3COH$)) were supplied by Sigma-Aldrich. Hydrogen peroxide (H_2O_2), formic acid (CH_2O_2), acetonitrile (ACN; C_2H_3N), and methanol (CH_3OH) were purchased from Thermo Fisher Scientific (Waltham, MA). TiO_2 (P25) was obtained from Degussa Corp (Parsippany, NJ). Water used for all experiments was Milli-Q water produced by a Millipore

Milli-Q system (Billerica, MA). Large molecule separation (LMS) solid phase extraction (SPE) cartridges (25 mg, 1 mL) were purchased from Agilent Technologies (Santa Clara, CA). Polyether sulfone syringes (0.22 μm pore size, 13mm) manufactured by Foxx Life Sciences (Salem, NH) were purchased through Thermo Fisher Scientific. Isotopically marked standards for parent and byproduct PFAS were obtained as mixtures in methanol from Wellington Laboratories (Guelph, ON, Canada).

4.2.2. Synthesis and characterization of TiO_2-Pb/rGO

TiO_2-Pb/rGO photocatalyst was prepared by the hydrothermal method following the procedure reported in literature [Zhou et al., 2011]. Briefly, rGO was dispersed in solution of water and ethanol (2:1) by ultrasonic treatment for 1 hr. Then, commercial P25 TiO_2 was added into 30 ml of the rGO dispersion and stirred for 2 hr. to achieve homogeneous suspension, where content of rGO was controlled to be 1% weight in TiO_2/rGO. The suspension was then placed in 40 mL Teflon-sealed autoclave and put in an oven maintaining at 120 °C for 3 hr. to deposit TiO_2 particles on rGO surface. Finally, the resulting composite was recovered by filtration, rinsed by deionized water several times, and dried at room temperature for 12 hr. Then, Pb was loaded onto TiO_2/rGO via a chemical bath deposition method. Amounts of TiO_2/rGO and Pb $(NO_3)_2$ as a Pb source were pre-determined to obtain TiO_2 and Pb ratio at 98:2 in TiO_2-Pb/rGO. TiO_2/rGO was taken into H_2O/ethanol (4:1) solution containing Pb $(NO_3)_2$ and then the mixture was stirred at 70 °C for 3 hr. The suspension was filtered, rinsed with distilled water, dried at room temperature for 12 hr, and finally annealed by heating at 400 °C for 2 hr. to form crystalline TiO_2-Pb/rGO particles.

Step 1

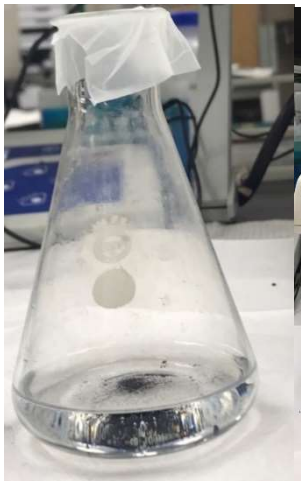

rGO in water/ethanol

Ultrasonic (1 hr.)

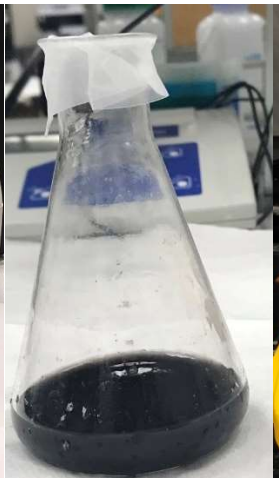

Dispersed rGO

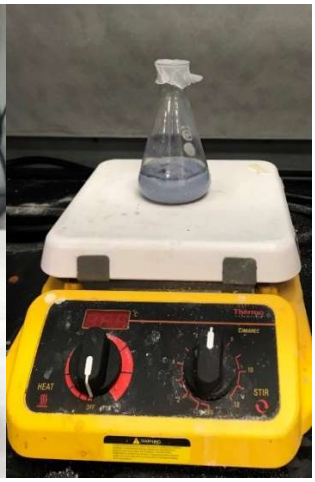

TiO_2/rGO mixing(2 hr.)

Autoclave

Heating (120 ^{0}C, 3 hr.)

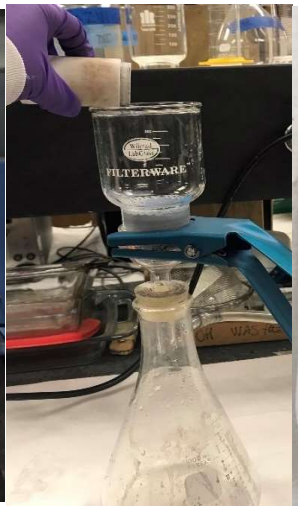

Filtration

Air dry (25 ^{0}C, 12 hr.)

Step 2

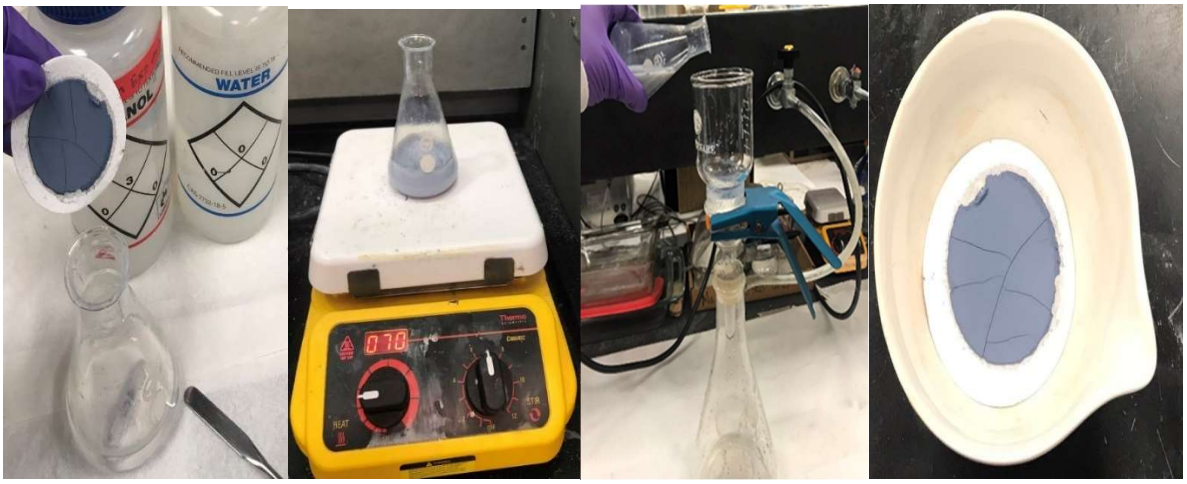

TiO_2-Pb/rGO Mixing (70 ^{0}C, 3 hr.) Filtration Air dry (25 ^{0}C, 12 hr.)

Annealed (400 ^{0}C, 2 hr.) Grinding

Figure 4.1. Synthesis of TiO_2-Pb/rGO photocatalyst

Then, TiO_2-Pb/rGO was briefly characterized to confirm its properties. X-ray diffraction (XRD) using a Bruker D8 X-Ray Diffractometer (Billerica, MA) with CuKα radiation at 1.5 Å and voltage at 40 KV was used to investigate the crystallographic properties. Scanning rate was 2°/min and scanning range was from 10 to 80°. Hitachi S-3000N (Hitachi, Tokyo) scanning electron microscope (SEM) was used to investigate the surface morphology, in combination with an energy dispersive X-ray spectroscopy (EDX) to determine the elemental composition. Light

adsorption characteristic was determined using UV-vis spectrophotometer (Shimadzu UV-2550; Kyoto, Japan). Absorption spectra were scanned from 300 to 800 nm and scanning rate was at 120 nm/min. The surface area was determined using a Tristar 3000 (Micromeritics, Norcross, GA) porosimetry analyzer employing N_2 adsorption and desorption isotherms.

4.2.3. Batch experiments

All reactions were carried out in a Pyrex glass beaker with effective volume of 21 mL containing PFAS at 10 mg/L. Concentration of photocatalysts tested was 0.33 g/L. Control experiments were conducted using other photocatalysts and materials at the same concentration. A 15 Watt 17-inch length lamp capable of producing 254 nm (UVC) was used as a UV source. Preliminary experiments showed that longer wavelengths such as UVA and UVB are ineffective for either photolytic or TiO_2 photocatalytic decomposition of PFAS. The lamp was placed on the top of the reactor, exhibiting 6.2 mW/cm^2 UV intensity measured by Ophir starlite energy meter (P/N7Z01565). No pH was adjusted to avoid any chemical and analytical interferences. Initial pH varied from around 4.5 to around 7.5 and it ended at 3.5-7.0, depending on the reaction conditions. Temperature was kept at around 25 $^{\circ}C$ using cool air flow around the reactor. A magnetic stirrer was used to agitate the reaction solution. The reactor was sealed using a clear plastic cover to prevent evaporation of PFAS solution during the experiment. Dissolved oxygen (O_2) at around 3.0 mg/L was not controlled. Radical scavengers such as TBA, pBQ, and NaN_3, and radical producers such as H_2O_2 were added at concentration of 100 mM, 4.5 mM, 7.5 mM, and 8mM, respectively, to identify and explain radicals responsible for any observed decomposition of PFAS. Consequently, many control and reference experiments were also conducted with/without UV, TiO_2, Pb, and rGO. At each time interval of 1, 2, 4, 12, and 24 hr., aqueous sample of 800 µL was collected and filtered with 0.22 µm syringe.

4. 3. Results and Discussion

Previous study and our preliminary test concluded that UVA and UVB absorption by PFOA in water was negligible [Chen et al., 2007]. As a result, UVC was used for the photolytic and photocatalytic decomposition of PFAS in this present study. **S**ome selected experiments, especially photocatalytic removal of PFOA using TiO_2, TiO_2-Pb, TiO_2/rGO and TiO_2-Pb/rGO, were triplicated. The standard deviation of triplicated results was small enough, indicating the reproducibility of the experiments.

4.3.1. Characterization data for the catalysts

Since similar materials to TiO_2-Pb/rGO, including TiO_2, TiO_2-Pb, and TiO_2/rGO, have been well characterized, [Chen et al., 2016; Ruiz et al., 2018] the properties of TiO_2-Pb/rGO were quickly checked in comparison to the base TiO_2 material, P-25. As expected, all XRD peaks of TiO_2 and TiO_2-Pb/rGO indicated combination of anatase (25.2 and 48.1°) and rutile phases (27.4, 55, 62.6, and 68.8°) according to their standard patterns (JCPDS No. 21-1272 and JCPDS No. 21-1276) (Figure 4.2). Previous studies showed that TiO_2-Pb based photocatalysts contain different Pb phases (JCPDS 78-0299) such as zero-valent lead (Pb^0 at 36.2°), lead monoxide (PbO at 28.4°), and lead dioxide (PbO_2 at 52.4°) [Kong et al., 2007; Murruni et al., 2008; Li et al. 2012]. However, those peaks were not significant for TiO_2-Pb/rGO used in this study, indicating no significant changes of the initial crystal structure after introduction of Pb most probably due to the small content of Pb at around 2%.

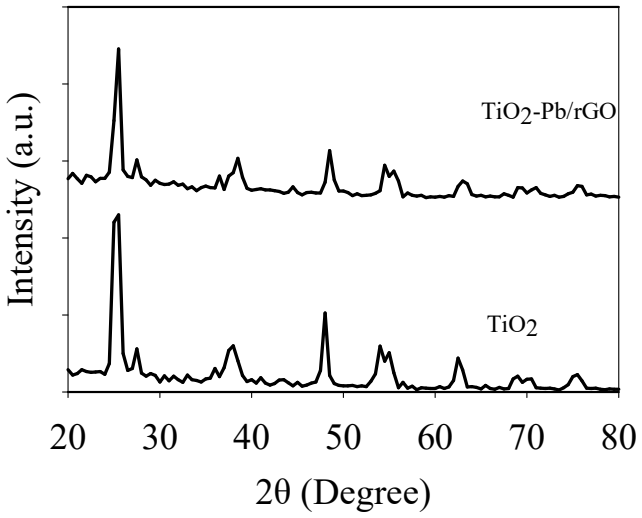

Figure 4.2. XRD patterns of TiO_2 and TiO_2-Pb/rGO photocatalysts

EDX results (Figure 4.3) showed that successful incorporation of Pb with weight contents of Pb and Ti at 1.58% and 74.78%, respectively, in TiO_2-Pb/rGO

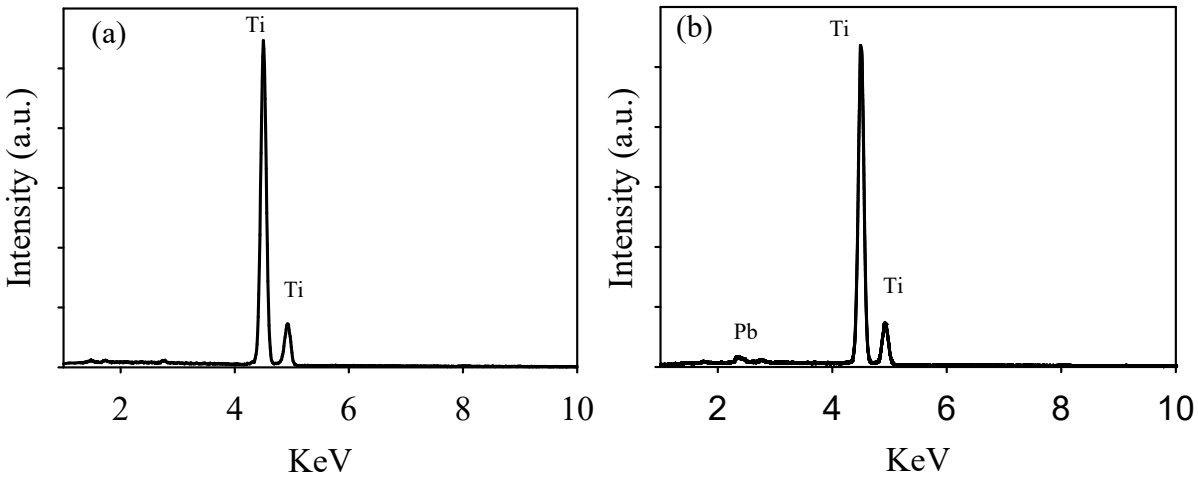

Figure 4.3. SEM-EDX elemental composition of (a) TiO_2 and (b) TiO_2-Pb/rGO photocatalyst

UV-vis absorption spectra of TiO_2, TiO_2-Pb, TiO_2/rGO, and TiO_2-Pb/rGO are shown in Figure 4.4. TiO_2 and TiO_2-Pb showed the very similar trend, absorbing only UV wavelengths less than 400 nm, while absorption band of both TiO_2/rGO and TiO_2-Pb/rGO was greatly expanded to

visible light range. Maximum absorption was shown in 379, 382, 407, and 415 nm for TiO_2, TiO_2-Pb, TiO_2/rGO, and TiO_2-Pb/rGO, respectively, which correspond to 3.27, 3.25, 3.05, and 2.99 eV according to bandgap energy (eV) = 1239.95/adsorption wavelength max (nm). Pb doping did not seem to induce significant bandgap reduction unlike other studies [Chen et al., 2016, Wang et al., 2009, Vijayan et al., 2009], while only 1% addition of rGO to TiO_2 greatly improved its visible light absorption.

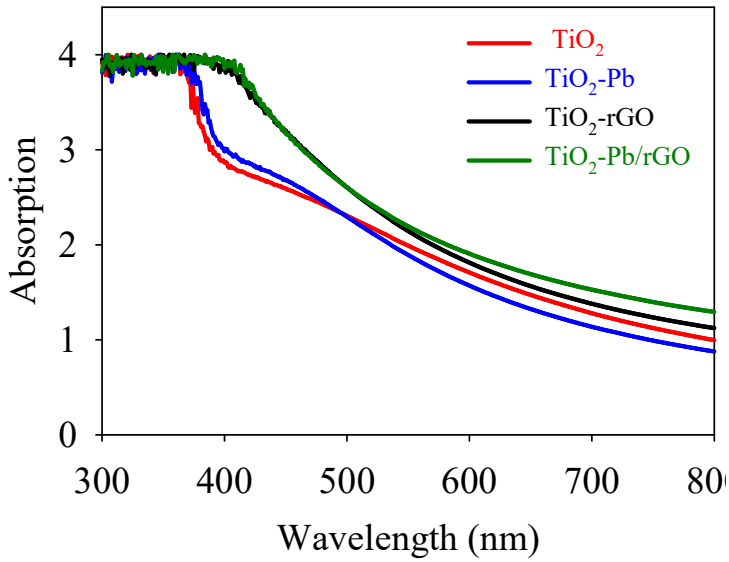

Figure 4.4. UV-vis absorption spectra of TiO_2, TiO_2-Pb, TiO_2/rGO, and TiO_2-Pb/rGO photocatalysts

Mean size of completely segregated TiO_2 particles was measured at 29.4 nm using Horiba SZ100 nanosizer (Figure 3.5). After the addition of lead and rGO into TiO_2 at ratio of 98:2/1 by weight, mean size of TiO_2-Pb/rGO nanoparticles is approximately 34.1 nm (Figure 4.5) Previous study also shows that Pb doping into TiO_2 increases particle size, because TiO_2 and lead formed the TiO_2 -Pb nanocomposite [Chen et al. 2016]. The size of agglomerated TiO_2 particles was well above tens µm.

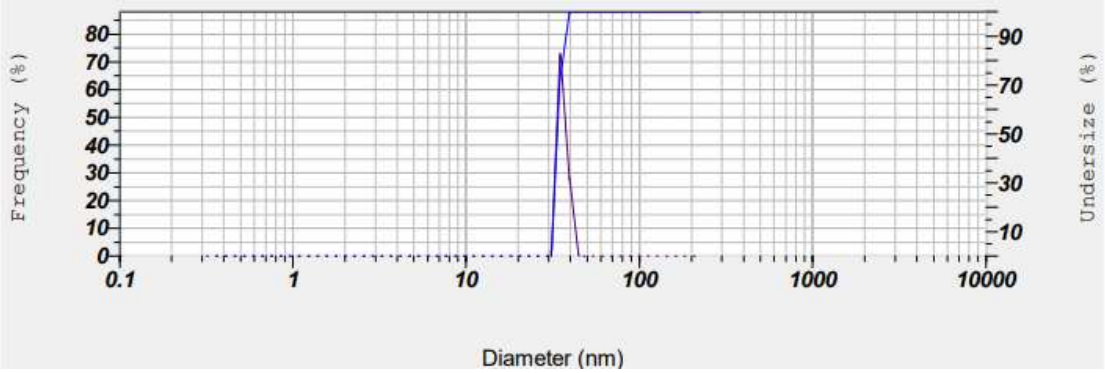

Figure 4.5: Particle size distribution of TiO_2-Pb/rGO photocatalyst

Specific surface area of TiO_2 was 50 m^2/g while that of rGO was 500 m^2/g. However, surface area of TiO_2-Pb/rGO was not increased significantly at around 53 m^2/g due to the low content of rGO at 1%.

4.3.2. Removal of PFOA

Figure 4.6 shows the removal and defluorination of PFOA by TiO_2-Pb/rGO under UVC. PFOA removal by TiO_2 via adsorption route and by Pb as control was negligible and thus there was also no defluorination. Alkyl chain of typical PFAS is hydrophobic while their functional groups are hydrophilic, which makes PFOA relatively less hydrophobic and more water-soluble in this experimental condition [Senevirathna et al., 2010; Deng et al. 2012]. UVC (220=270 nm) used in this study did not show any significant photolytic decomposition of PFOA and thus only negligible defluorination was observed, as expected considering PFOA absorbs wavelengths much shorter than 220 nm [Chen et al., 2007]. Meanwhile, rGO alone with high surface area of 500 m^2/g removed PFOA at around 65% via adsorption mechanism and thus no defluorination was observed. However, addition of 1% rGO into TiO_2-Pb (i.e., TiO_2-Pb/rGO) did not improve PFOA removal via adsorption mechanism. Only TiO_2-Pb/rGO under UVC showed highest PFOA

removal at 98% and significant defluorination at 34% (note Figure 4.9). As a result, only TiO_2-Pb/rGO under UVC was able to significantly decompose PFOA.

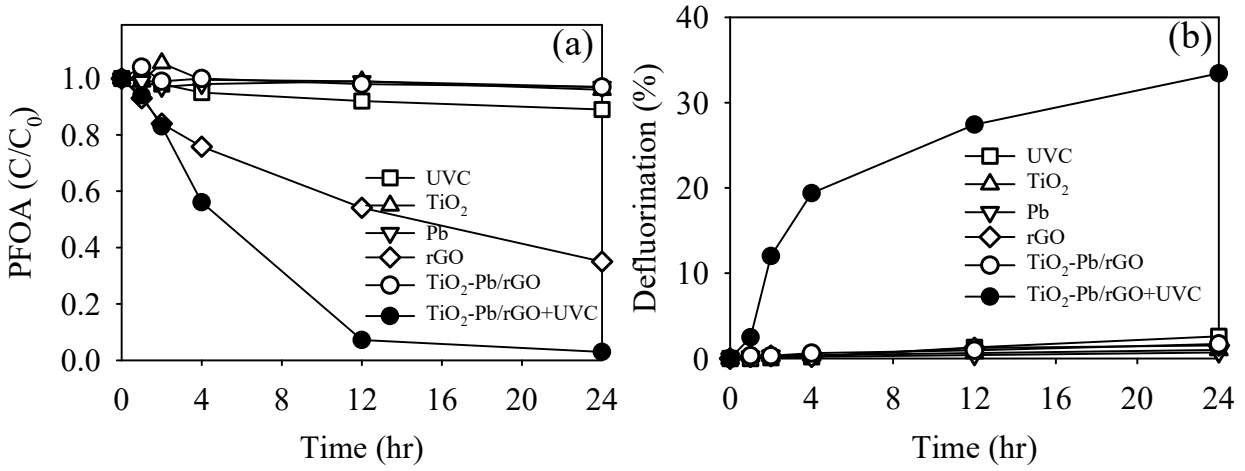

Figure 4.6. (a) removal and (b) defluorination of PFOA on TiO_2-Pb/rGO under UVC in comparison to controls (10 mg/L PFOA, 0.33 g/L photocatalyst, initial pH varied from around 4.5 to around 7.5 and final pH varied from around 4.5 to around 7.0 (no pH control), and temperature 25 °C). Defluorination % is simply calculated, based on observed F^- ion concentration in comparison to maximum F^- ion concentration when all fluorines are detached.

Further tests were conducted under UVC, employing TiO_2, Pb, rGO, TiO_2-Pb, TiO_2/rGO, and TiO_2-Pb/rGO, as shown in Fig. 4.7. First, significant PFOA removal by rGO/UVC at around 99% was ascribed to PFOA adsorption to rGO with surface area of 500 m^2/g because no significant defluorination was observed at 1.6%. Second, Pb/UVC showed certain PFOA removal and defluorination at 45% and 10%, respectively. It could be due to the formation of a complex between PFOA and Pb ion. Then the complex is excited and photolyzed by 254 nm UV light forming perfluoroalkyl radicals which rapidly reacts with water forming $C_6F_{13}COOH$ with less CF_2 unit than the original PFOA [Wang et al., 2008].

Third, TiO_2/UVC under the given experimental conditions did not show either significant PFOA removal or defluorination. Fourth, interestingly, TiO_2/rGO or TiO_2-Pb composite under UVC showed enhanced PFOA removal at 70% and 80% and defluorination at 25% and 8%, respectively, which is in agreement with results reported elsewhere [Chen et al., 2016; Ruiz et al., 2018]. Fifth, TiO_2-Pb/rGO under UVC showed superior PFOA removal at 98% and defluorination at 34% to any other systems. Assuming 1st order removal kinetics, rate constants (k) were calculated and summarized in Table 4.1.

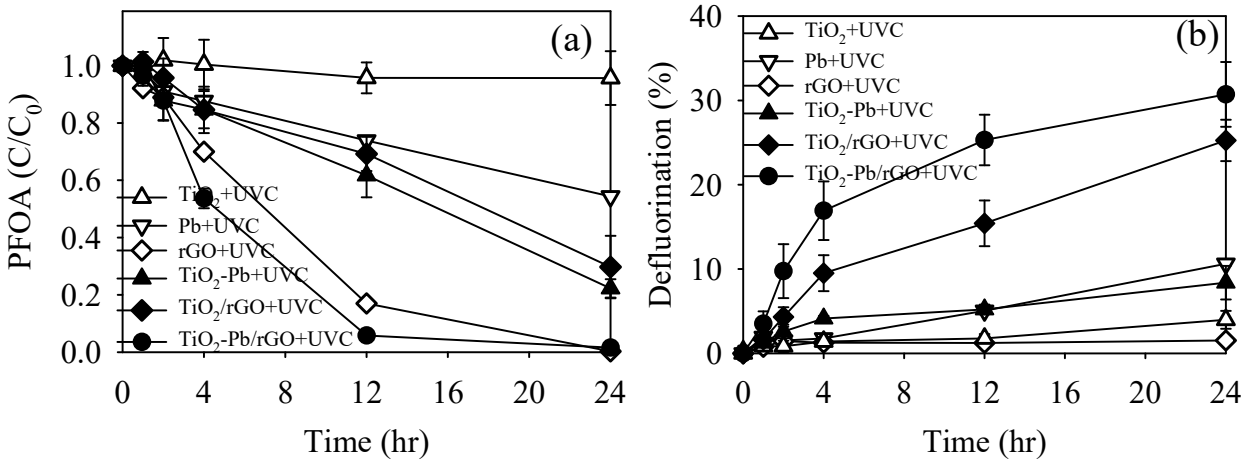

Figure 4.7. (a) removal and (b) defluorination of PFOA on various photocatalysts under UVC (10 mg/L PFOA, 0.33 g/L photocatalyst, initial pH varied from around 4.5 to around 7.5 and final pH varied from around 3.8 to around 6.5 (no pH control), and temperature 25 °C). Defluorination % is simply calculated, based on observed F^- ion concentration in comparison to maximum F^- ion concentration when all fluorines are detached.

Table1 4.1

1st order removal rate constant (k) of PFOA*

Group	Photocatalysis under UVC						Adsorption (no UVC)		Photolysis
Photocatalyst	TiO_2	Pb	rGO	TiO_2-Pb	TiO_2-rGO	TiO_2-Pb/rGO	TiO_2	TiO_2-Pb/rGO	-
k(1/hr)	0.0068	0.0254	0.0738	0.0571	0.0410	0.2193	0.0001	0.0004	0.0049

*$C=C_0 \times e^{-kt}$, where C_0 is initial concentration (mg/L) at t=0, k is 1st order rate constant (1/hr), and t is reaction time (hr)

Previous studies reported the effect of rGO or Pb doping on the reactivity of TiO_2/UV for decomposition of organic chemicals in water [Shi et al., 2007; Zhang et al.; 2009, Li et al.; 2013]. Combination of TiO_2 with rGO can lead to reduction in its band gap energy and Pb doping can also refine the crystallinity of TiO_2/rGO [Li et al., 2013; Shi et al., 2007]. The cooperative effects of Pb and rGO narrowed the band gap energy of TiO_2 as confirmed in Figure 4.5, activating TiO_2 more effectively and generating electrons(e^-) and holes (h^+) at wider wavelengths. The presence of rGO and Pb might also reduce electron-hole recombination by trapping e^-, where produced e^- migrates into rGO and difference in valence states between Ti^{4+} and Pb^{2+} may create O_2 vacancies for charge compensation [Yu et al., 2005; Ismail et al., 2007; Yao et al., 2008]. Oxygen may be adsorbed on the surface of rGO, which reacts with e^- and produces $^{\bullet}OH$ and other reactive oxygen species (ROS) such as superoxide radicals ($^{\bullet}O_2^-$) and singlet oxygen ($^1O_2$), which attack PFOA. [Chen et al., 2001].

4.3.3. Reaction mechanism

Since some of the systems were able to significantly remove PFOA and fluoride ions were also detected in Figure 4.8, targeted LC/MS analysis was applied to detect identifiable PFAS

byproducts if any, particularly shorter chain PFAS. Figure 4.8 shows evolution of aqueous short chain byproducts formation during decomposition of PFOA under UVC on TiO_2, Pb, rGO , TiO_2-Pb, TiO_2/rGO and TiO_2-Pb/rGO (also note Figure 4.9). The difference between parent PFOA removed from the aqueous phase ($PFAS_0$-$PFAS_t$) and total identifiable aqueous byproducts can be explained by various factors including adsorption of PFAS and byproducts to the materials used, presence of other byproducts, and complete mineralization. [Parenky et al., 2020] Decomposition of PFOA led to the formation of PFHpA (C7), PFHxA (C6), and PFPeA (C5) (note that all are PFCAs) but shorter chain PFCAs were rarely identified under the tested condition, which agrees with other studies [Park et al., 2016]. Only the cases showing significant defluorination in Figure 4.7(b), such as TiO_2-Pb/rGO/UVC, demonstrated significant reaction byproduct formation. For example, in case of TiO_2-Pb/rGO/UVC, total identifiable byproducts explained 68% of PFOA removed from the aqueous phase. The byproducts evolution also implied that PFOA is decomposed into short-chain intermediates through step-by-step removal of CF_2 units.

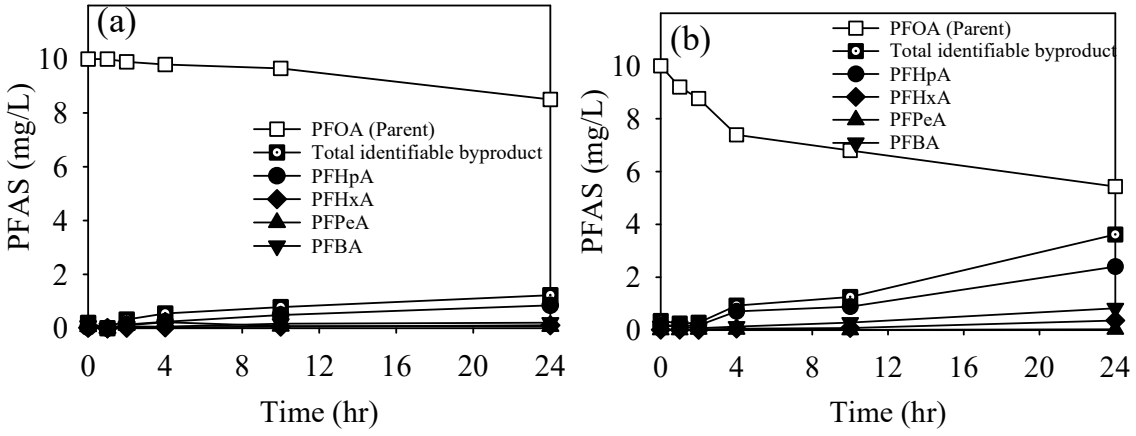

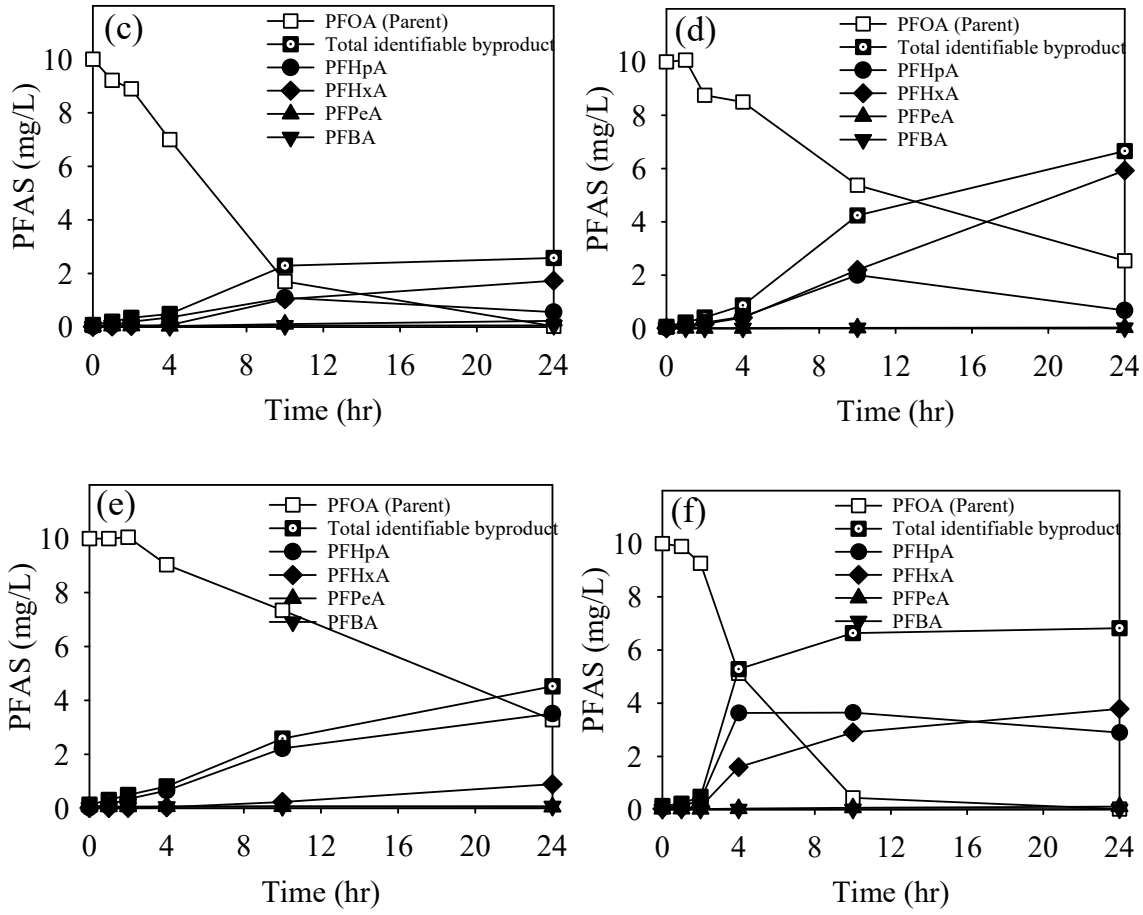

Figure 4.8. Evolution of aqueous short chain byproduct formation during decomposition of PFOA on (a) TiO_2, (b) Pb, (c) rGO, (d) TiO_2-Pb, (e) TiO_2/rGO, and (f) TiO_2-Pb/rGO under UVC (10 mg/L PFOA, 0.33 g/L photocatalyst, initial pH around 4.5 and final pH around 7.0 (no pH control), and temperature 25 $^{\circ}$C).

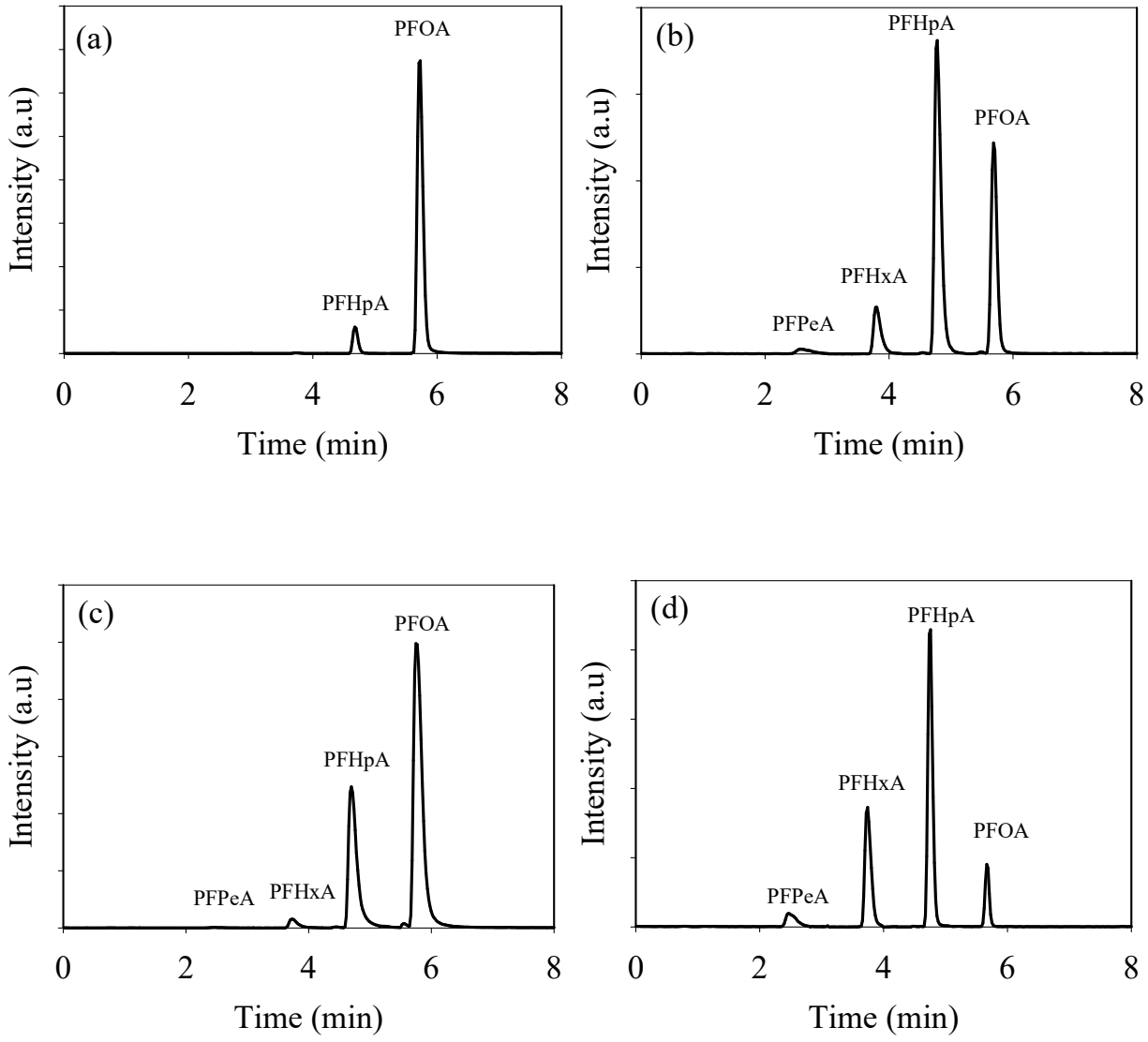

Figure 4.9. LC/MS chromatogram based on targeted analysis, showing identifiable aqueous byproducts formed during decomposition of PFOA on (a) TiO_2, (b) TiO_2-Pb, (c) TiO_2-rGO, and (d) TiO_2-Pb/rGO under UVC (10 mg/L PFOA, 0.33 g/L photocatalyst, initial pH around 4.5 to final pH around 7.0 (no pH control), and temperature 25 °C).

In order to find ROS responsible for PFOA decomposition on TiO_2-Pb/rGO/UVC, reaction quenching agents such as TBA, p-BQ, and NaN_3 were added to scavenge h^+, $^{\bullet}O_2^-$, and $^1O_2$,

respectively, as shown in Figure 4.10. [Monteagudo, et al., 2011] In all the cases, PFOA removal and defluorination was significantly inhibited, indicating that all h^+, $^{\bullet}O_2^-$, and $^1O_2$ in combination are somehow cooperatively responsible for the PFOA decomposition observed.

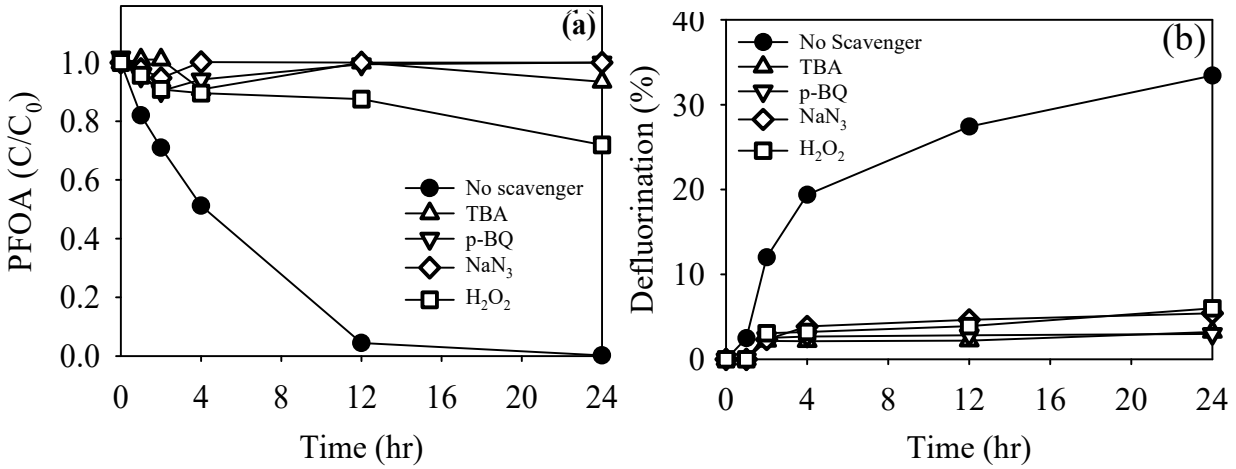

Figure 4.10 (a) removal and (b) defluorination of PFOA on TiO_2-Pb/rGO under UVC in the presence of TBA as a hole scavenger, p-BQ as a peroxy radical scavenger, NaN_3 as an oxygen scavenger, and H_2O_2 as a hydroxyl radical generator (10 mg/L PFOA, 0.33 g/L photocatalyst, 100 mmol/L TBA, 10 mmol/L pBQ, 75 mmol/L NaN_3, 1.5 g/L H_2O_2 initial pH varied from 7.5 to around 12.5 and final pH varied from around 5.2 to around 10.3 (no pH control), and temperature 25 °C).

In general, primary reactive species such as e^- and h^+ are generated on any TiO_2-based photocatalysts used in this study (Eq. 4.1). Stepwise decomposition of PFOA, in general PFCAs, was proposed previously [Hori et al., 2005]. Photocatalysis of PFOA starts with ionization and formation of perfluoroalkyl anions (Eq. 4.2), which are oxidized to perfluoroperoxy radicals by holes (Eq. 4.3) [Dillert et al., 2007]. Unstable perfluoroperoxy radicals undergo photo-Kolbe decarboxylation to form perfluoroalkyl radicals (Eq. 4.4). ROS or O_2 may react with the

perfluoroalkyl radicals, which are converted into intermediate PFCAs shortened by one CF_2-unit, thus releasing two fluoride ions (Eq. 4.5) [Panchangam et al., 2009]. This cycle repeats to form shorter chain PFCAs (Eq. 4.6). PFOA itself is inert with $^{\bullet}OH$, which might be, however, involved in decomposition of perfluoroalkyl radicals [Zhang et al., 2014].

$$TiO_2 + h\nu \rightarrow e^- + h^+ \quad (4.1)$$

$$F(CF_2)_nCOOH \rightarrow F(CF_2)_nCOO^- + H^+ \quad (4.2)$$

$$F(CF_2)_nCOO^- + h^+ \rightarrow F(CF_2)_nCOO^{\bullet} \quad (4.3)$$

$$F(CF_2)_nCOO^{\bullet} \rightarrow F(CF_2)_n^{\bullet} + CO_2 \quad (4.4)$$

$$F(CF_2)_n^{\bullet} + O_2/^1O_2 \rightarrow F(CF_2)_{n-1}COF + 2\ F^- \quad (4.5)$$

$$F(CF_2)_{n-1}COF + H_2O \rightarrow F(CF_2)_{n-1}COOH + HF \quad (4.6)$$

$$O_2 + e^- \rightarrow {}^{\bullet}O_2^- \rightarrow HO_2^{\bullet} \rightarrow H_2O_2 \rightarrow 2\,{}^{\bullet}OH \quad (4.7)$$

In general, O_2 present in water accepts photogenerated e^- to transform to $^{\bullet}O_2^-$, which can be further protonated to form hydroperoxyl radicals ($HO_2^{\bullet}$) and subsequently H_2O_2 (Eq. 4.7) [Sansotera et al., 2015]. However, the presence of rGO in the TiO_2 surface, along with Pb, can make the overall system complicated and may change the role of O_2, leading to formation of ROS which may function as sole reactants exclusively to perfluoroalkyl radicals. In particular, ROS transform to each other in a TiO_2/UV system. Previous studies showed that $^{\bullet}O_2^-$ can be converted to $^{\bullet}OH$ by the Haber–Weiss reaction while $^{\bullet}OH$ can also further transform to $^1O_2$ via disproportionation reaction [Salgado et al., 2013; Das et al., 2014; Dou et al., 2019]. And rGO on TiO_2 surface may inhibit $^{\bullet}OH$ generation and enhance the transformation of $^{\bullet}O_2^-$ to $^1O_2$. As an unstable excited oxygen molecule, $^1O_2$ can enhance PFOA decomposition [Macia et al., 2015; Macia et al., 2019; Qiuying et al., 2019]. The absence of the competition reaction for O_2 (as

electron acceptor) can also support the observed superior reactivity of TiO_2-Pb/rGO to others including bare TiO_2. Proposed

Meanwhile, h^+ also reacts with OH^- to yield $^{\bullet}OH$ [Nosaka et al., 2016]. As shown in Figure 4.10, $^{\bullet}OH$ was additionally produced by adding H_2O_2 in the reaction solution of TiO_2-Pb/rGO/UVC. PFOA removal and defluorination was significantly decreased with H_2O_2 at around 28% and 6%, respectively, compared to without H_2O_2 at around 98% and 32%, respectively. The result indicated that $^{\bullet}OH$ is less effective to decompose PFOA and/or H_2O_2 absorbs UVC quickly and thus UVC is less available to activate TiO_2-Pb/rGO or cleave C-F bonds. Proposed decomposition mechanism of PFAS by TiO_2-Pb/rGO photocatalyst is shown in Figure 4.11.

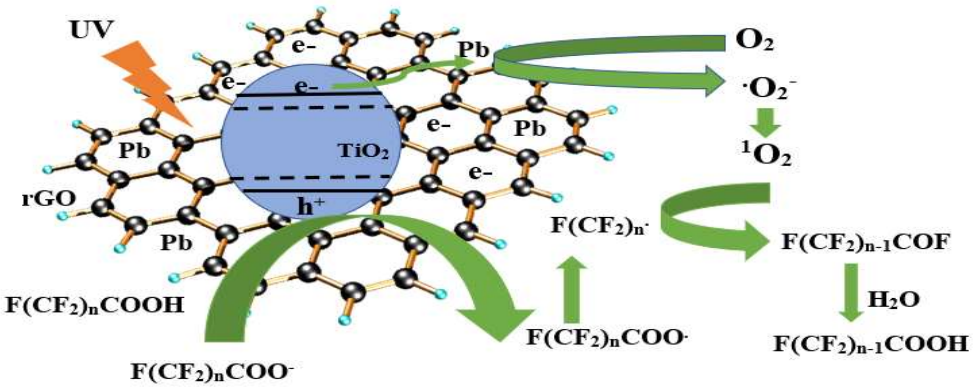

Figure 4.11. Proposed mechanism for decomposition of PFAS by TiO_2-Pb/rGO photocatalyst.

Since PFOA decomposition was successful in TiO_2-Pb/rGO/UVC, other PFAS were also examined (six perfluoroalkyl substances (3 PFCAs and 3 PFSAs) and one polyfluoroalkyl substance (6:2 FTS)), as shown in Figure 4.12. Overall removal increased in order of 6:2 FTS > PFOA >> PFOS > PFHpA ≈ PFHxS ≈ PFBA ≈ PFBS. Only 6:2 FTS (polyfluoroalkyl substance) and long chain PFCAs such as PFOA were significantly removed and defluorinated while PFSAs

and short chain PFCAs remained much less changed. Decomposition of only PFCAs is in agreement with their stepwise degradation explained in Eqs. 4.2-4.6 [Hori et al., 2005]. Bentel and co-workers also explained decomposition tendency of various PFAS with their bond dissociation energy (BDE) calculated using density functional theory, proposing that C-F BDE for long chain PFCAs are generally lower than those of PFSAs and short chain PFCAs [Bentel et al., 2019].

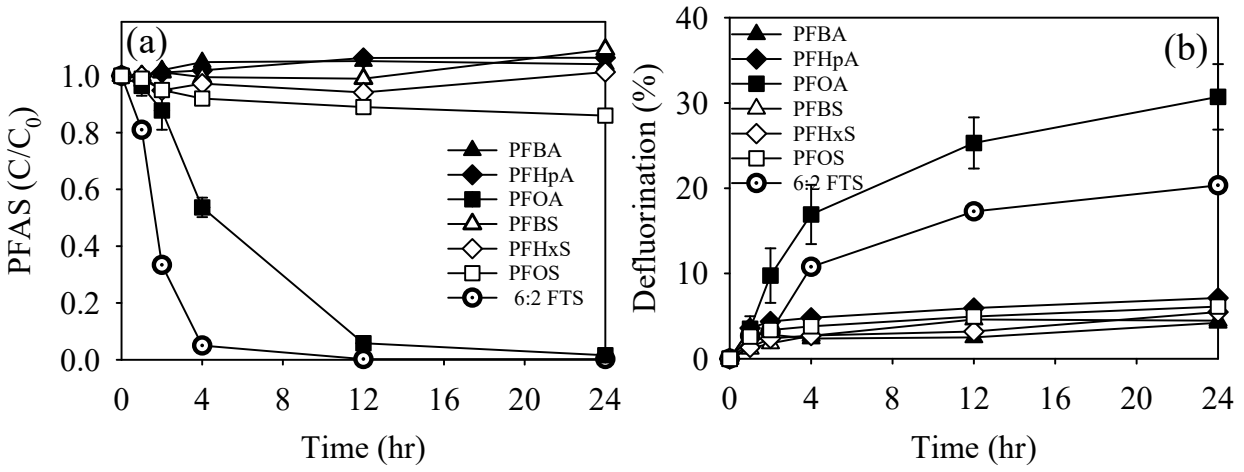

Figure 4.12. (a) removal and (b) defluorination of various PFAS on TiO_2-Pb/rGO under UVC (10 mg/L PFOA, 0.33 g/L photocatalyst, initial pH around 7.5 and final pH varied from around 4.0 to around 7.5 (no pH control), and temperature 25 $^{\circ}$C).

4.3.4 *System optimization*

Figures 4.13 and 4.14 demonstrate the effects of rGO and Pb content in TiO_2-Pb/rGO under UVC, respectively. PFOA removal and defluorination was significantly enhanced with introduction of rGO only up to 1-2% and introduction of Pb only to 2%. There might be trade-off effects between TiO_2 content as an essential photocatalyst and rGO or Pb content as a reactivity booster. In general,

introduction of secondary materials to TiO_2 may reduce UV penetration and utilization and they also occupy active sites on TiO_2 surface [Ravichandran et al., 2009].

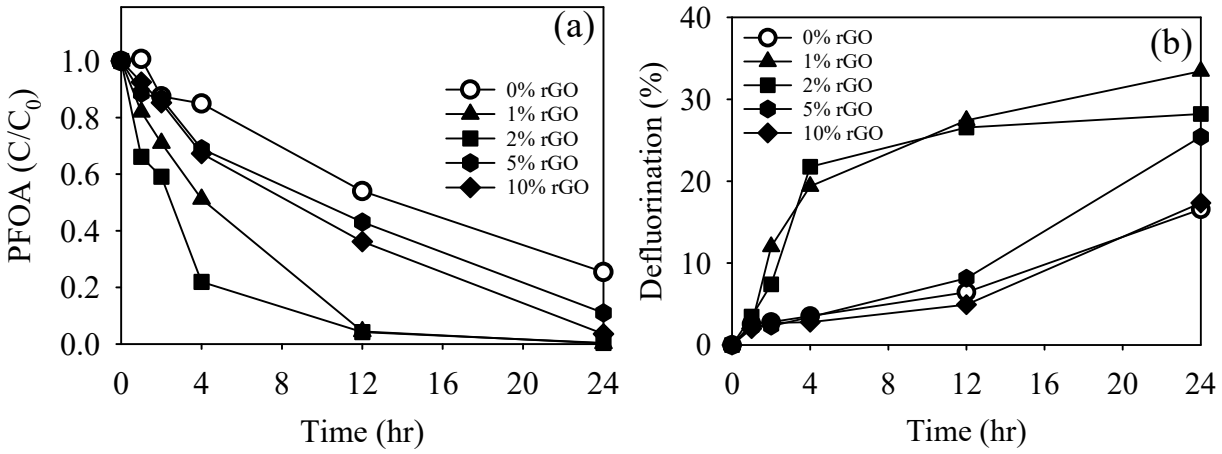

Figure 4.13. Effect of rGO content (weight %) in TiO_2-Pb/rGO on (a) removal and (b) defluorination of PFOA on TiO_2-Pb/rGO under UVC (10 mg/L PFOA, 0.33 g/L photocatalyst, initial pH around 7.5 and final pH varied from around 6.1 to around 6.6 (no pH control), and temperature 25 $^{\circ}$C).

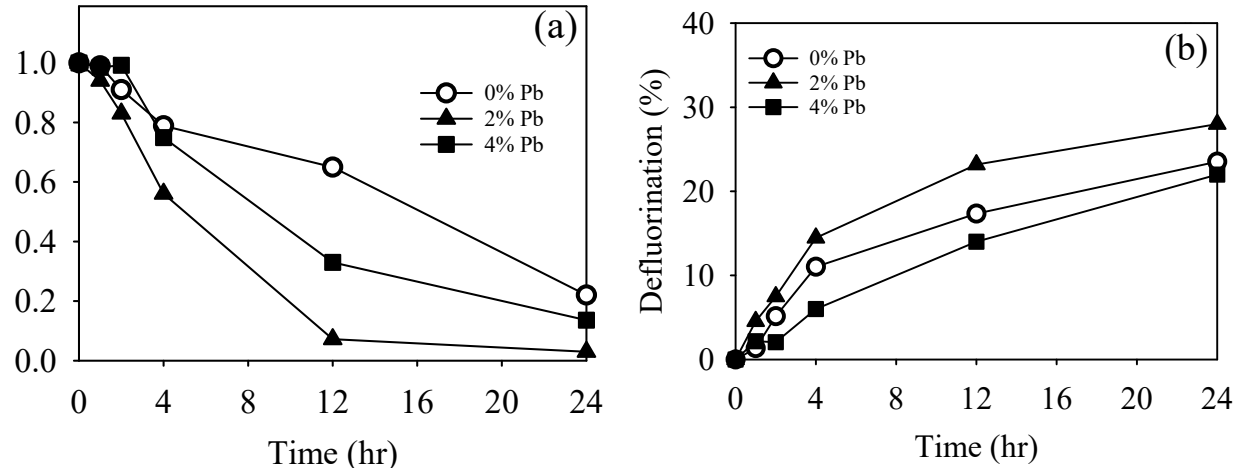

Figure 4.14. Effect of Pb content (weight %) in TiO_2-Pb/rGO on (a) removal and (b) defluorination of PFOA using TiO_2-Pb/rGO under UVC (10 mg/L PFOA, 0.33 g/L photocatalyst, initial pH

around 7.5 and final pH varied from around 4.8 to around 6.5 (no pH control), and temperature 25 °C).

As shown in Figure 4.15, PFOA removal and defluorination was also significantly enhanced with increase in TiO_2-Pb/rGO dose up to 0.33-0.66 g/L. Lowered PFOA removal and defluorination at 2.0 g/L of TiO_2-Pb/rGO can be ascribed to enhanced light scattering caused by high concentration of the solid particles [Aziz et al., 2016].

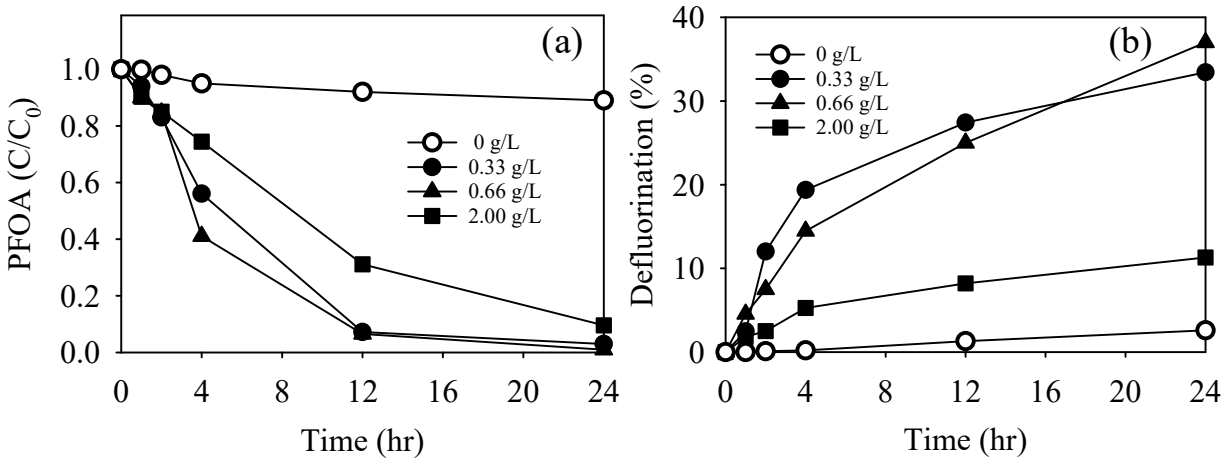

Figure 4.15. Effect of TiO_2-Pb/rGO dose on (a) removal and (b) defluorination of PFOA under UVC (10 mg/L PFOA, 0-2 g/L photocatalyst, initial pH around 7.5 and final pH varied from around 5.2 to around 7.8 (no pH control), and temperature 25 °C).

Lastly, Pb doping was compared with Fe doping as shown in Figure 4.16. The result showed that Pb doping is superior to Fe doping to enhance PFOA removal. Especially, Pb doping significantly improved PFOA defluorination at 34% in comparison to 15% by Fe doping. Previous studies showed the presence of zero-valent metal states in such TiO_2 photocatalysts, and thus the high activity of TiO_2-Pb/rGO can be explained by the standard reduction potential of Pb^{2+}/Pb^0 at -

0.13V in comparison to that of Fe^{2+}/Fe^{0} at -0.44 V for TiO_2-Fe/rGO. [Chen et al., 2015; Chen et al., 2016]

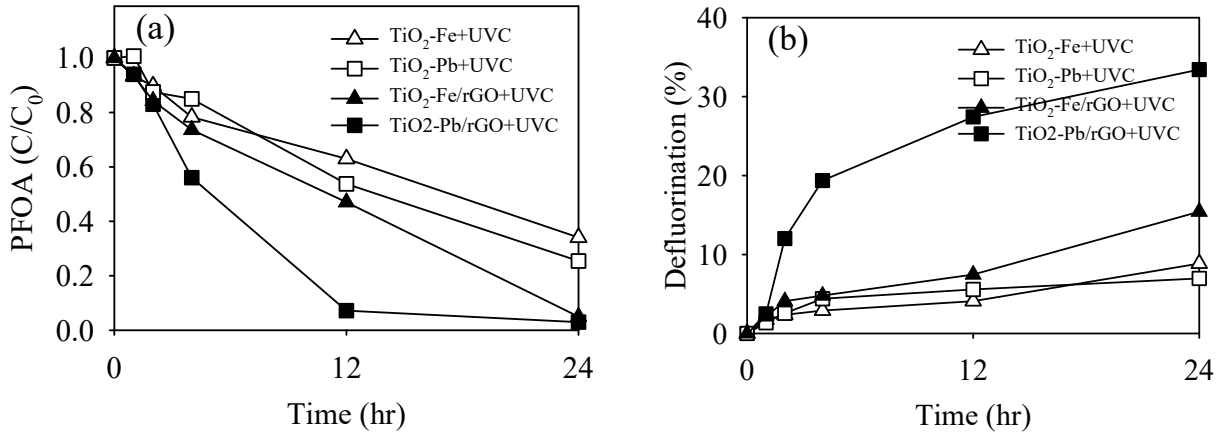

Figure 4.16. Comparison of Pb-doped and Fe-doped TiO_2/rGO with respect to (a) removal and (b) defluorination of PFOA under UVC (10 mg/L PFOA, 0.33 g/L photocatalyst, initial pH around 7.5 and final pH varied from around 5.2 to around 6.5 (no pH control), and temperature 25 $^{\circ}$C).

4.4 Conclusions

This study evaluated the reactivity of TiO_2-Pb/rGO composite photocatalyst under UVC to decompose PFAS, in particular PFOA. Doping of TiO_2 with Pb and introduction of rGO to TiO_2 greatly influenced the properties of TiO_2 such as UV-vis absorption characteristic and specific surface area, and substantially and positively affected PFOA removal and defluorination. All holes, superoxide radicals, and singlet oxygen in combination were responsible for the observed PFOA decomposition. PFOA was decomposed into short-chain intermediates through step-by-step removal of CF_2 units. Overall removal increased in order of 6:2 FTS > PFOA >> PFOS > PFHpA ≈ PFHxS ≈ PFBA ≈ PFBS. Only 6:2 FTS (polyfluoroalkyl substance) and long chain PFCAs such

as PFOA were significantly removed and defluorinated while PFSAs and short chain PFCAs remained less changed. Pb doping showed better performance than Fe doping. Although further studies and modifications to such TiO_2-based photocatalysts are needed to tackle decomposition of even PFSAs, this study overall implies that proper designing of TiO_2 photocatalytic materials has high potential to expedite decomposition of PFAS and, more broadly, similar halogenated organic chemicals in water at a given treatment cost.

4.5 References

[1] Aziz, A., Palaniandy, P., Aziz, H., Dahlan, I., (2016). Review of the mechanism and operational factors influencing the degradation process of contaminants in heterogenous photocatalysis. J. Chem. Res.; 40, 704-712.

[2] Bhattacharyya, K., Modak, B., Nayak, C., Nair, R.G., Bhattacharyya, D.; Jha, S., Tripathi, A., (2020). The formation and effect of O-vacancies in doped TiO_2. New J. Chem.; 44, 8559-8571.

[3] Bentel, M., Yu, Y., Xu, L., Li, Z., Wong, B., Men, Y., Liu, J., (2019). Defluorination of per- and polyfluoroalkyl substances (PFASs) with hydrated electrons: structural dependence and implications to PFAS remediation and management. Environ. Sci. Technol.; 53, 3718-3728.

[4] Chen, M., Lo, S., Lee, Y., Huang, C., (2015). Photocatalytic decomposition of perfluorooctanoic acid by transition-metal modified titanium dioxide, Journal of Hazardous Materials; 288, 168-175.

[5] Chen, M., Lo, S., Lee, Y., Kuo, J., Wu, C., (2016). Decomposition of perfluorooctanoic acid by ultraviolet light irradiation with Pb-modified titanium dioxide. J. Hazard. Mater.; 303, 111–118.

[6] Chen, J., Zhang, P., (2007). Photodegradation of perfluorooctanoic acid in water under irradiation of 254 nm and 185 nm light by use of persulfate. Water Sci. Technol.; 54, 317-325.

[7] Chen, F., Xie, Y., Zhao, J., Lu, G., (2001). Photocatalytic degradation of dyes on a magnetically separated photocatalyst under visible and UV irradiation; Chemosphere; 44, 1159-1168.

[8] Dillert, R., Bahenemann, D., Hidaka, H., (2007). Light-induced degradation of perfluorocarboxylic acids in the presence of titanium dioxide; Chemosphere; 67, 785-792.

[9] Das, T., Wati, M., Shad, K. (2014). Oxidative stress gated by Fenton and haber weiss reactions and its association with Alzheimer's disease. Arch Neurosci; 2, 1-8.

[10] Dastjerdi, R., Montazer, M., (2010). A review on the application of inorganic nano-structured materials in the modification of textiles: focus on anti-microbial properties; Colloids Surf. B. Biointerfaces, 79, 5-18.

[11] Deng, S., Zhang, Q., Nie, Y., Wei, H., Wang, B., Huang, J., Yu, G., Xing, B., (2012). Sorption mechanisms of perfluorinated compounds on carbon nanotubes. Environ. Pollut.; 168, 138–144.

[12] Dou, X., Zhang, Q., Shah, S.N., Khan, M., Uchiyama, K., Lin, L., (2019). MoS_2-quantum dot triggered reactive oxygen species generation and depletion: Responsible for enhanced chemiluminescence. Chem. Sci.; 10, 497-500.

[13] Dong, H., Zeng, G., Tang, L. Fan, C., Zhang, C., He, X., He, Y., (2015). An overview on limitations of TiO_2-based particles for photocatalytic degradation of organic pollutants and the corresponding countermeasures; Water Res.; 79, 128–146.

[14] Fujishima, A., Rao, T., Tryk, D., (2000). Titanium dioxide photocatalysis. J. Photochem. Photobiol. C: Photochemistry Reviews; 1, 1–21.

[15] Fujii, S., Tanaka, S., Lien, N., Qiu, Y., Polprasert, C., (2007). New POPs in the water environment: distribution, bioaccumulation and treatment of perfluorinated compounds. J. Water Supply Res. Technol., 56, 313-326.

[16] Hinderliter, P., DeLorme, M., Kennedy, G. (2006) Perfluorooctanoic acid: relationship between repeated inhalation exposures and plasma PFOA concentration in the rat. Toxicology; 222, 80-85.

[17] Hori, H., Yamamoto, A., Hayakawa, E., Taniyasu, S., Yamashita, N., Kutsuna, S., (2005). Efficient decomposition of environmentally persistent perfluorocarboxylic acids by use of persulfate as a photochemical oxidant. Environ. Sci. Technol.; 39, 2383-2388.

[18] Hori, H., Yamamoto, A., Hayakawa, E., Taniyasu, S., Yamashita, N., Kutsuna, S., (2005). Efficient decomposition of environmentally persistent perfluorocarboxylic acids by use of persulfate as a photochemical oxidant. Environ. Sci. Technol.; 39, 2383-2388.

[19] Ismail, A., Abboudi, M., Holloway, P., (2007). Photoluminescence from terbium doped silica–titania prepared by a sol–gel method. Mater. Res. Bull.; 42, 137-142.

[20] Kong, J., Shi, S., Kong, L., Zhu, X., Ni, J., (2007). Preparation and characterization of PbO_2 electrodes doped with different rare earth oxides; Electrochem. Acta; 53, 2048-2054.

[21] Krusic, P., Marchione, A., Roe, D., (2005). Gas-phase NMR studies of the thermolysis of perfluorooctanoic acid; J. Fluorine Chem.; 126, 1510-1516.

[22] Liao, Z., Farrell, J., (2009). Electrochemical Oxidation of Perfluoro butane Sulfonate using Boron-Doped Diamond Film Electrodes.; Journal of Applied Electrochemistry; 39, 1993-1999.

[23] Li, F., Duan, J., Tian, S., Ji, H., Zhu, Y., Wei, Z., Zhao, D., (2020). Short-chain per- and polyfluoroalkyl substances in aquatic systems: Occurrence, impacts and treatment. Chemical Engineering Journal; 380, 122506.

[24] Li, X., Yu, J., Wageh, S., Al-Ghamdi, A., Xie, J., (2016). Graphene in photocatalysis: a review. Small; 12, 6640-6696.

[25] Li, L., Zhang, Y., Schultz, A., Liu, X., Salvador, P., Rohrer, G., (2012). Visible light photochemical activity of hetero structured $PbTiO_3$–TiO_2 core–shell particles. Catal. Sci. Technol.; 2, 1945-1952

[26] Li, J., Zhou, S., Hong, G., Chang, C., (2013). Hydrothermal preparation of P25-graphene composite with enhanced adsorption and photocatalytic degradation of dyes; Chem. Eng. J.; 219, 486-491.

[27] Macia, N., Obach, R., Nonell, S., Heyne, B. (2019); Hybrid silver nanocubes for improved plasmon-enhanced singlet oxygen production and inactivation of bacteria. J. Am. Chem. Soc.; 141, 684-692.

[28] Macia, N., Heyne, B., (2015). Using photochemistry to understand and control the production of reactive oxygen species in biological environments. J. Photochem. Photobiol. A; 306, 1-12.

[29] Monteagudo, J., Durán, A., Martin, I., Carnicer, A., (2011). Roles of different intermediate active species in the mineralization reactions of phenolic pollutants under a UV-A/C photo-Fenton process. Appl. Catal., B; 106, 242-249.

[30] Moriwaki, H., Takagi, Y., Tanaka, M., Tsuruho, K., Okitsu, K., Maeda, Y., (2005). Sonochemical decomposition of perfluorooctane sulfonate and perfluorooctanoic acid. Environ. Sci. Technol.; 39, 3388-3392

[31] Murruni, L., Conde, F., Leyva, G., Litter, M., (2008). Photocatalytic reduction of Pb(II) over TiO_2: new insights on the effect of different electron donors; Appl. Catal. B: Environ.; 84, 563-569.

[32] Nosaka , Y., Nosaka, A. (2016). Understanding Hydroxyl Radical (•OH) Generation Processes in Photocatalysis; ACS Energy Lett.; 1, 356-359.

[33] Obo, H., Takeuchi, N., Yasuoka, K., (2015). Decomposition of perfluorooctanesulfonate (PFOS) by multiple alternating argon plasmas in bubbles with gas circulation. Int. J. Plasma Environ. Sci. Technol.; 9, 62-68.

[34] Oppong, S., Opoku, F., Govender, P., (2019). Tuning the electronic and structural properties of Gd-TiO_2-GO nanocomposites for enhancing photodegradation of IC dye: the role of Gd^{3+} ion. Appl. Catal. B Environ.; 243,106-120.

[35] Parenky, A., Souza, N., Asgari, N., Jeon, J., Nadagouda, M., Choi, H., (2020). Removal of perfluorooctane sulfonic acid (PFOS) in water by combining zerovalent iron particles with common oxidants. Environ. Eng. Sci.; 37, 472-481.

[36] Park, S., Lee, L., Medina, V., Zull, A., Waisner, S., (2016). Heat-activated persulfate oxidation of PFOA, 6:2 fluorotelomer sulfonate, and PFOS under conditions suitable for in-situ groundwater remediation. Chemosphere; 145, 376-383.

[37] Panchangam, S., Lin, A., Shaik, K., Lin, C., (2009). Decomposition of perfluorocarboxylic acids (PFCAs) by heterogeneous photocatalysis in acidic aqueous medium; Chemosphere; 77, 242-248

[38] Potera, C., (2009). Reproductive toxicology: study associates PFOS and PFOA with impaired fertility**;** Environ Health Perspect.; 117, 148.

[39] Qiuying, Y., Jiahui, J., Bin, S., Chencheng, D., Jun, L., Jinlong, Z., Mingyang, Z., (2019). Singlet oxygen triggered by superoxide radicals in a molybdenum cocatalytic Fenton

[40] Ravichandran, L., Selvam, K., Krishnakumar, B., Swaminathan, M., (2009). Photovalorisation of pentafluorobenzoic acid with platinum doped TiO_2; J. Hazard. Mater.; 167, 763-769

[41] Ruiz, B., Ribao, P., Diban, N., Rivero, M., Ortiz, I., Urtiaga, A., (2018). Photocatalytic degradation and mineralization of perfluorooctanoic acid (PFOA) using a composite TiO_2 −rGO catalyst. Journal of Hazardous Materials; 344, 950-957.

[42] Rayne, S., Forest, K., (2009). Perfluoroalkyl sulfonic and carboxylic acids: A critical review of physiochemical properties, levels and patterns in waters and wastewaters, and treatment methods; J. Environ. Sci. Heal. - Part A Toxic/Hazardous Subst. Environ. Eng.; 44, 1145–1199.

[43] Sansotera, M., Persico, F., Rizzi, V., Panzeri, W., Pirola, C., Bianchi, C.L., Mele, A., Navarrini, W., (2015). The effect of oxygen in the photocatalytic oxidation pathways of perfluorooctanoic acid; Journal of Fluorine Chemistry; 179, 159-168.

[44] Salgado, P., Melin, V., Contreras, D., Moreno, Y., Mansilla, H., (2013). Fenton reaction driven by iron ligands. J. Chil. Chem. Soc.; 58, 2096-2101.

[45] Senevirathna, S. (2010). Development of effective removal methods of PFCs (perfluorinated compounds) in water by adsorption and coagulation. Japan, School of Engineering, Kyoto University; Doctoral Thesis.

[46] Shi, J.W., Zhang, J.T., Hu, Y., Zhao, Y.C., (2007). Influence of Fe^{3+} and Ho^{3+} co-doping on the photocatalytic activity of TiO_2. Mater. Chem. Phys., 106, 247-249.

[47] . Song, C., Chen, P., Wang, C., Zhu, L., (2012). Photodegradation of perfluorooctanoic acid by synthesized TiO_2–MWCNT composites under 365 nm UV irradiation. Chemosphere, 86, 853-859.

[48] Swaminathan, M., Selvam, K., Ravichandran, L. (2010). Highly efficient activated carbon loaded TiO_2 for photo defluoridation of pentafluorobenzoic acid. J. Mol. Catal. A: Chem.; 317, 89-96.

[49] Vijayan, P., Mahendiran, C., Suresh, C., Shanthi, K., (2009). Photocatalytic activity of iron doped nanocrystalline titania for the oxidative degradation of 2,4,6-trichlorophenol. Catal. Today; 141, 220-224.

[50] Wang, S., Yang, Q., Chen, F., Sun, J., Luoa, K., Yaoa, F., Wang, X., Wang, D., Lia, X., Zeng, G., (2017). Photocatalytic degradation of perfluorooctanoic acid and perfluorooctane sulfonate in water: A critical review. Chemical Engineering Journal; 328, 927-942.

[51] Wang, F., Wong, R.J., Ho, J.H., Jiang, Y., Amal, R., (2017). Sensitization of Pt/TiO_2 using plasmonic Au nanoparticles for hydrogen evolution under visible-light irradiation; ACS Appl. Mater. Interfaces; 9, 30575-30582.

[52] Wang, Z., Chen, C., Wu, F., Zou, B., Zhao, M., Wang, J., Feng, C., (2009). Photodegradation of rhodamine B under visible light by bimetal co-doped TiO_2 nanocrystals. J. Hazard. Mater.; 164, 615-620.

[53] Wang, Y., Zhang, P., Pan, G., Chen, H., (2008). Ferric ion mediated photochemical decomposition of perfluorooctanoic acid (PFOA) by 254nm UV light. Journal of Hazardous Materials, 160, Issue 1, 181-186,

[54] Zhang, Z., Chen, J., Lyu, X., Yin, H., Sheng, G., (2014). Complete mineralization of perfluorooctanoic acid (PFOA) by gamma-irradiation in aqueous solution. Sci. Rep.; 4, 7418.

[55] Yu, Y., Yu, J., Chan, C., Che, Y., Zhao, J., Ding, L., Ge, W., Wong, P., (2005). Enhancement of adsorption and photocatalytic activity of TiO_2 by using carbon nanotubes for the treatment of azo dye; Appl. Catal. B-Environ.; 61, 1-11.

[56] Yao, Y., Li, G., Ciston, S., Lueptow, R., Gray, K., (2008). Photoreactive TiO_2/carbon nanotube composites: synthesis and reactivity. Environ. Sci. Technol.; 42, 4952-4957.

[57] Zhou, K., Zhu, Y., Yang, X., Jiang, X., Li, C., (2011). Preparation of graphene-TiO_2 composites with enhanced photocatalytic activity; New J. Chem.; 35, 353-359.

[58] Zhang, H., Lv, X., Li, Y., Wang, Y., Li, J., (2009). P25 graphene composite as a high performance photocatalyst. ACS Nano; 4, 380-386.

[59] Zhang, Z., Chen, J., Lyu, X., Yin, H., Sheng, G., (2014). Complete mineralization of perfluorooctanoic acid (PFOA) by gamma-irradiation in aqueous solution; Sci. Rep.; 4, 7418.

Chapter 5

Recommendations and Others

5.1 Recommendations for Future Studies

This study compared the TiO_2 photocatalytic and photochemical decomposition behaviors of 9 short and long chain PFAS, especially PFCAs and PFSAs which are two subgroups of PFAAs and investigated their removal mechanism. Many other PFAS subgroups are now present. PFPAs is another subgroup of PFAAs that recently gained scientific interest around the world. Future study should explore photocatalytic and photochemical removal of PFPAs and others and compare reaction kinetics to the results in this current work. In addition, since the reactions in this study were conducted in ultrapure water, future studies should explore the role of organic and inorganic matters present in water by conducting experiments with real field samples.

The successful decomposition of carboxylic long chain PFAS by TiO_2-Pb/rGO or TiO_2-Fe/rGO system raised certain questions such as feasibility of decomposing PFAS by doping other metals into TiO_2 coated with rGO. It would be important to understand elaborately how oxidation/reduction potential of doping metal affects decomposition kinetics. Simultaneously, the catalytic behavior of TiO_2-Pb/rGO towards PFAS should be evaluated in the presence of typical inorganic contaminants present in water. Although long chain PFCAs were successfully degraded under ambient conditions, short chain PFCAs and sulfonic PFAS still remained a challenge. Follow up studies investigating various TiO_2-Pb/rGO oxidant/reductant combinations could potentially decompose some PFAS groups and help in developing a comprehensive practical treatment technology. It is still not clear why all cases of scavenging h^+, $\bullet O_2^-$, and $^1O_2$ significantly inhibited photocatalytic removal of PFOA by TiO_2-Pb/rGO. The answer may lie in fast electron-

hole recombination in the absence of O_2 and ROS, while hole is primarily responsible for PFOA degradation. This needs to be thoroughly investigated for confirmation purpose. While this study was able to postulate some theories as to the interactions between TiO_2-Pb/rGO and PFOA, deeper studies using techniques like transmission electron microscopy and Fourier transform infrared are still needed to obtain a full understanding of the whole system.

5.2 Biographical Information

Nusrat Jahan Chowdhury began her academic journey in Bangladesh, where she earned her bachelor's degree in Chemical Engineering from Bangladesh University of Engineering and Technology, a renowned university in Dhaka, Bangladesh. Then she joined the University of Texas at Arlington (UTA) to pursue a master's degree in Material Science and Engineering. Then, she started working in industries as a research engineer, where she was responsible for improving the process performance of wastewater treatment plant. She was also involved in equipment selection projects. Nusrat restarted her graduate studies in the Department of Civil Engineering at UTA for her Ph.D. degree, aiming to pursue her main interest in environmental remediation. Her research focus involved the photocatalytic and photochemical decomposition of PFAS in water via oxidation and reduction mechanisms. She has also participated in many local and national conferences to present her research studies. She is now working to publish the research results in scientific journals. Her long-term goal is to secure a position in industries that involve applying some of the acquired skills and knowledge in real world environment.